symmetry

IMPACT FACTOR 2.940

CITESCORE 4.9

Review

Tetraquarks and Pentaquarks from Quark Model Perspective

Hongxia Huang, Chengrong Deng, Xuejie Liu, Yue Tan and Jialun Ping

Special Issue

Physics and Symmetry Section: Feature Papers 2022

Edited by

Prof. Dr. Tomohiro Inagaki and Dr. Olga Kodolova

MDPI

https://doi.org/10.3390/sym15071298

symmetry

MDPI

Review

Tetraquarks and Pentaquarks from Quark Model Perspective

Hongxia Huang [1,†], Chengrong Deng [2,†], Xuejie Liu [3], Yue Tan [4] and Jialun Ping [1,*]

[1] Department of Physics, Nanjing Normal University, Nanjing 210023, China; hxhuang@njnu.edu.cn
[2] School of Physics and Technology, Southwest University, Chongqing 400715, China; crdeng@swu.edu.cn
[3] School of Physics, Southeast University, Nanjing 210094, China; lxj1@seu.edu.cn
[4] School of Mathematics and Physics, Yancheng Institute of Technology, Yancheng 224051, China; tanyue@ycit.edu.cn
* Correspondence: jlping@njnu.edu.cn
† These authors contributed equally to this work.

Abstract: According to the classification of the quark model, the hadrons going beyond three-quark baryon and quark-antiquark meson pictures are called exotic hadrons. Many new hadrons have been observed since 2003, some of which exhibit exotic behaviors. There are a lot of excellent review articles on exotic hadrons available so far; the present article tries to focus on the recent experimental and theoretical progress on the exotic states from the perspective of the quark model. Although lattice quantum chromodynamics may give the final answer of the problem, the phenomenological models are still powerful tools to explore the exotic states and to provide insight on the phenomenology of hadrons. The spatial and color structures of multiquark states and the channel coupling calculation are emphasized through reviewing some bound states, molecular and color structure resonances. Finally, the unquench effects of some exotic states are reviewed. With the accumulation of experimental data on multiquark states and inspiration of underlying theory developments, more reasonable phenomenological models incorporating multi-body interactions and high Fock components to unify the description of normal hadrons and exotic hadrons are expectable.

Keywords: quark model; tetraquark; pentaquark; color structure; channel coupling

Citation: Huang, H.; Deng, C.; Liu, X.; Tan, Y.; Ping, J. Tetraquarks and Pentaquarks from Quark Model Perspective. *Symmetry* **2023**, *15*, 1298. https://doi.org/10.3390/sym15071298

Academic Editors: Tomohiro Inagaki and Olga Kodolova

Received: 22 May 2023
Revised: 17 June 2023
Accepted: 20 June 2023
Published: 22 June 2023

1. Introduction

Exotic hadrons, which cannot be accommodated in the usual schema of hadrons, three-quark baryons, and quark-antiquark mesons, are hot topics of both experimental and theoretical research in hadron physics. The fundamental theory of strong interaction, quantum chromodynamics (QCD), does not forbid the existence of multiquark states ($q^m\bar{q}^n$, $m-n=3k$ and $m+n>3$), hybrid states ($q\bar{q}g, q^3g, \cdots$), or glueballs (g^n, $n=2,3,\ldots$). There are two kinds of exotic hadrons. The first kind is the state with exotic quantum numbers, which cannot be produced by three-quark or quark-antiquark systems. The second kind is the state with normal quantum numbers, which can be produced by three-quark or quark-antiquark systems, but its properties cannot be understood as a normal hadron. One of the explanations for the exotic hadron is the multiquark state, in which there are various color structures. Therefore, multiquark states can provide the low-energy strong interaction information that may be absent in normal hadrons. Furthermore, invoking the multiquark and other components in the valence quark description of hadrons, it is possible to unify the treatment of normal and exotic hadrons.

However, too few exotic hadrons are confirmed by experiments so far. Nevertheless, there has been a lot of progress in the last two decades. In 2003, the BaBar Collaboration reported their observation of $D_{s0}(2317)$ in the inclusive $D_s^+\pi$ invariant mass spectrum [1], and the Belle Collaboration found a new charmonium state $X(3872)$ in the $J/\psi\pi^+\pi^-$ invariant mass spectrum of the process $B\to KJ/\psi\pi^+\pi^-$ [2]. Their observations stimulate the investigation of exotic hadron states. Afterwards, dozens of so-called XYZ particles

and other exotic states were claimed by experiments. In particular, the discovery of charged charmonium-like states, e.g., $Z_c(3900)$ [3], is regarded as the smoking gun of the existence of tetraquark states. Many near-threshold structures, e.g., the $Z_c(4020)^{\pm}$ [4,5], the $Z_b(10610/10650)^{\pm}$ [6,7], the $Z_{cs}(3985)^{-}$ [8], and the P_c states [9,10], have been observed in the worldwide high-energy experiments. Recently, a new narrow structure $X(6900)$ was observed by the LHCb Collaboration in the J/ψ-J/ψ mass spectrum [11], which arouses interest in fully heavy exotic hadrons. This state was later confirmed by the CMS Collaboration with higher standard deviations. In addition, two new fully heavy structures were also observed by the CMS Collaboration [12]. The report of two new exotic structures $X_0(2900)$ and $X_1(2900)$ in the D^-K^+ invariant mass distributions of the decay process $B^+ \to D^+D^-K^+$ by the LHCb Collaboration [13] renews our interest in four different flavors of hadron states. The doubly charmed bound state T_{cc}^+ with $I(J^P) = 0(1^+)$ was discovered by the LHCb Collaboration in the $D^0D^0\pi^+$ invariant mass spectrum [14], which invokes a renewed interest in the doubly heavy tetraquarks. These exotic states are clearly outside the scope of $q\bar{q}$ mesons and qqq baryons. Many theoretical works have been devoted to the study of these exotic hadrons. Several excellent review articles on exotic hadrons are available [15–20]. However, their internal structures are still under debate.

In this article, we mainly review the recent experimental and theoretical progress of exotic hadrons, focusing on current theoretical research on structures of these states from the perspective of quark models, emphasizing the multi-channel coupling and multi-body interaction effects. There are a lot of relevant references, and only part of them are referenced in the review for our goals. We apologize to the authors whose work is not referenced. In various theoretical approaches, the quark model is a phenomenological method in investigating the complicated strong-interaction systems. It can offer the most complete description of hadron properties and hadron–hadron interaction. For various exotic hadrons, the energy of some states is lower than the minimum threshold, so they may be stable bound states. The energy of some states is higher than the minimum threshold, which may be excited or resonant states, so the coupling effect with the scattering channel should be considered. Some states are not pure meson or baryon states, so the multi-quark coupling effect should be considered. In addition, the structure of exotic hadrons is always an open question. Exotic hadrons may be deuteron-like hadronic molecules; the reported near-threshold structures are good candidates of hadronic molecules. The compact objects with all quarks within one confinement volume are more interesting, as it is a new form of matter. Perhaps colorful sub-structures, diquark, color octet cluster, play an important role in the compact exotica. It is quite possible that both kinds of structures and their mixing appear in nature.

1.1. Color Structures

Based on QCD, the color structures of states will clearly play an important role in understanding exotic hadrons. In the lattice QCD, the color-electric flux is confined to narrow, flux-tube joining quarks and antiquarks. A color flux tube starts from each quark and ends at an antiquark or a Y-shaped junction, where three color flux tubes are either annihilated or created [21]. To some extent, the color flux tubes should be very similar to the chemical bond in the molecular system. In the QED world, there are almost countless structures of matter. Among organic molecules, there are very interesting varieties such as methane, benzene, fullerene, etc. The topological structures of the color flux tubes should be various, which may lead to even more varieties of QCD matter.

The quark and antiquark in mesons are linked with a color flux tube. Three quarks in baryons are connected by a Y-shape flux-tube [22]; $\boldsymbol{y}$ denotes a junction where three color flux tubes meet (see Figure 1). The unique color structure of normal hadrons, which are made of three quarks or quark-antiquark, makes the construction of the model to describe these hadrons easy and effective.

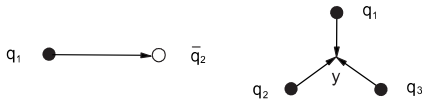

Figure 1. Mesons and baryons.

Based on the color flux-tube structures of baryons and mesons, as well as the similarity between the color flux tubes and chemical bonds, those of a multiquark system with $N+1$ particles can be generated by replacing a quark or an antiquark in an N particle state by a Y-shaped junction and two antiquarks or two quarks. Therefore, the multiquark states should possess abundant color flux-tube structures. In the following, we concentrate on the color flux-tube structure of the tetraquark and pentaquark states, which are presented in Figure 2. A thin line only stands for a **3**- or $\bar{\mathbf{3}}$-dimension color flux-tube starting from a quark or ending at an antiquark. A thick line represents a **3**-, $\bar{\mathbf{3}}$-, **6**-, $\bar{\mathbf{6}}$-, or **8**-dimension compound color flux-tube coming from the coupling of the other two color flux tubes.

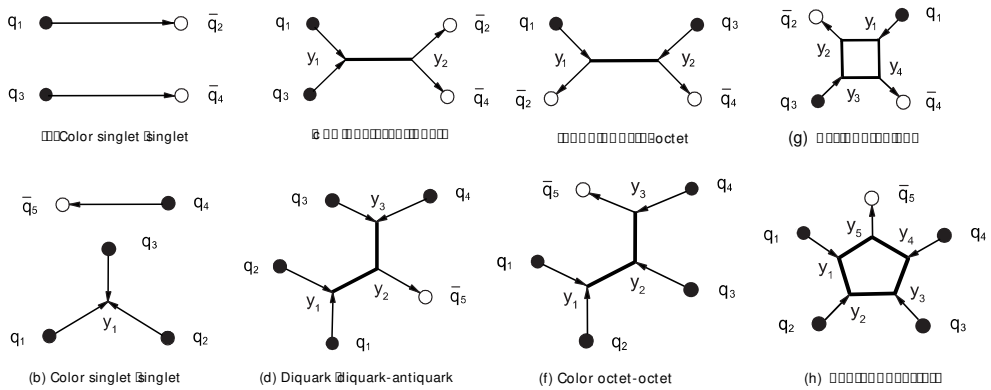

Figure 2. Color flux-tube structures for the tetraquark and pentaquark states.

Figure 2a,b show the color singlet–singlet configuration, in which two isolated colorless states are combined to form a tetraquark or a pentaquark state. This color form is usually called molecular structure. The formation of such molecular states mainly depends on the meson exchange interaction and the residual interaction between two colorless objects. Therefore, the molecular states prefer the loose spatial configuration. Many newly observed exotic hadrons are discussed in the molecular picture within various theoretical frameworks because of their proximity to the thresholds of two mesons or meson–baryon [19,20,23].

Figure 2c shows the diquark–antidiquark configuration, in which two quarks and two antiquarks are coupled into colored diquark and antidiquark, respectively, and then diquark and antidiquark are coupled into a colorless system. The tetraquark states with diquark–antidiquark configuration $[q_1q_3][\bar{q}_2\bar{q}_4]$ have two different color coupling modes according to the colorless requirement, $[[q_1q_3]_{\bar{\mathbf{3}}_c}[\bar{q}_2\bar{q}_4]_{\mathbf{3}_c}]_{1_c}$ and $[[q_1q_3]_{\mathbf{6}_c}[\bar{q}_2\bar{q}_4]_{\bar{\mathbf{6}}_c}]_{1_c}$. The $[[q_1q_3]_{\bar{\mathbf{3}}_c}[\bar{q}_2\bar{q}_4]_{\mathbf{3}_c}]_{1_c}$ is favored because of the strong attractive interaction in the diquark $[q_1q_3]_{\bar{\mathbf{3}}_c}$ and the antidiquark $[\bar{q}_2\bar{q}_4]_{\mathbf{3}_c}$, which is widely adopted to investigate the properties of the new hadrons. In general, the $[[q_1q_3]_{\mathbf{6}_c}[\bar{q}_2\bar{q}_4]_{\bar{\mathbf{6}}_c}]_{1_c}$ is unpopular because the interactions in the diquark $[q_1q_3]_{\mathbf{6}_c}$ and the antidiquark $[\bar{q}_2\bar{q}_4]_{\bar{\mathbf{6}}_c}$ are repulsive. However, it is favored in the fully heavy tetraquark states because of the strong Coulomb interaction between the diquark $[q_1q_3]_{\mathbf{6}_c}$ and the antidiquark $[\bar{q}_2\bar{q}_4]_{\bar{\mathbf{6}}_c}$ [24]. The coupling of two color modes is usually taken into account, which can further push down the energy of the tetraquark states [25].

The pentaquark state with a similar configuration is usually called diquark–diquark–antiquark configuration; see Figure 2d. It has three color coupling modes, $[[q_1q_2]_{\bar{\mathbf{3}}_c}[q_3q_4]_{\bar{\mathbf{3}}_c}\bar{q}_5]_{1_c}$, $[[q_1q_2]_{\bar{\mathbf{3}}_c}[q_3q_4]_{\mathbf{6}_c}\bar{q}_5]_{1_c}$, and $[[q_1q_2]_{\mathbf{6}_c}[q_3q_4]_{\bar{\mathbf{3}}_c}\bar{q}_5]_{1_c}$. The $[[q_1q_2]_{\bar{\mathbf{3}}_c}[q_3q_4]_{\bar{\mathbf{3}}_c}\bar{q}_5]_{1_c}$ was pioneered by Jaffe and Wilczek to explain the structure of the pentaquark state Θ^+ [26]. However, the

mass of this mode is not the lowest in the state Θ^+ mainly because the P-wave excitation between two "good" diquarks $[q_1q_2]_{\bar{3}_c}$ and $[q_3q_4]_{\bar{3}_c}$ occurs due to the requirements of the Bose–Einstein statistics [27].

Figure 2e,f show the color octet–octet configuration, in which two color octets are combined to form a tetraquark or a pentaquark state. In this configuration, the colored baryons and mesons generally have high mass due to the repulsive interactions. The tetraquark and pentaquark states consisting of two color octets usually have higher mass than that of other configurations. Thus, the color octet–octet configurations are often neglected in the study of multiquark states. Sometimes, they are combined with the molecular configuration to construct a complete color space [28].

Many organic molecules possess ring-like chemical bonds, such as the well-known benzene. Based on the similarity between the color flux tubes and the chemical bonds, possible ring-like color flux-tube structures for the tetraquark and pentaquark states and their properties were discussed in Refs. [29,30]. The structure of the tetraquark in Figure 2g is named a QCD quark cyclobutadiene. Of course, the existence of another QCD quark cyclobutadiene is also allowed in which two quarks or anti-quarks locate at neighboring positions in the flux-tube ring. The structure of the pentaquark state in Figure 2h is called the pentagonal state and it has no counterpart in the organics. In addition, the QCD benzene for the structure of the hexaquark states was also proposed in the string models [31,32].

Generally, the state with the configuration of Figure 2a or Figure 2b is classified as the colorless channel, and the one with the other configuration of Figure 2 is classified as the hidden color channel. The hidden color component is an inescapable novel degree of freedom of the multi-quark states. The physical effects of the hidden color components in the multiquark states are interesting and further investigation is expected. It is easy to construct the color wave functions of multiquark states with the molecular, diquark, and color octet configurations according to the color $SU^C(3)$ coupling rule. The starting point is always the color coupling of quark–quark or quark–antiquark. However, there is a problem in constructing the color wave functions of the state in ring-like structure, where none of the quark–quark or quark–antiquark is connected by a flux tube or a Y-shape color flux tube directly; any two quarks are connected by two or more Y-shape color flux tubes.

1.2. Multi-Body Interaction

Another feature of the multiquark system is that the multi-body interaction will emerge. In most calculations so far, the two-body interactions used in the normal hadrons are directly extended to the multiquark systems based on the "Casimir scaling" [33,34], i.e., the interactions between color antisymmetric interacting quark pair, which work well in the normal hadron spectrum, are generalized to that between color symmetric interacting quark pair by adding $\boldsymbol{\lambda}_i \cdot \boldsymbol{\lambda}_j$, the second-order Casimir operator of color $SU^C(3)$. The extension will lead to power-law van der Waals forces between color-singlet hadrons, which contradicts the experimental data [35,36]. The problems are related to the fact that the models do not respect local color gauge invariance [37,38]. In addition, it also leads to anti-confinement for symmetric color structure in the multiquark systems [39]. However, the recent Lattice QCD calculations showed that multi-body string-like or flux-tube interactions exist in multiquark systems. For a connected multiquark system, the one-gluon exchange plus multi-Y ansatz works well [40,41]. The potentials for the multiquark system are

$$V_{4Q} = \frac{\alpha_s}{4}\sum_{i<j}\frac{\boldsymbol{\lambda}_i \cdot \boldsymbol{\lambda}_j}{r_{ij}} + \sigma_{4Q}L_{\min} + C_{4Q}, \quad (1)$$

$$V_{5Q} = \frac{\alpha_s}{4}\sum_{i<j}\frac{\boldsymbol{\lambda}_i \cdot \boldsymbol{\lambda}_j}{r_{ij}} + \sigma_{5Q}L_{\min} + C_{5Q}. \quad (2)$$

The potentials for normal hadrons are [42]

$$V_{Q\bar{Q}} = \frac{\alpha_s}{4}\frac{\boldsymbol{\lambda}_1\cdot\boldsymbol{\lambda}_2}{r_{12}} + \sigma_{Q\bar{Q}} r_{12} + C_{Q\bar{Q}}, \tag{3}$$

$$V_{3Q} = \frac{\alpha_s}{4}\sum_{i<j}\frac{\boldsymbol{\lambda}_i\cdot\boldsymbol{\lambda}_j}{r_{ij}} + \sigma_{3Q} L_{\min} + C_{3Q}, \tag{4}$$

with $L_{\min}$ being the minimal values of the total flux-tube length for each system,

$$L_{\min} = \sum_i L_i. \tag{5}$$

The following relations hold:

$$\sigma_{Q\bar{Q}} \simeq \sigma_{3Q} \simeq \sigma_{4Q} \simeq \sigma_{5Q}. \tag{6}$$

For $3Q$ systems, the Y-structure (three-body interaction) can be well approximated by Δ-structure (two-body interactions) [43]. For multiquark systems, the validity of the approximation needs to be checked. Incorporating the multi-body interaction in the multiquark systems is expected in the further study of exotic hadrons. In addition, the fact that the contribution of three-gluon exchange among three quarks is zero for antisymmetric systems and non-zero for other systems [44] also calls for the employment of multi-body interactions in the multiquark systems.

The traditional constituent quark models can describe the properties of normal baryons and mesons well because their color structures are unique and trivial. Extended to multiquark systems, the direct extension of models is problematic. Recently, a color flux-tube model has been developed based on the lattice QCD picture and the concept of constituent quark [31,45,46]. The most salient feature of this model is that a multi-body confinement potential is employed. Such multi-body interaction may actually exist in the multiquark states. The color flux-tube model permits the appearance of some novel color structures [29,31,47].

1.3. Resonances

The most exotic hadrons reported recently in experiments are resonances. The bound states which are stable against the strong interaction can be identified unambiguously because they lie below the lowest relevant strong decay thresholds. The identification of resonances turns out to be a challenging and complicated task because the resonance states lie above some strong decay thresholds so that they will decay strongly to other hadrons. Then the coupling between the resonances (closed channels) and the continuum states (decay channels) is important for the observation of the resonances. For color singlet–singlet resonances (molecule-like states), two hadrons with higher energies attract each other to form a composite object with given quantum numbers, which is a bound state if it stands alone. However, if there are two-hadron states with lower energies and the same set of quantum numbers, the composite object can decay to the two-hadron states, so the composite object becomes a resonance. For example, the attraction between Σ_c^* and $\bar{D}^*$ is strong enough to form a bound state with $I(J^P) = \frac{1}{2}(\frac{1}{2}^-)$. However, there are some two-hadron states, such as $\Lambda_c\bar{D}$, $N\eta_c$, etc., with lower energies and the same quantum numbers. So $\Sigma_c^*\bar{D}^*$ can decay to $\Lambda_c\bar{D}$, $N\eta_c$, etc., and then it becomes a resonance [48]. There is another type of resonance called "color structure resonances". In this case, the composite object cannot fall apart into colored sub-clusters directly because of color confinement, for example, the tetraquark system in diquark–antidiquark structure or color octet–octet structure. The energies of these states are stable against the variation of the volume. Hence, they are all bound states if they stand alone, although they have higher energies than the corresponding states in color singlet–singlet structure. The possibility of these states decaying to several hadrons turns them into resonances.

The coupling not only attributes the decay width to the resonances but also shifts the masses of the resonances. In some cases, the coupling may push the mass of a resonance above the threshold which leads to the disappearance of the resonance. For example, $\Delta\Delta$ with quantum numbers $I(J^P) = 0(1^+)$ is a bound state if it stands alone, but it can couple to NN channel, and the coupling pushes the state above the threshold of two Δs; then, the state disappears after the coupling [49]. The general rule for pushing up the resonance states is that the lower channel can form a bound state itself. Otherwise, the coupling between the closed channels and the open channels will pull down the mass of the resonances. Another possible reason for the disappearance of the resonance is that the resonance strongly couples to the continuum states; the decay width may be too large so that the resonance cannot be observed. In the calculation with finite volume, the situation will become more complicated. The obtained energies are all discrete ones. To identify the genuine resonances in the states with discrete energies, some means have to be adopted. So far there are several methods used in the phenomenological model calculations, channel coupling phase shifts calculation, stabilization method (real scaling method), and complex scaling method. We shall give a practical description of three methods in Section 2.2.

The structure of the article is as follows. Section 2 introduces models and methods for identifying the bound states and resonance states. Section 3 reviews the bound states, especially the doubly heavy tetraquark states $QQ\bar{q}\bar{q}$. Section 4 reviews some molecular resonances, giving the theoretical explanation to the molecular picture of some pentaquarks. Sections 5 and 6 review some color structure resonances and possible unquenched states, respectively. The summary and perspective are shown in the last section. In addition, the natural unit system is used in this review.

2. Models and Methods

2.1. Various Quark Models

At the hadronic scale, the fundamental theory of strong interaction QCD is non-perturbative due to its property of color confinement. At present, it is still impossible to obtain the hadron spectrum analytically from the QCD. The QCD-inspired constituent quark model (CQM) is therefore a useful tool for obtaining physical insight into these strong interacting systems. Although the systematics to obtain corrections in the quark model and the connection between the models and the underlying theory QCD are missing, the models can provide simple physical pictures, which connect the phenomenological regularities observed in the hadron data with the underlying structure. CQM can offer the most complete description of hadron properties and is probably the most successful phenomenological model of hadron structure [50].

2.1.1. Naïve Quark Model

The pioneering model of hadron structure was established in the 1960s by Gell-Mann and Zweig [51,52], in which the hadron representations could be constructed by introducing the quarks as the members of the triplet representation of SU(3) flavor group. In order to solve the model contradiction with the spin-statistics theorem in the baryon Δ^{++}, the color degree of freedom was proposed [53,54] and then the underlying theory of strong interaction QCD was formulated. Rújula et al. derived the OGE potential from the one-gluon exchange diagram in QCD and applied it in an effective manner to reproduce energy splittings in hadron spectroscopy [55]. However, the confinement potential cannot be rigorously derived from QCD in an analytic manner.

In the 1970s, the naïve quark model involving the effective OGE and confinement potentials was established and it can describe the properties of the heavy mesons and light baryons well [56–60]. The model was able present the short-range repulsive core when the model was applied to investigate the NN interaction [61]. However, the medium-range attraction in the NN interaction is absent so that the deuteron cannot be reproduced in the model.

2.1.2. Hybrid Quark Model

In order to overcome the difficulties in the naïve quark model, Oka et al. proposed the hybrid quark model [62]. The model Hamiltonian contains not only the quark–quark potential (confinement and OGE) but also the one-pion, one-sigma, or two-pion exchange potentials occurring between two nucleons. The effective meson exchange potential between two nucleons is considered to simulate the effects of the meson cloud surrounding the quark core. However, the relation between the meson exchange force and the quark exchange interaction was not clarified. In the model, the short-range part of the nuclear force is given by the quark exchange interaction as the naïve quark model. The long-range part is described by the one-pion exchange potential and the medium-range part is provided by the one-sigma exchange. The model can reproduce the observed deuteron properties (binding energy and quadrupole moment) and NN scattering phase shifts.

2.1.3. Chiral Quark Model

For the sake of consistency, it is compelling to find a justification for the meson exchange potential between two nucleons at the quark level. Due to the meson clouds surrounding the nucleon's quark core, the implementation of chiral symmetry at the quark potential level was needed [63]. The chiral symmetry breaking is the most important nonperturbative phenomenon for hadron structure at low energies [64,65]. The constituent quark mass appears because of the spontaneous breaking of the chiral symmetry at some momentum scale. Once a constituent quark mass is generated, such particles have to interact through Goldstone modes. The introduction of sigma–meson as well as pion–meson exchanges between the quarks results in the SU(2) chiral quark model. The model can describe the hadron spectrum, NN phase shifts, and the properties of the deuteron well [66–68]. Subsequently, the SU(3) quark model was developed to describe the baryon and meson spectra successfully [69,70]. Furthermore, the model can interpret the properties of the NN and nucleon–hyperon interactions well [71–74].

2.1.4. Quark Delocalization and Color Screening Model

In order to solve the difficulty in obtaining intermediate-range attraction of the nuclear force, the quark delocalization and color screening model (QDCSM) have been proposed on the basis of the similarity between the nuclear force and molecular force [75,76]. In molecular physics, experience shows that electron delocalization is an important effect contributing to the formation of chemical bonds. There may exist a similar effect for the nuclear bond due to quark delocalization. The quark delocalization is realized by writing the single particle orbital wave function as a linear combination of left and right Gaussians, the single particle orbital wave functions in the ordinary quark cluster model.

$$\psi_L(\mathbf{r}) = \phi_L(\mathbf{r}) + \epsilon\phi_R(\mathbf{r}),\ \psi_R(\mathbf{r}) = \phi_R(\mathbf{r}) + \epsilon\phi_L(\mathbf{r}), \tag{7}$$

$$\phi_L(\mathbf{r}) = \left(\frac{1}{\pi b^2}\right)^{3/4} e^{-\frac{1}{2b^2}(\mathbf{r}-\mathbf{S}_i/2)^2}, \tag{8}$$

$$\phi_R(\mathbf{r}) = \left(\frac{1}{\pi b^2}\right)^{3/4} e^{-\frac{1}{2b^2}(\mathbf{r}+\mathbf{S}_i/2)^2}, \tag{9}$$

where ϵ is a variational parameter determined by a variational calculation. $\mathbf{S}$ is the separation between two baryons. It indicates that the quark in one baryon orbit has some probability to roam into the other baryon orbit. ϕ_L and ϕ_R are the single particle orbital wave functions, respectively.

In addition, the model adopts the phenomenological color screening confinement potential,

$$V_{ij}^{con} = \begin{cases} -a_c \boldsymbol{\lambda}_i^c \cdot \boldsymbol{\lambda}_j^c r_{ij}^2 & \text{if } i, j \text{ occur in the same baryon,} \\ -a_c \boldsymbol{\lambda}_i^c \cdot \boldsymbol{\lambda}_j^c \frac{1-e^{-\mu_c r_{ij}^2}}{\mu_c} & \text{if } i, j \text{ occur in different baryons.} \end{cases}$$

The color screening confinement potential can automatically match the quadratic one in the short-distance region ($\mu_c r^2 \ll 1$). When two baryons are separated by large distances, the confinement potential can guarantee that the energy of the hexaquark system evolves into the sum of the two-baryon internal energy calculated by the model Hamiltonian. In the intermediate range region, hybrid confinement can give a different picture from that given by a single form confinement. The model can describe the nuclear intermediate range attraction and reproduce the NN scattering data and the properties of the deuteron. However, the detailed relation between quark delocalization and meson exchange is not yet clear. In addition, the model can avoid the spurious van der Waals color force between two color singlets arising from the direct extension of the single-hadron Hamiltonian to the multiquark states [75,76]. The model has been widely applied to investigate the properties of the baryon–baryon, baryon–meson, and meson–meson interactions [77–81].

2.1.5. Color Flux-Tube Model

Color confinement is a long-distance behavior, whose understanding continues to be a challenge in theoretical physics [82]. In the traditional CQM, a two-body confinement potential proportional to the color charges $\boldsymbol{\lambda}_i^c \cdot \boldsymbol{\lambda}_j^c$ and r_{ij}^n, namely $V_{ij}^C = a_c \boldsymbol{\lambda}_i^c \cdot \boldsymbol{\lambda}_j^c \cdot r_{ij}^n$, where $n = 1$ or 2 and r_{ij} is the distance between two quarks, was introduced to phenomenologically describe the quark confinement interaction [83]. The model can automatically prevent overall color singlet multiquark states disintegrating into several colored subsystems by means of color confinement with an appropriate $SU^C(3)$ Casimir constant [84]. The model also allows a multiquark system disintegrating into color-singlet clusters, and it leads to interaction potential within meson-like $q\bar{q}$ and baryon-like qqq subsystems in accord with the empirically known potentials [84]. However, the model is known to be flawed phenomenologically because it leads to power law van der Waals forces between color-singlet hadrons [35]. It is also flawed theoretically in that it is very implausible that the long-range static multibody potential is just a sum of the two-body ones [84]. The problems are related to the fact that this model does not respect local color gauge invariance [37]. Robson proposed to use many-body confinement potentials for meson–meson and baryon–baryon systems [85], which contains the essential features of the solution which emerges from the flux model based on the strong coupling limit of LQCD Hamiltonian and on the explicit local color gauge invariance [21].

The structures of multiquark systems and hadron–hadron interactions are abundant [31,47] and provide important information that is absent in ordinary hadrons, such as the $qq\bar{q}\bar{q}$ interaction [39]. Recently, LQCD calculations on mesons, baryons, tetraquark, and pentaquark states reveal flux-tube or string-like structure [40,41,86,87]. The confinement interaction of multiquark states is a multibody interaction and can be simulated by a potential which is proportional to the minimum of the total length of strings connecting the quarks to form a multiquark system.

The CFTM has been developed based on the lattice QCD color flux-tube picture and the traditional quark models. Compared with the traditional constituent quark models, the CFTM merely modifies the sum of three pairs of two-body confinement potential in the traditional models to a multi-body quadratic one. Relative to the lattice QCD, we replace the linear potential with the quadratic one. In the baryons, the three-body quadratic confinement potential can be written as

$$V^C(3) = K\Big((\boldsymbol{r}_1 - \boldsymbol{y})^2 + (\boldsymbol{r}_2 - \boldsymbol{y})^2 + (\boldsymbol{r}_3 - \boldsymbol{y})^2\Big). \tag{10}$$

The junction $\boldsymbol{y}$ can be fixed by minimizing the energy of baryons. The minimum of the confinement potential therefore has the following forms:

$$V^C(3) = K\left(\left(\frac{\boldsymbol{r}_1 - \boldsymbol{r}_2}{\sqrt{2}}\right)^2 + \left(\frac{2\boldsymbol{r}_3 - \boldsymbol{r}_1 - \boldsymbol{r}_2}{\sqrt{6}}\right)^2\right). \tag{11}$$

This formula can also be expressed as the sum of three pairs of two-body interactions,

$$V^C(3) = \frac{K}{3}\Big((\boldsymbol{r}_1 - \boldsymbol{r}_2)^2 + (\boldsymbol{r}_2 - \boldsymbol{r}_3)^2 + (\boldsymbol{r}_1 - \boldsymbol{r}_3)^2\Big). \tag{12}$$

It can be seen that the three-body quadratic confinement potential of the baryons is totally equivalent to the sum of the two-body one so that the CFTM reduces to the traditional quark model when it was used in the baryons. In the case of the multiquark states, the multibody confinement potential is determined by their color flux-tube structure and can be simplified into several independent harmonic oscillators [30,46,88], which cannot be transformed into the sum of some pairs of two-body interactions.

For the ground hadron states, their sizes are generally less than or around 1 fm, in which the difference between the quadratic potential and the linear one is not obvious. The difference can be further diluted by the adjustable stiffness of the color flux tube. The replacement is therefore reasonable in the ground states. Note that the replacement in the excited states needs to be addressed with great caution because they are spatially more extended (>1 fm). In addition, the quadratic confinement potential can greatly simplify the numerical calculation in the dynamical investigation on the multiquark states.

2.1.6. Unquenched Quark Model

In quantum field theory, the number of particles is not a conserved quantity. Generally, a physical state is a vector in the Fock space, which is a linear combination of states with given particle numbers. For hadrons, the states can be written as

$$\begin{aligned} |\text{Meson}\rangle &= c_0|q\bar{q}\rangle + c_1|q\bar{q}q\bar{q}\rangle + c_2|q\bar{q}g\rangle + \cdots, \\ |\text{Baryon}\rangle &= c_0|qqq\rangle + c_1|qqqq\bar{q}\rangle + c_2|qqqg\rangle + \cdots. \end{aligned} \tag{13}$$

As the LQCD goes beyond the quenched approximation, it is time for the quark model to take into account the unquenching effects, which is initialized by Törnqvist [89]. To ensure the effectiveness of the unquenched quark model, it is necessary to establish that the valence quark model serves as a reliable zeroth-order approximation for the low-lying hadrons. This entails a rapid convergence of the Fock expansion. Taking the meson state as an example, the two-quark (quark–antiquark) configuration must be dominated the low-lying state; the four-quark configuration makes a small modification. As for the hybrid term, generally the gluon degree of freedom is frozen in the quark model, so this term is neglected. In the early time of the unquenched quark model, the model for mesons and baryons only considers the first two terms in Equation (13).

In the unquenched quark model, the wave functions of hadrons are composed of a valence term and additional terms involving an extra quark–antiquark pair, which can be expressed as

$$\Psi_{meson} = c_0\Psi_{2q} + \sum_{i=1}^{N} c_1^i \Psi_{4q}^i, \qquad \Psi_{baryon} = c_0\Psi_{3q} + \sum_{i=1}^{N} c_1^i \Psi_{5q}^i \tag{14}$$

Here, Ψ_{2q} (Ψ_{3q}) and Ψ_{4q}^i (Ψ_{5q}^i) represent the wave functions of the two-quark (three-quark) and four-quark (five-quark) components, respectively. The expansion coefficients, denoted as c_0 and c_1^i, are determined by the dynamics of the system. The four-quark (five-quark) components, at present, are limited to two-hadron states. In the nonrelativistic quark model, the Schrödinger equation is employed, and the conservation of particle number is assumed. However, in the non-relativistic approach, it is not possible to express the Hamiltonian of the nonrelativistic unquenched quark model in the usual manner due to the inclusion of additional quark–antiquark pairs. Generally, the Hamiltonian can be written as

$$H = H_{2q(3q)} + H_{4q(5q)} + T_{24(35)}. \tag{15}$$

$H_{2q(3q)}$ acts only on the wave function $\Psi_{2q(3q)}$; $H_{4q(5q)}$ acts only on the wave functions $\Psi^i_{4q(5q)}$; and $T_{24(35)}$ couples the two-quark (three-quark) and four-quark (five-quark) components.

To find the mass shifts, which are introduced by four-quark (five-quark) components of a hadron, one needs to solve the following eigenvalue equation:

$$H|\Psi_{meson(baryon)}\rangle = E|\Psi_{meson(baryon)}\rangle. \tag{16}$$

By expanding the orbital wave functions of $\Psi_{2q}(\Psi_{3q}), \Psi_{4q}(\Psi_{5q})$ in Equation (14) with Gaussians, the above eigenvalue equation turns into a generalized eigenvalue problem of a matrix. Usually, the dimension of the matrix is very large, so an approximate method, an accumulating approach [90], is widely adopted. In this approach, one always performs a two-channel coupling calculation, $\Psi_{2q(3q)}$ and one of $\Psi^i_{4q(5q)}$ with given channel i, to obtain the mass shift Δm_i. The total mass shift is the summation of each Δm_i. This approach is a good approximation when the coupling among different four (five)-quark channels can be neglected. Otherwise, the diagonalization of a high-dimensional matrix is necessary.

The key problem in the unquenched quark model is the transition operator T, which relates two-quark (three-quark) and four-quark (five-quark) terms. Generally, the transition operator in the $^3P_0$ model is employed due to its effectiveness in dealing with strong decay of hadrons and simplicity of its mechanism. The $^3P_0$ model is first proposed by Micu in studying the decay rates of meson resonances with quantum numbers J^P=0^+, 1^+, and 2^+ [91]. The $^3P_0$ model was popularized in hadron spectroscopy by Le Yaouanc et al. [92–94] and Roberts [95]. It can be applied to the OZI rule allowing two-body strong decays of a hadron. Now, the $^3P_0$ operator is used to investigate not only the decay behavior but also the mass shift of hadrons [90,96–101].

In the $^3P_0$ model, the transition operator for a meson can be expressed as follows:

$$T = -3\,\gamma \sum_m \langle 1m1-m|00\rangle \int d\boldsymbol{p}_3 d\boldsymbol{p}_4 \delta^3(\boldsymbol{p}_3+\boldsymbol{p}_4)\mathcal{Y}_1^m(\tfrac{\boldsymbol{p}_3-\boldsymbol{p}_4}{2})\chi^{34}_{1-m}\phi_0^{34}\omega_0^{34}b_3^\dagger(\boldsymbol{p}_3)d_4^\dagger(\boldsymbol{p}_4), \tag{17}$$

where we assign γ as the probability associated with the creation of a quark–antiquark pair from the vacuum. It is important to note that due to the negative intrinsic parity of the antiquark, the resulting quark–antiquark pair must be in the state $^{2S+1}LJ = {}^3P_0$. Here, we define ϕ_0^{34} as the flavor singlet state, represented by $\frac{1}{\sqrt{3}}(u\bar{u}+d\bar{d}+s\bar{s})$, while ω_0^{34} represents the color singlet state, given by $\frac{1}{\sqrt{3}}(r\bar{r}+g\bar{g}+b\bar{b})$. It is worth noting that the quark and antiquark within the original meson are indexed as 1 and 2, respectively, whereas the quark pairs created in the vacuum are indexed as 3 and 4. However, the operator leads to unusually large mass shifts for the mesons with light and/or strange quarks, even for ground states [102]. Large mass shifts have been observed in other calculations as well [103,104]. These findings challenge the validity of the valence quark model for describing low-lying meson states and give rise to convergence issues in the Fock expansion. In Ref. [105], the convergence problem was addressed by considering only the nearest set of meson–meson states and assigning a global constant to represent the contribution of other states. Perhaps the more rigorous way to solve the problem is to introduce suppression factors to the transition operator based on physical consideration. In Ref. [102], the convergence factor $e^{-r^2/4f^2}$ ($e^{-f^2p^2}$ in momentum space, $\boldsymbol{p} = \boldsymbol{p}_3 - \boldsymbol{p}_4$) for the created quark–antiquark pair with high energies and the damping factor $e^{-R^2_{AV}/R_0^2}$ for the distance between the valence particles and created quark–antiquark pair are introduced to modify the transition operator in the $^3P_0$ model,

$$\begin{aligned} T_{modify} \quad = \quad & -3\,\gamma \sum_m \langle 1m1(-m)|00\rangle \\ & \int d\boldsymbol{p}_3 d\boldsymbol{p}_4 \delta^3(\boldsymbol{p}_3+\boldsymbol{p}_4) \times \mathcal{Y}_1^m(\hat{\boldsymbol{p}})\, \mathrm{e}^{-f^2p^2} e^{-R^2_{AV}/R_0^2} \chi^{34}_{1-m}\phi_0^{34}\omega_0^{34}b_3^\dagger(\boldsymbol{p}_3)d_4^\dagger(\boldsymbol{p}_4). \end{aligned} \tag{18}$$

By using the modified transition operator, the mass shifts from meson–meson states to the ground states of light mesons are reduced to 10∼20% of the mass with only valence quarks.

Another transition operator which has been used in the unquenched quark model comes from the ^{3}C model [106,107], which was developed in studying the charmonium spectrum. In this model, the operator is defined as

$$T = \frac{3}{8}\sum_{a=1}^{8}\int :\rho_a(\boldsymbol{r})V(\boldsymbol{r}-\boldsymbol{r}')\rho_a(\boldsymbol{r}'):d^3rd^3r', \quad \rho_a(\boldsymbol{r}) = \frac{1}{2}\psi^\dagger(\boldsymbol{r})\lambda_a\psi(\boldsymbol{r}), \tag{19}$$

where $\psi(\boldsymbol{r})$ is the quark field operator, $\lambda_a, a = 1,\cdots,8$ are the Gell-Mann matrices, V is the charmonium potential. In the beginning, only confinement potential is included in the potential V [106]; later, the potential was extended to include the color Coulomb potential [107]. The advantage of this method is that no new parameter is introduced when the high Fock components are incorporated into the unquenched quark model.

2.2. Methods for Identifying the Genuine Resonance States

Many theoretical approaches to multiquark systems have been reviewed in several excellent review articles [15–20]. In this section, we limit our description to the methods for identifying genuine resonances.

Resonance is defined as a pole in a scattering amplitude and it is not directly accessible. It generally has multiple decay channels, involving two or three stable hadrons. In principle, a calculation with multiple channels of multi-particles is needed to explore the properties of a resonance. In lattice QCD, the calculation is performed in finite volume to restore the results in the infinite volume; the periodic boundary condition and Lüscher method are employed. In this way, the discrete spectrum obtained in the finite volume is related to the hadron scattering amplitude in the infinite volume. The details of identifying the resonances in lattice QCD can be found in the recent review article [108] and references therein.

In QCD sum rule, the coupling between resonance and two-particle intermediate states is taken into account by adding a term in the phenomenological side of the sum rule; a coupling between the currents, representing the resonance and two particles, has to be introduced [109–112]. The details can be found in the review article [113].

Effective field theory is a rigorous method to perform the calculation of exotic hadrons in a specific range, and it has a clear connection to the fundamental theory of strong interaction, QCD. Its application to hadronic molecules can be seen in the review article [23] and references therein.

In the following, three methods to identify the genuine resonances in the phenomenological model are presented.

2.2.1. Channel Coupling Phase Shift Calculation

When a resonance state couples to the continuum states of its two-body decay channels, the scattering phase shifts of the two particles in the decay channel will change rapidly as the collision energy tunes through the resonance [114]. The rapid phase change is a general feature of resonance phenomena; see Figure 3. The center of mass energy with phase shift $\frac{\pi}{2}$ gives the mass of the resonance (E_R in Figure 3), and the difference of the energies with phase shift $\frac{3\pi}{4}$ and $\frac{\pi}{4}$ gives the partial decay width of the resonance (Γ in Figure 3).

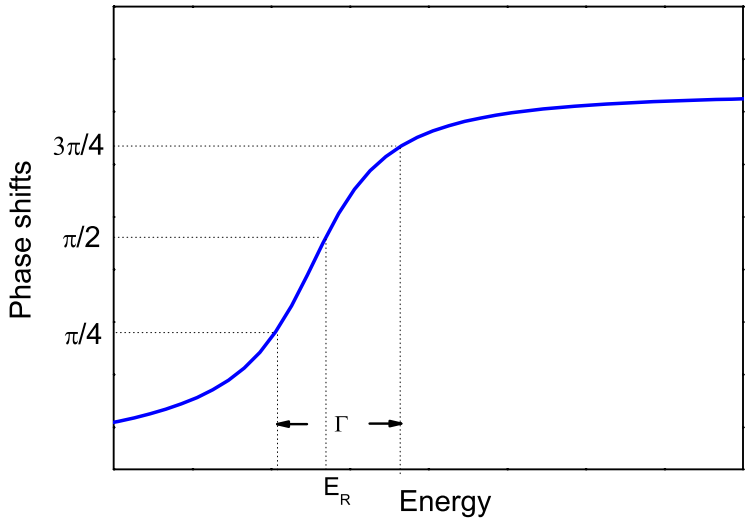

Figure 3. The resonance phenomena in scattering phase shifts.

To perform the scattering phase shift calculation at the quark level in hadron physics, the resonating group method (RGM) [115,116], which was developed to deal with the bound and scattering problems of two composite particles, is generally employed. In RGM, the internal degrees of freedom of two composite particles are frozen, and only the relative motion between two composite particles needs to be investigated. Taking the pentaquark system as an example and assuming that there are two channels—the first is the scattering channel, for example, pJ/ψ ($\gamma = 1$), and the second is a resonance channel, $\Sigma_c \bar{D}$ ($\gamma = 2$)—the wave functions of the system can be written as

$$\Psi^c = \sum_{\gamma=1}^{2} \mathcal{A}_\gamma \Big[\Phi_\gamma(\xi) \chi_\gamma^c(R_\gamma) \Big], \quad c = 1, 2, \tag{20}$$

where Φ_γ is the internal wave functions of baryon and meson with internal Jacobi coordinates ξ, R_γ is the separation between two composite particles, and $\chi_\gamma^c(R_\gamma)$ is the wave function for the relative motion between two composite particles. $\mathcal{A}_\gamma$ is the appropriate antisymmetrization operator. The effect of the finite volume is removed by using the physical boundary condition. The boundary is denoted by R_γ^c, beyond which the interaction between two composite particles can be neglected. The asymptotic behavior of $\chi_\gamma(R_\gamma)$ is

$$\chi_\gamma^c(R_\gamma) = \chi_\gamma^-(k_\gamma, R_\gamma)\delta_{\gamma c} + S_{\gamma c}\chi_\gamma^+(k_\gamma, R_\gamma), \quad R_\gamma > R_\gamma^c, \tag{21}$$

where $S_{\gamma c}$ is the transition $c \to \gamma$ matrix element. For the scattering channel,

$$\chi_\gamma^\pm(k_\gamma, R_\gamma) = \frac{1}{\sqrt{v_\gamma}} h_{L_\gamma}^\pm(k_\gamma, R_\gamma), \quad R_\gamma > R_\gamma^c, \tag{22}$$

$h_{L_\gamma}^\pm$ is the Hankel function, and v_γ is the relative speed. For the resonance channel,

$$\chi_\gamma^\pm(k_\gamma, R_\gamma) = 0, \quad R_\gamma > R_\gamma^c. \tag{23}$$

To solve the Schrödinger equation, the Kohn–Hulthén–Kato variational method [116] is used. In this approach, the relative motion wavefunction is expanded by a set of basis functions (for example, Gaussians with different centers), $u_i^{(in)}, i = 0, 1, \ldots, n_\gamma$,

$$\chi_\gamma^c(R_\gamma) = \sum_{i=0}^{n_\gamma} C_{\gamma i}^c u_{\gamma i}(R_\gamma), \tag{24}$$

where

$$u_{\gamma i}(R_\gamma) = \begin{cases} b_{\gamma i} u_i^{(in)}, & R_\gamma < R_\gamma^c, \\ \chi_\gamma^-(k_\gamma, R_\gamma) + s_{\gamma i}\chi_\gamma^+(k_\gamma, R_\gamma), & R_\gamma > R_\gamma^c. \end{cases} \tag{25}$$

From the requirement that the wave functions are continuous at $R = R_\gamma^c$, the coefficients $b_{\gamma i}$ and $s_{\gamma i}$ can be determined. Substituting $u_{\gamma i}(R_\gamma)$ into the Schrödinger equation and using the variational principle, one arrives at the following algebraic equation:

$$\sum_\beta \sum_{j=1}^{n_\beta} \mathcal{L}_{\gamma i,\beta j} C_{\beta j}^c = \mathcal{M}_{\gamma i}^c, \;\; i = 1, 2, \ldots, n_\gamma. \tag{26}$$

In deriving the above equation, the following condition, which is obtained by comparing Equation (21) with Equations (24) and (25), has been used:

$$\sum_{i=0}^{n_\gamma} C_{\gamma i}^c = \delta_{\gamma c}. \tag{27}$$

The matrix elements in Equation (26) are defined as follows:

$$\mathcal{L}_{\gamma i,\beta j} = \mathcal{K}_{\gamma i,\beta j} - \mathcal{K}_{\gamma 0,\beta j} - \mathcal{K}_{\gamma i,\beta 0} + \mathcal{K}_{\gamma 0,\beta 0}, \tag{28}$$

$$\mathcal{M}_{\gamma i}^c = -\mathcal{K}_{\gamma i,c0} + \mathcal{K}_{\gamma 0,c0}, \tag{29}$$

$$\mathcal{K}_{\gamma i,\beta j} = \int d\tau \, \langle \mathcal{A}_\gamma \left[\Phi_\gamma u_{\gamma i}\right] | H - E | \mathcal{A}_\beta \left[\Phi_\beta u_{\beta j}\right] \rangle. \tag{30}$$

By solving Equation (26), one can obtain the coefficients $C_{\beta j}^c$, and the approximate S-matrix element is given by

$$S_{\gamma c} = \sum_{i=0}^{n_\gamma} C_{\gamma i}^c s_{\gamma i}. \tag{31}$$

Finally, the stable S-matrix element is obtained:

$$S_{\beta\alpha,st} = S_{\beta\alpha} - \frac{ik^2}{\hbar} \sum_\gamma \sum_{i=0}^{n_\gamma} \mathcal{K}_{\beta 0,\gamma i} C_{\gamma i}^\alpha. \tag{32}$$

The phase shift comes from the following equation:

$$S_{\beta\alpha,st} = |S_{\beta\alpha,st}| e^{2i\delta_L}. \tag{33}$$

2.2.2. Real Scaling Method

The real scaling method (also called stabilization method) [117] has been developed to identify the genuine resonances from the states with discrete energies in the calculation with finite volume. In this method, a factor α is used to scale the finite volume. The energies of scattering states will fall off towards their thresholds, and the resonance will show up as an avoided crossing structure with the increase in α (see Figure 4). The reason is as follows. If the energy of a scattering state is far away from that of the resonance, the coupling between the resonance and the scattering states is weak, and the energy of the resonance is almost stable. When the energy of the scattering state approaches that of the resonance due to the increase in α, the coupling will become strong. If α is increased further, the separation between the energies of resonance and scattering states will increase and the coupling will become weak again. In this way, an avoided crossing structure appears. This is a general feature of two interacting energy levels. Because of the continuum nature of the scattering states, the avoided crossing structure will show up repeatedly with increasing α. In addition, from the slopes of resonance and scattering states, the decay width can be estimated by the following formula:

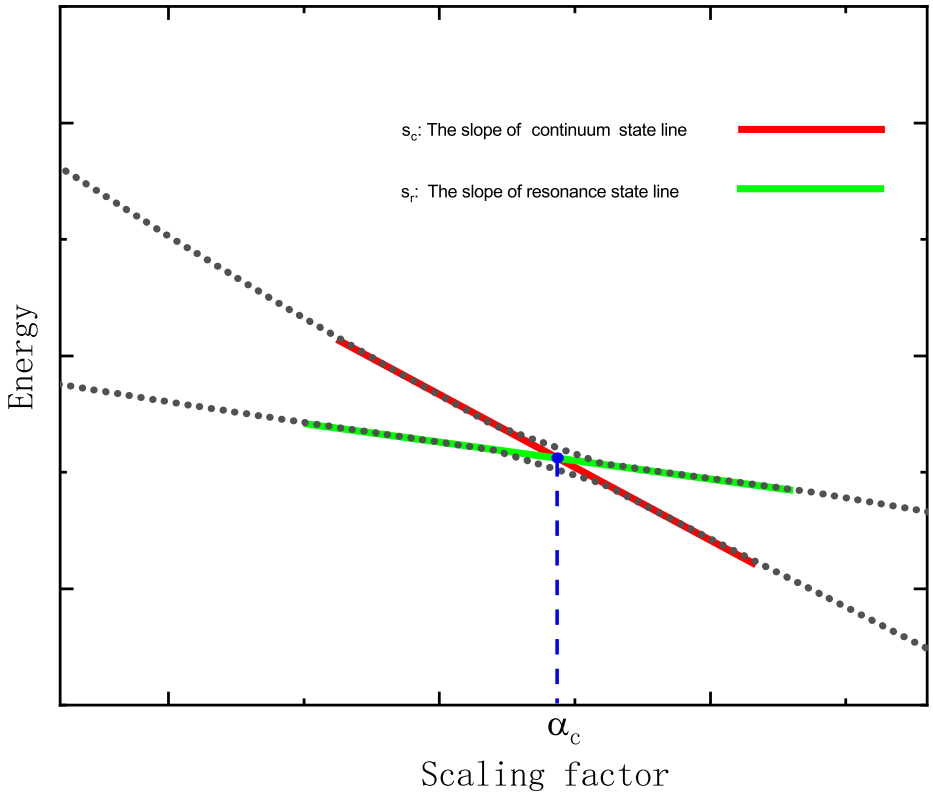

Figure 4. The schematic energy spectrum in the real scaling method.

$$\Gamma = 4|V(\alpha_c)|\frac{\sqrt{|s_r||s_c|}}{|s_r - s_c|}, \tag{34}$$

where s_r and s_c are the slopes of the resonance and scattering states, respectively, and $V(\alpha_c)$ is the energy difference between the resonance and the scattering state at the avoided crossing point.

Note that not all avoided crossing structures correspond to genuine resonance. If there are two scattering states ψ_1 and ψ_2 with many different thresholds, E_1 and E_2, and $E_2 > E_1$, then just above E_2, avoided crossing structures often show up; these structures do not imply resonance states, because ψ_2 with energy just above E_2 will fall down slowly to its threshold with increasing α, while ψ_1 with energy above E_2 will fall down rapidly to its threshold E_1. The interaction between two scattering states will produce avoided crossing structure just above the threshold E_2.

2.2.3. Complex Scaling Method

In the quantum theory of a two-body system, the momenta k_S, $k_B = i\gamma_b$, and $k_R = \kappa_r - i\gamma_r$ for scattering states, bound states, and resonances are real, imaginary, and complex (k_S, γ_b, κ_r, and γ_r are real), respectively. For all states, the asymptotic wavefunctions are proportional to the outgoing wave $e^{ik_p r}$. Then only for bound states, a damp form of the radial wavefunction $e^{-\gamma_b r}$ is obtained and it is a square integrable function.

The complex scaling method was proposed in 1971 [118,119] and was extensively applied in atomic and molecular physics. In this approach, the resonance is associated with a square integrable eigenfunction of the complex scaled Hamiltonian. There are several excellent review articles on the complex scaling method [120–122]. Here only a brief introduction is given.

In the complex scaling method, a transformation $U(\theta)$ is introduced to scale the radial coordinate:

$$U(\theta)\mathbf{r}U^{-1}(\theta) = \mathbf{r}e^{i\theta}. \tag{35}$$

The Schrödinger equation is transformed to

$$H^\theta \Psi^\theta = E^\theta \Psi^\theta, \quad H^\theta = U(\theta) H U^{-1}(\theta). \tag{36}$$

Using complex-scaled coordinates, the asymptotic wavefunctions for bound states and resonances become square integrable functions,

$$\begin{aligned} e^{ik_B r e^{i\theta}} &= e^{-\gamma_b r \cos\theta - i\gamma_b r \sin\theta}, \\ e^{ik_R r e^{i\theta}} &= e^{-(\kappa_r \sin\theta - \gamma_r \cos\theta) r + i(\kappa_r \cos\theta + \gamma_r \sin\theta)}, \ \theta > \tan^{-1}\left(\frac{\gamma_r}{\kappa_r}\right). \end{aligned} \tag{37}$$

Aguilar, Combes, and Balslev proved that the complex-scaled Schrödinger equation has the following properties:

1. The energies of the bound states are invariant with respect to the scaling.
2. The resonances are described by the square integrable functions, like bound states.
3. The continuum spectra are rotated clockwise by an angle 2θ from the positive real energy axis.

The schematic eigen-energy distribution of the complex-scaled Hamiltonian is shown in Figure 5.

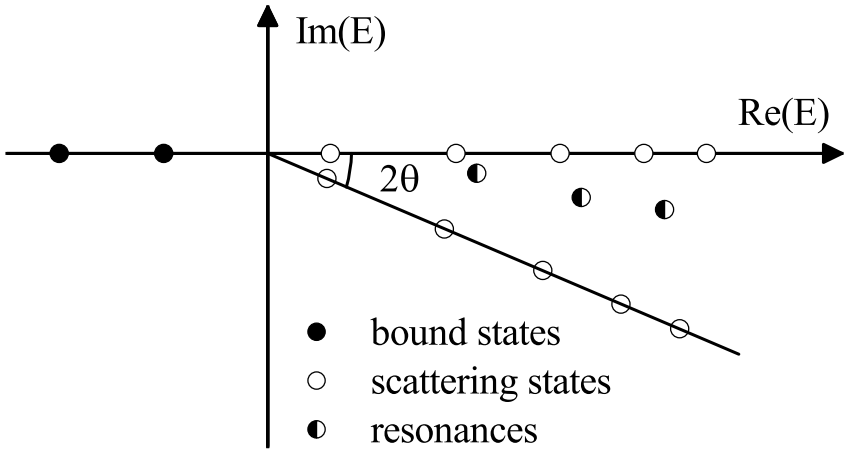

Figure 5. The schematic eigen-energy distribution of the complex-scaled Hamiltonian.

In the actual calculation, the eigenfunction Ψ^θ are often expanded by a set of basis functions, $u_i(\mathbf{r}), i = 1, 2, \ldots, n$ [123],

$$\Psi^\theta(\mathbf{r}) = \sum_{i=1}^{n} c_i^\theta u_i(\mathbf{r}). \tag{38}$$

The θ-dependent coefficients c_i^θ and eigen-energies E^θ can be obtained by solving the eigenvalue problem,

$$\sum_{j=1}^{n} H_{ji}^\theta c_i^\theta = E^\theta \sum_{j=1}^{n} N_{ji} c_i^\theta, \tag{39}$$

with

$$H_{ji}^\theta = \langle u_j(\mathbf{r}) | H^\theta | u_i(\mathbf{r}) \rangle, \quad N_{ji} = \langle u_j(\mathbf{r}) | u_i(\mathbf{r}) \rangle. \tag{40}$$

3. Bound States

A system of particles is a bound state if the relative motion of the particles occurs in a limited region of phase space. For bound states, the mass of the system is less than the sum of the masses of the constituent particles. To form a bound state, attractive forces must

exist between at least some particles of the system at certain distances between the particles. In hadron physics, the well-defined bound state is the deuteron composed of a proton and a neutron with a binding energy of 2.22 MeV. In recent decades, many theoretical investigations indicated that the doubly heavy tetraquark state $QQ\bar{q}\bar{q}$ may establish a stable bound state similar to the hydrogen molecule. Experimentally, the deuteron-like bound state T_{cc}^{+} was observed by the LHCb Collaboration recently, which will open a new gate for a family of the T_{cc}^{+}-like multiquark states.

3.1. T_{cc}^{+} *and* T_{bb}^{-}

The theoretical explorations on the question of whether or not the stable doubly heavy tetraquark states $QQ\bar{q}\bar{q}$ can exist under the strong interactions were pioneered in the early 1980s [124,125]. Subsequently, a lot of attention has been paid to the states in various nonperturbative methods, such as the MIT bag model [126], constituent quark models [127–131], chiral perturbation theory [132], string model [133,134], lattice QCD [135,136], and QCD sum rule approach [137,138]. It is widely accepted that the state $bb\bar{u}\bar{d}$, denoted as T_{bb}^{-}, with $I(J^P) = 0(1^+)$ can establish a stable state because the large mass of b-quark [123,139–149]. The binding energy of the state T_{bb}^{-} is about 200 MeV with respect to the threshold of two mesons $\bar{B}\bar{B}^*$ in various theoretical frameworks. A large center of momentum energy is required to produce the state T_{bb}^{-} and hence its discovery may be delayed. The predicted mass of the ground state $cc\bar{u}\bar{d}$ with $I(J^P) = 0(1^+)$, denoted hereafter as T_{cc}^{+}, hovers around its threshold DD^* in the range of $\pm$300 MeV [123,139–149].

In 2021, the LHCb Collaboration reported the existence of the doubly charmed state T_{cc}^{+} with $0(1^+)$ by analyzing the $D^0D^0\pi^+$ invariant mass spectrum, which has a minimal quark configuration of $cc\bar{u}\bar{d}$ [14]. Its binding energy relative to the DD^* threshold and width is

$$E_b = -273 \pm 61 \pm 5^{+11}_{-14}\ \text{keV},\ \Gamma = 410 \pm 165 \pm 43^{+18}_{-38}\ \text{keV}.$$

The LHCb Collaboration also released a more profound decay analysis, in which the unitarized Breit–Wigner profile was used [150]. Its binding energy and width were changed as

$$E_b = -361 \pm 40\ \text{keV},\ \Gamma = 47.8 \pm 1.9\ \text{keV}.$$

The binding energy and decay width of the T_{cc}^{+} signal can match very well with the prediction of the DD^* molecular state [151,152]. Furthermore, the LHCb collaboration examined several important parameters, including the characteristic size, the scattering length, the effective range, etc., which can be helpful to understand the deuteron-like nature of the state T_{cc}^{+} [14,150]. The observation of the state T_{cc}^{+} is another great breakthrough after the doubly charmed baryon Ξ_{cc}^{++} for hadron physics. In recent decades, the discovery of the $X(3872)$ pioneered the observation of a family of hidden-charm and hidden-bottom tetraquark and pentaquark states [2]. Similarly, the T_{cc}^{+} shall open a gate for a hadron world of the T_{cc}^{+}-like doubly heavy tetraquark, pentaquark, and hexaquark states.

The state T_{cc}^{+} has been inspiring a large amount of study on its properties and structure within the different theoretical frameworks. The properties of known T_{cc}^{+} so far indicated that the state can be generally consistent with a loose molecular picture [152–163]. In addition, only a few investigations were dedicated to the properties of the state T_{cc}^{+} in the compact tetraquark picture [164–167]. One can consult the comprehensive reviews on the doubly heavy tetraquark states [19,20]. In the following, we browse the properties of the doubly heavy tetraquark states from the perspective of the diquark–antidiquark and meson–meson configurations.

The color freedom follows the color SU^C(3) group, and it is sometimes denoted in short as SU^C(3). According to the SU^C(3) coupling rule, the state $QQ\bar{q}\bar{q}$ has meson–meson configuration and diquark–antidiquark configuration. The meson–meson configuration is composed of color singlet–singlet $[Q\bar{q}]_{\mathbf{1}_c}[Q\bar{q}]_{\mathbf{1}_c}$ and color octet–octet $[Q\bar{q}]_{\mathbf{8}_c}[Q\bar{q}]_{\mathbf{8}_c}$. The diquark–antidiquark configuration includes two color components: $[QQ]_{\bar{\mathbf{3}}_c}[\bar{q}\bar{q}]_{\mathbf{3}_c}$ and $[QQ]_{\mathbf{6}_c}[\bar{q}\bar{q}]_{\bar{\mathbf{6}}_c}$.

Prior to the state T_{cc}^{+} reported by the LHCb Collaboration, the diquark–antidiquark configuration seems to prevail over the meson–meson configuration, while the situation has been completely reversed due to the subsequent observation of the T_{cc}^{+} [19,20].

3.1.1. Diquark–Antidiquark Configuration

The diquark was first proposed by Gell-Mann in his pioneering work in 1964 [51]. Up to now, there exists some phenomenological evidence of the relevance of the diquarks in hadron physics [168–170]. The diquark is not a point-like fundamental object, unlike the quark. In the quark models, the diquark is a spatially extended object with various color-flavor-spin-space configurations. The substructure of the diquarks may affect the structure and nature of the multiquark states [168–170]. In this subsection, we mainly concentrate on the properties of the states $QQ\bar{q}\bar{q}$ from the perspective of diquark–antiquark configuration.

Recently, the nature of the $[QQ]$ and $[\bar{q}\bar{q}]$ was reviewed in detail in quark models [28]. Similar to spin or isospin, the authors defined the color quantum number $c = 0$ and $c = 1$ for the diquark in the color $\bar{\mathbf{3}}$ and $\mathbf{6}$ representation, respectively. For the $[QQ]$, its spin s, isospin i, orbital angular momentum l, and color c should satisfy the constraint $s + i + l + c = odd$ due to the Pauli principle. Therefore, the inner structure of the $[QQ]$ is abundant.

The S-wave diquark $[QQ]_{\bar{\mathbf{3}}}$ must be spin triplet. Its Coulomb interaction is strongly attractive because the small kinetic energy allows the heavy quarks to approach each other. The heavier the heavy quark, the stronger the Coulomb interaction. However, its color-magnetic interaction is weakly repulsive because it is suppressed by the heavy quark mass. Thus, the S-wave diquark $[QQ]_{\bar{\mathbf{3}}}$ in the spin triplet is favored. The S-wave diquark $[QQ]_{\mathbf{6}}$ must be spin singlet. Both the color-magnetic interaction and Coulomb interaction are repulsive so that it is disfavored. Such two types of diquark $[QQ]$ are generally adopted within various theoretical frameworks [19].

The color-magnetic interaction in the excited diquarks $[QQ]$ is still weak due to the large mass of heavy quarks. The Coulomb interaction gradually decreases because they are more extended and spatially induced by the orbital excitations. In addition, the orbital excitation tends to increase the kinetic energy. In general, the excited diquarks are much heavier than the S-wave diquark so that the excited diquarks are usually ignored. However, the low excited diquark $[QQ]$ and good antidiquark $[\bar{u}\bar{d}]$ can establish a bound state if the mass M_Q is enough large, which leads to the stable excited state $[bb][\bar{u}\bar{d}]$ with $I(J^P) = 0(1^+)$.

For the light antidiquark $[\bar{q}\bar{q}]$, its quantum numbers should obey the constraint $s + i + l + c = even$ due to the Pauli principle. The situation in the antidiquark $[\bar{q}\bar{q}]$ is completely opposite to that of the heavy diquark $[QQ]$ because of the obvious mass difference. Relative to the diquark $[QQ]$, the color-magnetic interaction in the antidiquark $[\bar{q}\bar{q}]$ increases owing to the small mass of the light quark. On the contrary, the Coulomb interaction decreases because the distances between light quarks increase. In this way, the color-magnetic interaction tends to prevail over the Coulomb interaction in the antidiquark $[\bar{q}\bar{q}]$.

The S-wave antidiquark $[\bar{q}\bar{q}]$ has four possible spin-isospin-color combinations. The spin-singlet, isospin-singlet, and color-triplet diquark is often called the good diquark [168], in which the Coulomb interaction, color-magnetic interaction, as well as the one-pion exchange interaction, if chiral symmetry is involved, are attractive. Other combinations are sometimes called bad diquarks. Therefore, such a good diquark generally has lower mass because of its strong color-magnetic interaction and one-pion exchange interaction, while bad diquarks have higher mass.

A good diquark $[qq]_{\bar{\mathbf{3}}_c}$ and a good anti-diquark $[\bar{q}\bar{q}]_{\mathbf{3}_c}$ generally do not form a stable tetraquark state because of the low mass threshold of two light pseudoscalar mesons. Similarly, the combination of a good diquark $[cc]_{\bar{\mathbf{3}}_c}$ and a good antidiquark $[\bar{c}\bar{c}]_{\mathbf{3}_c}$ is apparently higher than the threshold of $\eta_c\eta_c$ in the different theoretical investigations [24,171].

In this way, neither the fully light nor the fully heavy tetraquark states can form stable states. Experimentally, the fully charmed tetraquark states recently reported by the LHCb Collaboration are much higher than their thresholds [11].

In principle, there may exist many combinations of the $[QQ]$ and $[\bar{q}\bar{q}]$ with various $I(J^P)$, if including various excited states, the ground states of which were investigated in the different theoretical frameworks [19]. The states with $I(J^P) = 0(1^+)$ are the most promising stable state, especially the state $[bb][\bar{u}\bar{d}]$ with $0(1^+)$. Recently, six spin-isospin-color-orbit combinations (see Table 1) of the $[QQ]$ and $[\bar{u}\bar{d}]$ with $0(1^+)$ are researched in the quark model [28].

The ground state $[Q_1Q_3][\bar{q}_2\bar{q}_4]$ with $0(1^+)$ only contains two channels; see the cases (1) and (2), which are the generally adopted in the diquark–antidiquark configurations. After coupling the two channels, the two states $[c_1c_3][\bar{q}_2\bar{q}_4]$ and $[b_1b_3][\bar{q}_2\bar{q}_4]$ with $I(J^P) = 0(1^+)$ can form deep compact bound states with the binding energy of about -60 and -205 MeV, respectively. Case (1) is dominant with a probability almost reaching 100% so that the channel coupling effect is insignificant. The four lowest excited states with $0(1^+)$ are much higher than the ground states. Cases (3) and (4) have the same orbital excitation mode, where the channel coupling effect is also very weak. However, the color configuration $\mathbf{6} \otimes \bar{\mathbf{6}}$ is dominant. Cases (5) and (6) cannot couple with each other because of their orbital different excitation modes if the noncentral forces are not taken into account in the model [19]. Furthermore, the channel coupling effect is still very weak between the same orbital excitation modes in the higher excited states.

A good diquark $[QQ]_{\bar{\mathbf{3}}_c}$ and a good antidiquark $[\bar{q}\bar{q}]_{\mathbf{3}_c}$ (i.e., case (1)) are an optimal combination to produce a possible stable doubly heavy tetraquark state with $I(J^P) = 0(1^+)$. The strong attractive Coulomb interaction in the diquark $[QQ]_{\bar{\mathbf{3}}_c}$ alone can ensure that the state lies below the threshold of two $Q\bar{q}$ mesons if the mass ratio of M_Q and m_q exceeds a critical value. In the limit of the very large M_Q, the diquark $[QQ]_{\bar{\mathbf{3}}_c}$ shrinks into a tiny and compact core and the light quarks move around the QQ-core [154]. Therefore, the doubly heavy tetraquark state likes a helium-like QCD-atom. Moreover, the strong attractive color-magnetic interaction and pseudoscalar meson exchange forces if the chiral symmetry is involved in the good antiquark $[\bar{q}\bar{q}]_{\mathbf{3}_c}$. To some extent, the light antidiquark $[\bar{q}\bar{q}]_{\mathbf{3}_c}$ plays the similar role as the electron pair in the hydrogen molecule, where two electrons are in spin-singlet and form a σ bond. Furthermore, the above two binding mechanisms are independent and do not occur in the two-$Q\bar{q}$ meson threshold, which is beneficial to produce the compact tetraquark state with $0(1^+)$. This combination is also pointed out as a good candidate for a stable exotic in other approaches, such as effective Lagrangians [172], lattice QCD [173], and QCD sum rules [174].

Table 1. Six lowest combinations of $[Q_1Q_3]$ and $[\bar{q}_2\bar{q}_4]$ and their energy in terms of MeV; l_{13}, l_{24}, and $l_{13,24}$ are orbital angular momenta. Taken from Ref. [28].

Case	Color	Spin	l_{13} l_{24} $l_{13,24}$	$[c_1c_3][\bar{q}_2\bar{q}_4]$	$[b_1b_3][\bar{q}_2\bar{q}_4]$
(1)	$\bar{\mathbf{3}} \otimes \mathbf{3}$	$\mathbf{1} \oplus \mathbf{0}$	0 0 0	3820, 98.7%	10,355, 99.8%
(2)	$\mathbf{6} \otimes \bar{\mathbf{6}}$	$\mathbf{0} \oplus \mathbf{1}$	0 0 0	4112, 1.3%	10,679, 0.2%
	(1) + (2)			3817	10,355
(3)	$\bar{\mathbf{3}} \otimes \mathbf{3}$	$\mathbf{0} \oplus \mathbf{1}$	1 1 0	4439, 1.5%	10,973, 0.3%
(4)	$\mathbf{6} \otimes \bar{\mathbf{6}}$	$\mathbf{1} \oplus \mathbf{0}$	1 1 0	4285, 98.5%	10,841, 99.7%
	(3) + (4)			4282	10,840
(5)	$\bar{\mathbf{3}} \otimes \mathbf{3}$	$\mathbf{1} \oplus \mathbf{1}$	0 1 1	4440	10,987
(6)	$\mathbf{6} \otimes \bar{\mathbf{6}}$	$\mathbf{1} \oplus \mathbf{1}$	1 0 1	4311	10,873

3.1.2. Meson–Meson Configuration

Deuteron-like T_{cc}^+. The diquark–antidiquark configuration is obviously contradictive with the properties of the state T_{cc}^+ reported by the LHCb Collaboration [14,150]. Therefore, a large amount of study was devoted to the properties of the state T_{cc}^+ in the meson–meson configuration with the different theoretical frameworks [152–163]. In the meson–meson configuration, the wave function of the state T_{cc}^+ with $I(J^P) = 0(1^+)$ should include two color singlet channels,

$$DD^* = \frac{1}{\sqrt{2}}(D^{0*}D^+ - D^+D^*),\ D^*D^* = \frac{1}{\sqrt{2}}(D^{*0}D^{*+} - D^{*+}D^{*0}),$$

and two color octet channels

$$D_8D_8^* = \frac{1}{\sqrt{2}}(D_8^{0*}D_8^+ - D_8^+D_8^*),\ D_8^*D_8^* = \frac{1}{\sqrt{2}}(D_8^{*0}D_8^{*+} - D_8^{*+}D_8^{*0}).$$

Recently, the state T_{cc}^+ with the meson–meson configuration was systematically studied in a nonrelativistic quark model including a color screening confinement potential, meson exchange interactions, and one-gluon exchange interactions [154]. In the model, the state T_{cc}^+ can be described as a very loosely deuteron-like bound state with a binding energy around 0.34 MeV and a huge size of 4.32 fm. The spatial configuration is qualitatively consistent with that given by the LHCb Collaboration according to the characteristic sizes calculated from the binding energy [150]. The long-range π and intermediate-range σ-meson exchange interactions between D and D^* play an important role in the formation of the state T_{cc}^+.

Neither of the single DD^* and D^*D^* channels alone can form a bound state in the model. However, the stable state T_{cc}^+ can be achieved by the coupling of the two channels, in which the dominant component of the state T_{cc}^+ is the DD^* channel. In this way, the channel coupling effect plays a critical role in the formation of the state T_{cc}^+ in the model description [154].

In general, the state T_{cc}^+ should be a mixture of the color singlets and color octet configurations. Consequently, the state was further investigated by taking the mixing of two color configurations into account [28]. Numerical results indicated that the colorless components in the T_{cc}^+ state reach 81%, while the hidden color components are 19%. The distance between the two subclusters is about 2.62 fm, which still supports the deuteron-like configuration. Compared with the pure colorless components, the channel coupling effect is not very strong in the state T_{cc}^+, which also holds for the state T_{bb}^-.

These numerical results indeed justify the consideration of all possible colorless components only in the loose deuteron-like configuration [28]. However, the physical effects of the hidden color components, especially in the deeply bound multiquark states, are interesting and deserve further investigation.

T_{bb}^- *with various spatial structures*. In the meson–meson configuration, the state T_{bb}^- with $0(1^+)$ is sensitive to different dynamical effects and may have three different physical pictures [154]: the compact state, deuteron-like state, and hydrogen molecule-like state. Their binding energies are less than 50 MeV and qualitatively consistent with the latest lattice QCD predictions on the state [175].

A. Compact molecular state. The state T_{bb}^- with $I(J^P) = 0(1^+)$ is a rather deeply bound state with a binding energy of about 30∼50 MeV in the ChQM [154], which is very close to the latest lattice QCD predictions in the range of 20∼40 MeV [175]. However, the earlier lattice QCD results indicated that these states were over 100 MeV below the $\bar{B}\bar{B}^*$ threshold [143,176]. The main component of the state T_{bb}^- with $0(1^+)$ is the $\bar{B}\bar{B}^*$ in the quark model [154]. The two subclusters $\bar{B}$ and $\bar{B}^*$ become obscure and strongly overlap with each other severely because the sizes of the subclusters $\langle \mathbf{r}^2 \rangle^{\frac{1}{2}}$ and $\langle \mathbf{R}^2 \rangle^{\frac{1}{2}}$ are bigger than the relative distance $\langle \boldsymbol{\rho}^2 \rangle^{\frac{1}{2}}$ between the two subclusters [154]; see Figure 6. In this way, the state T_{bb}^- is a compact molecular state, which is completely different from the traditional deuteron-like molecular states from the perspective of spatial configuration. The large

b-quark mass allows the two subclusters to get as close as possible. In addition, the strong attraction between the $\bar{B}$ and $\bar{B}^*$ originating from the one-gluon exchange and π exchange interactions bind them together to establish the compact molecule state T_{bb}^-.

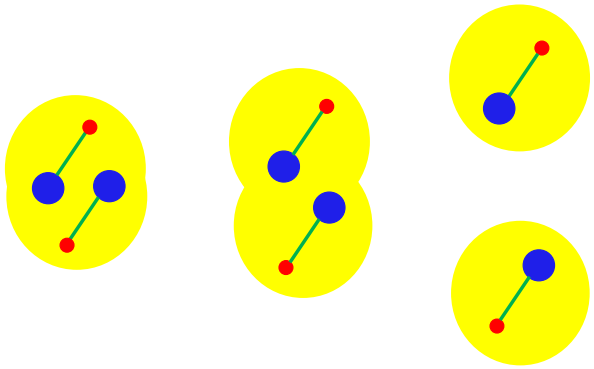

Figure 6. The spatial configuration. **Left**: compact molecule state; **middle**: hydrogen molecule-like state; **right**: deuteron-like state. Big blue ball and small red ball represent Q and $\bar{q}$, respectively. A large yellow ball represents a subcluster. Taken from Ref. [154].

B. Hydrogen-like state. The state T_{bb}^- with $I(J^P) = 0(1^+)$ can form a bound state with $E_b = -10$ MeV in the QDCSM [154]. The two subclusters $\bar{B}$ ($\bar{B}^*$) and $\bar{B}^*$ moderately overlap with each other; see Figure 6, where the attraction mainly arises from the decrease in the kinetic energy. Such an appropriate spatial overlapping greatly enlarges the phase space of the light quarks $\bar{q}_2$ and $\bar{q}_4$ and allows them to roam into the opposite subcluster freely, which helps to lower the kinetic energy of the T_{bb}^- system. This is the realization of the uncertainty principle.

The delocalization of the light quarks in the state T_{bb}^- is extremely similar to the valence bond in the hydrogen molecule, where the electron pair is shared by two protons. Therefore, the state T_{bb}^- with $I(J^P) = 0(1^+)$ is very similar to the hydrogen molecular state, which is formed by the delocalization of the light quarks with the color screening effect in the present model. The idea of the QCD valence bond was proposed and investigated in Ref. [137] and discussed extensively in the review [17]. Richard et al. also studied the hydrogen molecule-like doubly heavy tetraquark states [177].

In atom physics, the Born–Oppenheimer approximation, also known as adiabatic approximation, assumes that the electronic wave functions and energy levels at any instant depend only on the positions of the nuclei and not on the motions of the nuclei at that instant because of the obvious mass difference between the electron and the nuclei. The state T_{bb}^- is similar to the hydrogen molecule so that Maiani et al. discussed the hydrogen molecule-like T_{bb}^- state recently when the $[bb]$ pair is in color sextet based on the Born–Oppenheimer approximation to treat the hydrogen bond of QCD [178].

C. Deuteron-like state. In the naïve quark model, the T_{bb}^- state with $0(1^+)$ can still produce a shallow bound state with $E_b = -3.9$ MeV, where the attraction mainly comes from the weak residual OGE potential (Coulomb interaction plus color-magnetic interaction) [154]. The Coulomb interaction between two b-quarks and the color-magnetic interaction between two light quarks are weakly attractive. The $\bar{B}$ and $\bar{B}^*$ are separated too far away to overlap each other because the sum of the sizes of the two subclusters is less than their relative distance; see Figure 6. Quarks are only allowed to move in the isolated subclusters. Therefore, the T_{bb}^- state with $0(1^+)$ looks like a loosely bound deuteron-like molecular state.

3.1.3. Correlation between Two Configurations

The diquark–antidiquark configuration $[Q_1Q_3][\bar{q}_2\bar{q}_4]$ is apt to yield a deep compact bound state, while the meson–meson configuration $[Q_1\bar{q}_2][Q_3\bar{q}_4]$ is prone to produce a

shallow bound state in the quark models [123,140,154,179]. In principle, if all possible orbital excitations are considered properly, either the diquark or molecule bases are complete and orthogonal. In this way, one can apply either set of these bases to make the model calculations.

Recently, the underlying mechanism of these two obviously different physical pictures was decoded from the perspective of the quark clustering [28]. Two color configurations of the doubly heavy tetraquark states, $\{\mathbf{1}_{12}\otimes\mathbf{1}_{34}, \mathbf{8}_{12}\otimes\mathbf{8}_{34}\}$ for $[Q_1\bar{q}_2][Q_3\bar{q}_4]$ and $\{\bar{\mathbf{3}}_{13}\otimes\mathbf{3}_{24}, \mathbf{6}_{13}\otimes\bar{\mathbf{6}}_{24}\}$ for $[Q_1Q_3][\bar{q}_2\bar{q}_4]$, are completely equivalent:

$$\begin{pmatrix} \mathbf{1}_{12}\otimes\mathbf{1}_{34} \\ \mathbf{8}_{12}\otimes\mathbf{8}_{34} \end{pmatrix} = \begin{pmatrix} \frac{1}{\sqrt{3}} & \frac{\sqrt{2}}{\sqrt{3}} \\ -\frac{\sqrt{2}}{\sqrt{3}} & \frac{1}{\sqrt{3}} \end{pmatrix} \begin{pmatrix} \bar{\mathbf{3}}_{13}\otimes\mathbf{3}_{24} \\ \mathbf{6}_{13}\otimes\bar{\mathbf{6}}_{24} \end{pmatrix}.$$

The spin configurations of the states with $0(1^+)$, $\{\mathbf{1}_{12}\oplus\mathbf{1}_{34}, \mathbf{1}_{12}\oplus\mathbf{0}_{34}, \mathbf{0}_{12}\oplus\mathbf{1}_{34}\}$ and $\{\mathbf{1}_{13}\oplus\mathbf{1}_{24}, \mathbf{1}_{13}\oplus\mathbf{0}_{24}, \mathbf{0}_{13}\oplus\mathbf{1}_{24}\}$, are also completely equivalent:

$$\begin{pmatrix} \mathbf{1}_{12}\oplus\mathbf{1}_{34} \\ \mathbf{1}_{12}\oplus\mathbf{0}_{34} \\ \mathbf{0}_{12}\oplus\mathbf{1}_{34} \end{pmatrix} = \begin{pmatrix} 0 & \frac{1}{\sqrt{2}} & \frac{1}{\sqrt{2}} \\ -\frac{1}{\sqrt{2}} & \frac{1}{2} & -\frac{1}{2} \\ -\frac{1}{\sqrt{2}} & -\frac{1}{2} & \frac{1}{2} \end{pmatrix} \begin{pmatrix} \mathbf{1}_{13}\oplus\mathbf{1}_{24} \\ \mathbf{1}_{13}\oplus\mathbf{0}_{24} \\ \mathbf{0}_{13}\oplus\mathbf{1}_{24} \end{pmatrix}.$$

For the orbital space, one can define the relative coordinates $\mathbf{r}_{ij}$ and $\mathbf{r}_{ij,kl}$ as

$$\mathbf{r}_{ij} = \mathbf{r}_i - \mathbf{r}_j,\ \mathbf{r}_{ij,kl} = \frac{m_i\mathbf{r}_i+m_j\mathbf{r}_j}{m_i+m_j} - \frac{m_k\mathbf{r}_k+m_l\mathbf{r}_l}{m_k+m_l},$$

where $\{\mathbf{r}_{12}, \mathbf{r}_{34}, \mathbf{r}_{12,34}\}$ and $\{\mathbf{r}_{13}, \mathbf{r}_{24}, \mathbf{r}_{13,24}\}$ are the Jacobi coordinates for the meson–meson configuration and the diquark–antidiquark configuration, respectively. They can reciprocally transform into each other through a unitary matrix depending on the quark masses.

To explore the correlation between two configurations, one can express the orbit wave function $\phi(\mathbf{r}_{12}, \mathbf{r}_{34}, \mathbf{r}_{12,34})$ in terms of the explicit diquark configuration, namely $\phi(\mathbf{r}_{12}, \mathbf{r}_{34}, \mathbf{r}_{12,34}) = \phi'(\mathbf{r}_{13}, \mathbf{r}_{24}, \mathbf{r}_{13,24})$. If the Gaussian function is adopted as the orbit trial wave function, the coordinate-related parts can be expressed as

$$e^{-\nu_i\mathbf{r}_{12}^2-\nu_j\mathbf{r}_{34}^2-\nu_k\mathbf{r}_{12,34}^2} = e^{-a\mathbf{r}_{13}^2-b\mathbf{r}_{24}^2-c\mathbf{r}_{13,24}^2}\times e^{-d\mathbf{r}_{13}\cdot\mathbf{r}_{24}-e\mathbf{r}_{13}\cdot\mathbf{r}_{13,24}-f\mathbf{r}_{24}\cdot\mathbf{r}_{13,24}},$$

in which the coefficients a-f depend on the variational parameters νs and the elements of the transformation matrix from $\{\mathbf{r}_{12}, \mathbf{r}_{34}, \mathbf{r}_{12,34}\}$ to $\{\mathbf{r}_{13}, \mathbf{r}_{24}, \mathbf{r}_{13,24}\}$. The radial wave function includes all possible relative orbital angular momenta coupled to zero angular momentum [180],

$$\begin{aligned} e^{-d\mathbf{r}_{13}\cdot\mathbf{r}_{24}-e\mathbf{r}_{13}\cdot\mathbf{r}_{13,24}-f\mathbf{r}_{24}\cdot\mathbf{r}_{13,24}} &= \tfrac{1}{4\sqrt{\pi}}\textstyle\sum_{l_{13}=0}^{\infty}\sum_{l_{24}=0}^{\infty}\sum_{l_{13,24}=0}^{\infty}\left[[Y_{l_{13}}(\hat{\mathbf{r}}_{13})Y_{l_{24}}(\hat{\mathbf{r}}_{24})]_{l_{13,24}}Y_{l_{13,24}}(\hat{\mathbf{r}}_{13,24})\right]_0 \\ &\times\textstyle\sum_{l_1,l_2,l_3}(2l_1+1)(2l_2+1)(2l_3+1)\langle l_10l_20|l_{13}\rangle\langle l_10l_30|l_{24}\rangle\langle l_20l_30|l_{13,24}\rangle\begin{Bmatrix} l_{13} & l_{24} & l_{13,24} \\ l_3 & l_2 & l_1 \end{Bmatrix} \\ &\times\left(\sqrt{\tfrac{\pi}{2dr_{13}r_{24}}}I_{l_1+\frac{1}{2}}(dr_{13}r_{24})\right)\left(\sqrt{\tfrac{\pi}{2er_{13}r_{13,24}}}I_{l_2+\frac{1}{2}}(er_{13}r_{13,24})\right)\left(\sqrt{\tfrac{\pi}{2fr_{24}r_{13,24}}}I_{l_3+\frac{1}{2}}(fr_{24}r_{13,24})\right), \end{aligned}$$

where $I_a(x)$ are the modified Bessel functions.

In this way, one can decompose the ground state $[Q_1\bar{q}_2][Q_3\bar{q}_4]$ with $0(1^+)$ as the superposition of a large number of the $[Q_1Q_3][\bar{q}_2\bar{q}_4]$ states with various angular excitations of l_{13}, l_{24}, and $l_{13,24}$. With the probability of each component in the states in Table 2 and their color-spin wave functions, the percentage of each type of the $[Q_1Q_3]$ and $[\bar{q}_2\bar{q}_4]$ combination can be approximately calculated [28]. The optimal combination, a good diquark $[QQ]$ and a good antidiquark $[\bar{u}\bar{d}]$, should be responsible for the formation of the shallow bound state T_{cc}^+ from the perspective of diquarks. It implies the possible existence of another compact

doubly heavy tetraquark state T_{cc}^{+} by replacing the light quark in the doubly charmed baryon Ξ_{cc}^{++} with an optimal antidiquark $[\bar{u}\bar{d}]$ [28].

Table 2. Components, ratio, and binding energy E_b in unit of MeV. Taken from Ref. [28].

State	Component	E_b	Ratio (%)
T_{cc}^{+}	D^*D:D^*D^*:$D_{\mathbf{8}}^*D_{\mathbf{8}}$:$D_{\mathbf{8}}^*D_{\mathbf{8}}^*$	-1.24	74.2:6.8:0.2:18.8
$T_{cc}^{+\prime}$	D^*D:D^*D^*	-0.86	98.8:1.2
T_{bb}^{-}	$\bar{B}^*\bar{B}$:$\bar{B}^*\bar{B}^*$:$\bar{B}_{\mathbf{8}}^*\bar{B}_{\mathbf{8}}$:$\bar{B}_{\mathbf{8}}^*\bar{B}_{\mathbf{8}}^*$	-48.9	49.0:40.0:7.0:4.0
$T_{bb}^{-\prime}$	$\bar{B}^*\bar{B}$:$\bar{B}^*\bar{B}^*$	-43.8	62.4:37.6

The diquark and molecule configurations have different orbitally excited modes. Therefore, their corresponding ground state spaces in the diquark and molecule bases are not equivalent. The construction of the trial wave function in the model space depends on the orbitally excited modes in the realistic model calculations, which may result in the difference between the two configurations.

3.1.4. Mixing of Two Configurations

By considering the meson–meson and diquark–antidiquark configurations as well as their coupling, the authors studied the doubly heavy tetraquark states within the framework of the chiral quark model [123,179]. Within the meson–meson structure, a weakly bound DD^* molecular state has a binding energy of about 1.8 MeV relative to the DD^* threshold so that it is a good candidate for the state T_{cc}^{+} observed by the LHCb Collaboration. In addition, they also applied the diquark–antidiquark structure to research the state T_{cc}^{+}. They obtained a deeper bound state with a mass about 3700 MeV so that it should not be the candidate of the state T_{cc}^{+}. The conclusions are qualitatively consistent with those of other similar model studies on the state T_{cc}^{+} [140,154].

Ref. [123] pointed out that either structure is enough for the model calculation if all orbital excitation states are taken into account properly. It is clearly too difficult in the realistic calculations. An economic way is to combine different structures which are all kept in the ground state to perform the calculation. However, there is an overcomplete problem in the multiquark calculation of the structure mixing, which induces the singularity of the Hamiltonian matrix. To solve this problem, the eigenfunction method was employed. By mixing of the meson–meson structure and diquark–antidiquark structure, they found that the main component is the diquark–antidiquark structure. The energy of the system can be further decreased to about 3660 MeV [123].

In addition, a two-body Bethe–Salpeter equation was applied to study the internal competition between the meson–meson and diquark–antidiquark components in the wave functions of the state T_{cc}^{+} [181]. However, the results indicate that the state T_{cc}^{+} is dominated by an internal DD^* component, while its diquark–antidiquark component is negligible.

Each so-called structure was named according to the trial wave function, especially the color part, in the realistic model calculations. In fact, the color configurations of the two structures are equivalent if they are complete [28]. The difference between the two structures completely originates from their orbital excited models. Essentially, the mixing of two different structures just enlarges the model space, which results in the further decrease in the mass of the doubly heavy tetraquark states.

3.2. Other Doubly Heavy Tetraquark States

The state T_{cc}^{+} as a deuteron-like hadronic molecule evoked the possibility of other doubly heavy tetraquark states which are related to the state T_{cc}^{+} through various symmetries such as the heavy quark symmetry, SU(3) flavor symmetry, and so on. In this section, we

mainly review the partners of the state T_{cc}^{+} predicted by various theoretical frameworks after the discovery of the state T_{cc}^{+}.

3.2.1. T_{bbs}^{-}

The corresponding SU(2) groups of the isospin, V-spin, and U-spin are three subgroups of the flavor SU(3) group. Therefore, the states T_{bbs}^{-} and T_{bb}^{-} with the same spin-parity should share analogous behaviors when their V-spin and iso-spin have the same symmetry.

In the quark model [154], the V-spin antisymmetric state T_{bbs}^{-} with $I(J^P) = \frac{1}{2}(1^+)$ is a shallow bound state with a binding energy of about 10 MeV relative to the threshold $\bar{B}\bar{B}_s^*$, where the attraction mainly comes from the σ-meson exchange interaction. The result agrees with that of Ref. [151] but is less than the latest lattice QCD result of about 80 MeV in Ref. [182]. Similar to the state T_{bb}^{-} with $0(1^+)$, the state T_{bbs}^{-} with $\frac{1}{2}(1^+)$ can also form a compact state in the case of the meson exchange interaction, which should therefore be a compound of color singlet and other hidden color components. The lattice result indicated that the meson–meson percentage is about 84%, while the hidden color percentage is about 16% in Ref. [182]. Turning off the meson exchange interaction, the state T_{bbs}^{-} can also establish a hydrogen-like bound state and a deuteron-like state [154]. In the potential chiral-diquark model and chromomagnetic interaction model [153,164,165], the state T_{bbs}^{-} can also form a compact stable bound state.

The interactions of the doubly bottom systems $\bar{B}\bar{B}_s^*$, $\bar{B}^*\bar{B}_s$, and $\bar{B}^*\bar{B}_s^*$ were studied by means of vector meson exchange with Lagrangians from an extension of the local hidden gauge approach [183]. The binding energy of the states $\bar{B}\bar{B}_s^*$-$\bar{B}^*\bar{B}_s$ and $\bar{B}^*\bar{B}_s^*$ with $I(J^P) = \frac{1}{2}(1^+)$ below their threshold around 10∼20 MeV and the decay widths vary from one system to the other in the order of 10∼100 MeV for the state $\bar{B}\bar{B}_s^*$-$\bar{B}^*\bar{B}_s$ and about 0.5 MeV for the state $\bar{B}_s^*\bar{B}^*$ with $\frac{1}{2}(1^+)$. Recently, the lattice QCD study on the doubly heavy tetraquark states indicated that the state T_{bbs}^{-} with $\frac{1}{2}(1^+)$ can form a stable state and has a binding energy of about 80 MeV below the threshold $\bar{B}\bar{B}_s^*$ [182]. In the heavy quark limit [149], the state T_{bbs}^{-} are bound into compact states by their color-Coulomb potential in the diquark–antidiquark configuration.

3.2.2. T_{bc}^{0} and T_{bcs}^{0}

The state T_{bc}^{0} locates between the states T_{cc}^{+} and T_{bb}^{-} so that their behaviors are to some extent similar. In addition, the behaviors of the states T_{bc}^{0} and T_{bcs}^{0} are also analogous because V-spin and U-spin are similar. The state T_{bc}^{0} with $I(J^P) = 0(1^+)$ has a binding energy of several MeVs and its dominant component is the $\bar{B}^*D$ channel in Ref. [154]. The intuitive physical pictures, compact state, hydrogen-like state, or deuteron-like state, in the state T_{bb}^{-} with $0(1^+)$ reappear in the state T_{bc}^{0} with $0(1^+)$. The bound states T_{bc}^{0} with $0(0^+)$ and $0(2^+)$ can appear because there is no symmetry between c-quark and b-quark. They can form bound states with a binding energy of several MeVs because of the σ-meson exchange interaction [154]. Similar quark model studies on the state T_{bc}^{0} also indicated that the states T_{bc}^{0} with $0(0^+)$ and $0(1^+)$ can establish bound states [141,184]. The hydrogen-like state disappears in the states with $0(0^+)$ and $\frac{1}{2}(0^+)$, while it reappears in the states with $0(2^+)$ and $\frac{1}{2}(2^+)$. The state T_{bc}^{0} with $0(2^+)$ should not be stable because it can decay into D-wave $\bar{B}D$ through the strong interaction. The state should have a narrow width if it really exists as the model predicts [154]. The V-spin antisymmetrical states T_{bcs}^{0} with $\frac{1}{2}(0^+)$ and $\frac{1}{2}(2^+)$ can also establish a shallow bound state [154]. However, the hydrogen-like state cannot occur in the V-spin antisymmetrical states T_{bcs}^{0} with $\frac{1}{2}(1^+)$. Similar to the state T_{bc}^{0} with $0(2^+)$, the state T_{bcs}^{0} with $\frac{1}{2}(2^+)$ is not stable and can decay into $\bar{B}_sD$, $\bar{B}_sD\pi$, $\bar{B}_sD^*\gamma$, $\bar{B}_s^*D\gamma$, $\bar{B}_sD\gamma\gamma$ [154].

Lattice QCD investigated the states T_{bc}^{0} and T_{bcs}^{0} [182,185,186]. In Ref. [185], the state T_{bc}^{0} with $I(J^P) = 0(1^+)$ is a stable state against the strong interactions and its binding energy is in the range of 20∼40 MeV below the threshold $\bar{B}^*D$. However, the states T_{bc}^{0} with $0(0^+)$ and $0(1^+)$ are slightly above the corresponding thresholds in Ref. [182]. An

$n_f = 2 + 1$ lattice study of a number of channels indicated that the states T^0_{bcs} with 0^+ and 1^+ lie below their corresponding lowest thresholds $D\bar{B}_s$ and $D\bar{B}^*_s$ [186], respectively.

The QCD sum rule approach is also used to study the states T^0_{bc} and T^0_{bcs} [138,187]. Ref. [138] researched the state T^0_{bc} by constructing the corresponding diquark–antidiquark currents with $J^P = 0^+$ and 1^+. The results indicated that the masses of both the scalar and axial vector tetraquark states are about 7.1∼7.2 GeV for the state T^0_{bc}, which lies below the threshold of $D^{(*)}\bar{B}^*$. Ref. [187] studied the masses of the state T^0_{bcs} with 0^+ and 1^+ by constructing all diquark–antidiquark interpolating currents and calculated the two-point correlation functions and spectral densities. The masses are below the thresholds of $\bar{B}_s D$ and $\bar{B}^*_s D$ for the scalar and axial-vector channels, respectively.

3.2.3. T^+_{ccs}

Prior to the discovery of the state T^+_{cc} with $I(J^P) = 0(1^+)$ reported by the LHCb Collaboration, the lattice calculation of the state T^+_{ccs} ($cc\bar{u}\bar{s}$) with $\frac{1}{2}(1^+)$ indicated that it lies below its threshold by about 10 MeV [176]. After the discovery of T^+_{cc}, Ref. [188] took advantage of the experimental information on the binding of the state T^+_{cc} to fix the cutoff regulator of the loops in the Bethe–Salpeter equation. The state $D^*_s D^*$ with $J^P = 1^+$ can form a bound state. Using input needed to describe the T^+_{cc} state, the $D^*_s D^*$ system develops a strong cusp around the threshold with a width of the order of 70∼100 keV. In the color-magnetic model [189], both the states T^+_{cc} and T^+_{ccs} can establish stable states against the strong interactions. However, the state is not stable in the quark model with various dynamical effects [154], which may be changed if the mixing of the *S*-*D* wave by noncentral forces is taken into account.

3.2.4. Isospin, V-Spin, and U-Spin Symmetrical States

Inspired by the discovery of T^+_{cc}, naturally one would ask whether the stable state T^{++}_{ccss} can exist or not. Recently, Belle Collaboration searched for the tetraquark state X_{ccss} in $D_s D_s$ ($D^*_s D^*_s$) final states, but no significant signals were observed [190]. In the quark models [154,191], T^{++}_{ccss}, T^+_{bcss}, and T^0_{bbss} cannot form stable states because all interactions in the states cannot provide enough attraction because the ground state antidiquark $\bar{s}\bar{s}$ cannot form a good antidiquark [28]. The lattice QCD investigations on the states T^{++}_{ccss}, T^0_{bbss}, and T^+_{bcss} indicated that no clear indication of any level below their respective threshold can be found [176]. Ref. [192] employed heavy meson chiral perturbation theory and one-boson exchange approximation to calculate the interaction kernels in the Bethe–Salpeter equations. The state $B^*_s B^*_s$ perhaps forms a molecular state with $J^P = 0^+$.

The lattice QCD investigations on the isospin symmetric states indicated that no clear signal of any level below their respective thresholds can be found [176]. All of the isospin symmetrical states T^+_{cc}, T^-_{bb}, and T^0_{bc} and the V-spin symmetrical states T^+_{ccs}, T^-_{bbs}, and T^0_{bcs} cannot form stable states because all interactions in the states cannot provide enough attraction in the models [140,154,191]. The optimal spin-isospin-color-orbital combination of a good heavy diquark QQ and a good light antidiquark $\bar{q}\bar{q}$ is a necessary condition to produce a stable double heavy tetraquark state from the perspective of diquarks [28]. Therefore, one can understand the reason that there do not exist stable doubly heavy tetraquark states which contain the isospin, *U*-spin or *V*-spin symmetric light antidiquarks in various theoretical frameworks.

3.3. Nucleon-η_c Bound State

In 1990, Brodsky et al. showed that the QCD van der Waals interaction due to multiple-gluon exchange provides a new kind of attractive nuclear force capable of binding heavy quarkonia to nuclei [193]. They used a nonrelativistic Yukawa-type attractive potential $V_{(Q\bar{Q})A} = -\alpha e^{-\mu r}/r$ to characterize the QCD van der Waals interaction. They determined the constants α and μ using the phenomenological model of high-energy Pomeron interactions developed by Donnachie and Landshoff [194]. Using a variational wave function $\Psi(r) = (\gamma^3/\pi)^{1/2} e^{-\gamma r}$, they predicted bound states of η_c with ^3He and heavier nuclei.

Their prediction was confirmed by Wasson [195] using a more realistic $V_{(Q\bar{Q})A}$ potential taking into account the nucleon distribution inside the nucleus.

The work of QDCSM also supported the existence of the nucleon-η_c bound state [78]. In Ref. [78], the interaction between the nucleon and η_c was observed, and a weak attraction was obtained. Although the attraction is not strong enough to form a bound state directly, the coupling with other channels (NJ/ψ, $\Lambda_c\bar{D}$, $\Lambda_c\bar{D}^*$, $\Sigma_c\bar{D}$, $\Sigma_c\bar{D}^*$ and $\Sigma_c^*\bar{D}^*$) leads to a bound state $N\eta_c$ with $J^P = \frac{1}{2}^-$. Similarly, the $N\eta_b$ with $J^P = \frac{1}{2}^-$ is also a bound state with the help of channel coupling.

3.4. Short Summary

In this section, the doubly heavy tetraquark states with the molecular and diquark–antidiquark configurations and their correlation and mixing are reviewed. The dominant component of the T_{cc}^+ state by the LHCb Collaboration is the DD^* molecular component. The T_{cc}^+ state is a loosely bound deuteron-like state with a binding energy of 0.34 MeV and a huge size around 4.32 fm in the model description. The coupled channel effect between the DD^* and D^*D^* channels plays a critical role in the formation of the T_{cc}^+. In addition, the long-range π and intermediate-range σ exchange interactions also play a pivotal role. Within the meson–meson configuration, the state T_{bb}^- with $I(J^P) = 0(1^+)$ can establish a bound state and its binding energy is less than 50 MeV. The state is sensitive to different dynamical effects and can present three different physical pictures: the compact state, deuteron-like state, and hydrogen molecule-like state. In addition, other doubly heavy tetraquark states are reviewed from the heavy quark symmetry, SU(3) flavor symmetry, and so on.

A good diquark $[QQ]_{\bar{\mathbf{3}}_c}$ and a good antidiquark $[\bar{q}\bar{q}]_{\mathbf{3}_c}$ are an optimal combination to produce a deep compact bound state with $I(J^P) = 0(1^+)$, in which the Coulomb interaction in the diquark $[QQ]_{\bar{\mathbf{3}}_c}$ and the color-magnetic interaction in the antiquark $[\bar{q}\bar{q}]_{\mathbf{3}_c}$ play an important role. The two binding mechanisms are independent and do not occur in the threshold of two $Q\bar{q}$ mesons, which is beneficial to produce the compact tetraquark states with $0(1^+)$. In the realistic calculations, the two configurations have the orbitally excited modes so that the models' space of their ground states are different, which may result in the two different physical pictures in the doubly heavy tetraquark states.

The hidden color component is an inevitable degree of freedom in the multiquark states, the energy of which is in general higher than that of the colorless states. However, the doubly heavy tetraquark states just happen to be an exception. The existence of the deuteron-like T_{cc}^+ state implies the advent of other compact double heavy tetraquark states from the perspective of quark models. The doubly charmed baryon Ξ_{cc}^{++} indicates the possible existence of the similar doubly charmed multiquark states with the light quark replaced by a strongly correlated light anti-diquark.

4. Molecular Resonances

Among the exotic states, the hadronic molecules, which are mainly composed of two color-singlet hadrons, have received extensive attention. Hadronic molecules are analogs of light nuclei, most notably the deuteron. They can be treated to a good approximation as composite systems made of two or more hadrons which are bound together via strong interactions.

The $\Lambda(1405)$ resonance is possibly a meson–baryon molecule composed of one kaon and one nucleon, which was predicted by Dalitz and Tuan in 1959 [196] and observed in the hydrogen bubble chamber at Berkeley in 1961 [197] several years before the quark model was proposed. In the meson sector, the $a_0(980)$ and $f_0(980)$ were proposed to be the $K\bar{K}$ molecular states by Weinstein and Isgur [83,84,198]. However, their partner states σ and κ within the nonet cannot be explained within this molecular scheme. In 1976, the interaction of a pair of charmed mesons and possible molecular states were investigated by Voloshin and Okun [199]. Later, the work of Ref. [200] studied the possibility of the $\psi(4040)$ as a $D^*\bar{D}^*$ molecular charmonium. Furthermore, the possible $D\bar{D}^*$ and $D^*\bar{D}^*$ molecular states

were also investigated within the the quark–pion interaction model [201,202]. However, the early theoretical efforts on molecular states were not supported by experimental progress until 2003. Since 2003, more and more new light hadrons and charmonium-like states have been reported experimentally. Some of them are considered as good candidates of the molecular states because they lie close to the threshold of two mesons.

In 2003, the $X(1835)$ was reported by the BESII Collaboration in the radiative decay $J/\psi \to p\bar{p}$ [203], with mass $M = 1859^{+3+5}_{-10-25}$ MeV and width $\Gamma < 30$ MeV. Since the mass of this structure is close to the $p\bar{p}$ threshold, the $X(1835)$ was suggested to be a baryonium state in Refs. [204–206]. The charmonium-like state $X(3872)$ announced by the Belle Collaboration [2], which sits on the $D\bar{D}^*$ threshold, inspired the $D\bar{D}^*$ molecular explanation [207]. Particular interest has been paid to the positive-parity charm-strange mesons $D^*_{s0}(2317)$ and $D_{s1}(2460)$ observed by BaBar [1] and CLEO [208] Collaborations in 2003. The masses of $D^*_{s0}(2317)$ and $D_{s1}(2460)$ are below the DK and D^*K thresholds, respectively, which makes them natural candidates for hadronic molecules [209–222]. However, the interpretation of the structure of these states is still controversial. The unquenched picture has been proposed by some theoretical work. We will give more discussion in Section 6. Since 2015, the LHCb's new report of the hidden-charm pentaquarks [9,10] triggered many theoretical investigations again. Since the $P_c(4312)$, $P_c(4440)$, and $P_c(4457)$ are located only tens of MeV below the threshold of $\Sigma_c^{(*)}\bar{D}^{(*)}$ states, the molecular scheme is a more natural interpretation for these states. In this section, we will take the pentaquark states as an example to discuss the theoretical study of molecular resonances in detail.

4.1. Hidden-Charm Pentaquarks

The most noteworthy states in recent years are the hidden-charm pentaquarks. In 2015, the LHCb Collaboration observed two hidden-charm pentaquark states in the $J/\psi p$ invariant mass spectrum of $\Lambda_b^0 \to J/\psi K^- p$ [9]. The mass and the width of $P_c(4380)$ and $P_c(4450)$ are

$$\begin{aligned} P_c(4380): M &= 4380 \pm 8 \pm 29 \text{ MeV}, \quad \Gamma = 205 \pm 18 \pm 86 \text{ MeV}; \\ P_c(4450): M &= 4449.8 \pm 1.7 \pm 2.5 \text{ MeV}, \quad \Gamma = 39 \pm 5 \pm 19 \text{ MeV}. \end{aligned}$$

Four years later, the LHCb Collaboration reported the observation of three new pentaquarks, named $P_c(4312)$, $P_c(4440)$, and $P_c(4457)$ [10]. Their widths are $\Gamma = 9.8 \pm 2.7^{+3.7}_{-4.5}$ MeV, $\Gamma = 20.6 \pm 4.9^{+8.7}_{-10.1}$ MeV, and $\Gamma = 6.4 \pm 2.0^{+5.7}_{-1.9}$ MeV, respectively. The $P_c(4312)$ was discovered with 7.3σ significance by analyzing the $J/\psi p$ invariant mass spectrum. The previously reported $P_c(4450)$ structure was resolved at 5.4σ significance into two narrow states: the $P_c(4440)$ and $P_c(4457)$. As mentioned in Ref. [10], since all three states are narrow and below the $\Sigma_c^+\bar{D}^0$ and $\Sigma_c^+\bar{D}^{*0}$ thresholds within plausible hadron–hadron binding energies, they provide the strongest experimental evidence to date for the existence of molecular states composed of a charmed baryon and an anti-charmed meson.

Recently, the LHCb Collaboration reported a new structure with a relatively low statistical significance of 3.1∼3.7 σ in the $J/\psi p$ and $J/\psi\bar{p}$ systems in $B_s^0 \to J/\psi p\bar{p}$ decay, while no evidence was found for the $P_c(4312)$ discovered earlier in $\Lambda_b^0 \to J/\psi K^- p$. The mass of this structure is $4337^{+7}_{-4}{}^{+2}_{-2}$ MeV and the width is $29^{+26}_{-12}{}^{+14}_{-14}$ MeV [223].

Before the LHCb observation of the P_c states, many studies had been performed on the existence of possible hidden-charm pentaquarks [224–231]. For example, in 2010, Wu et al. predicted the hidden-charm N^* and Λ^* resonances above 4 GeV in the molecule picture by using the coupled-channel unitary approach [224]; the possible hidden-charm molecular states composed of an S-wave anti-charmed meson and an S-wave charmed baryon were studied extensively in the framework of the OBE model in 2011 [227]. The observations of the hidden-charm pentaquarks bring great interest in theoretical investigations. Most theoretical works before 2019 were devoted to the interpretation of the nature of the $P_c(4380)$ and $P_c(4450)$. The explanations include baryon–meson molecules [78,232–241], the diquark–triquark states [242,243], the diquark–diquark–antiquark states [244–247], the

genuine multiquark states [248], the topological soliton [249], the kinematical threshold effects in the triangle singularity mechanism [250–252], etc. The lattice QCD simulation of NJ/ψ and $N\eta_c$ scattering was also performed to find these P_c states [253].

The LHCb's new report of the hidden-charm pentaquarks $P_c(4312)$, $P_c(4440)$, and $P_c(4457)$ triggered many theoretical investigations again. Since the $P_c(4312)$, $P_c(4440)$, and $P_c(4457)$ locate only tens of MeV below the threshold of $\Sigma_c^{(*)}\bar{D}^{(*)}$ states, the molecular scheme is a more natural interpretation for these states. The main interpretations with $\Sigma_c^{(*)}\bar{D}^{(*)}$ molecular configurations are provided by QCD sum rule [254], constituent quark models [48], potential models [255–260], effective field theory [261,262], heavy hadron chiral perturbation theory [263], and heavy quark spin multiplet structures [264,265]. During these theoretical works, the $P_c(4312)$ is widely accepted as an S-wave $\Sigma_c\bar{D}$ molecule state with $J^P = \frac{1}{2}^-$. Although the $P_c(4440)$ and $P_c(4457)$ are generally treated as the S-wave $\Sigma_c\bar{D}^*$ molecule states, the spin of these two states is controversial. One point of view is that the spin-parity of $P_c(4440)$ and $P_c(4457)$ is $\frac{1}{2}^-$ and $\frac{3}{2}^-$, respectively [262,266–269]. Another point of view is that their spin-parity is $\frac{3}{2}^-$ and $\frac{1}{2}^-$, respectively [270–274]. Moreover, the decay properties [269,275–283] and production [280,284–293] of these pentaquarks were also investigated extensively. More details about the hidden-charm pentaquarks can be found in the review articles [15,294]. Here we concentrate on recent developments within the molecular scheme.

4.1.1. Hidden-Charm Pentaquark Resonances in Quark Models

In QDCSM, possible hidden-charm molecular pentaquarks with $Y = 1$, $I = \frac{1}{2}$, $J^P = \frac{1}{2}^\pm$, $\frac{3}{2}^\pm$, and $\frac{5}{2}^\pm$ have been investigated by using the RGM [48,78]. Seven baryon–meson channels, $N\eta_c$, NJ/ψ, $\Lambda_c\bar{D}$, $\Lambda_c\bar{D}^*$, $\Sigma_c\bar{D}$, $\Sigma_c\bar{D}^*$, and $\Sigma_c^*\bar{D}^*$ with $\frac{1}{2}^\pm$, five baryon–meson channels, NJ/ψ, $\Lambda_c\bar{D}^*$, $\Sigma_c\bar{D}^*$, $\Sigma_c^*\bar{D}$, and $\Sigma_c^*\bar{D}^*$ with $\frac{3}{2}^\pm$, and one baryon–meson channel $\Sigma_c^*\bar{D}^*$ with $\frac{5}{2}^\pm$ are studied. The energies of the positive parity states are higher than the experimental data, so the authors mainly present the results of the negative parity states. The single channel calculation showed that the interaction between Σ_c/Σ_c^* and $\bar{D}/\bar{D}^*$ is strong enough to form bound states. The energy of each bound state is shown below.

$J^P = \frac{1}{2}^-$: $\Sigma_c\bar{D}$: 4300∼4306 MeV, $\Sigma_c\bar{D}^*$: 4441∼4444 MeV, $\Sigma_c^*\bar{D}^*$: 4503∼4506 MeV;
$J^P = \frac{3}{2}^-$: $\Sigma_c^*\bar{D}$: 4367∼4372 MeV, $\Sigma_c\bar{D}^*$: 4445∼4450 MeV, $\Sigma_c^*\bar{D}^*$: 4510∼4514 MeV;
$J^P = \frac{5}{2}^-$: $\Sigma_c^*\bar{D}^*$: 4512 ∼ 4517 MeV.

However, these bound states can couple to the corresponding open channels and become resonance states or scattering states. Furthermore, the coupling between the bound states and the decay channels can shift the energy of the resonance and give the width to the resonance states. So in Ref. [48], the channel-coupling calculation of the bound-state channels and the open channels was carried out and the corresponding baryon–meson scattering process was also investigated. Figures 7 and 8 show the phase shifts of the scattering channels. Table 3 shows the resonance mass and decay width of resonance states.

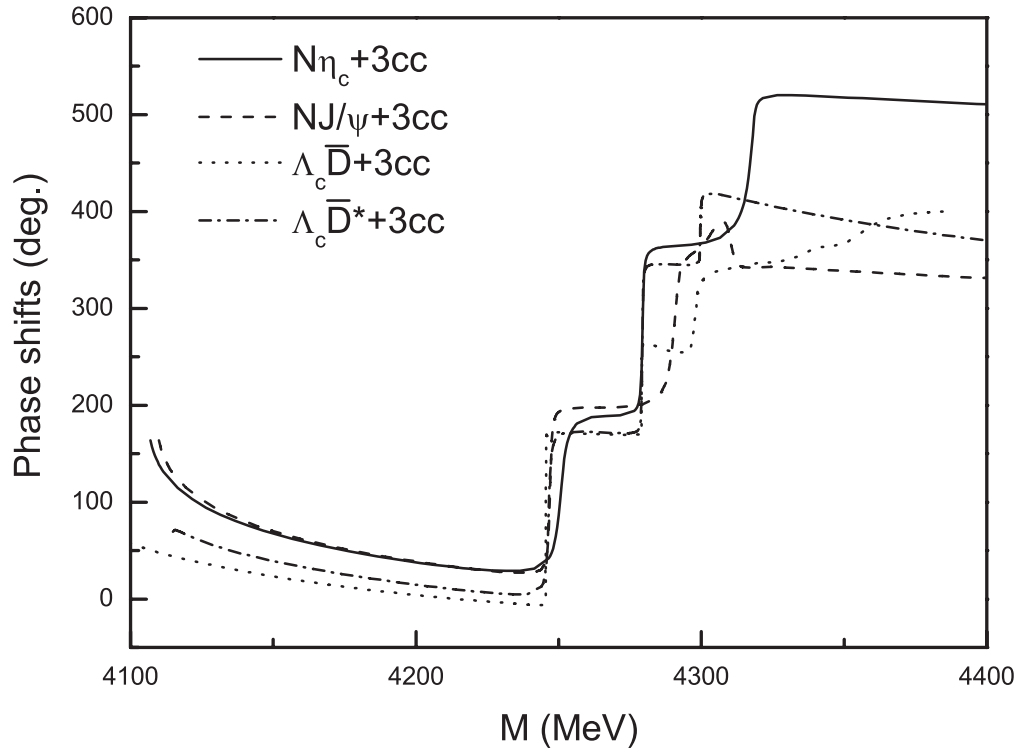

Figure 7. The $N\eta_c$, NJ/ψ, $\Lambda_c\bar{D}$, and $\Lambda_c\bar{D}^*$ S-wave phase shifts with four-channel coupling for the $I(J^P) = \frac{1}{2}(\frac{1}{2}^-)$ system. Taken from Ref. [48].

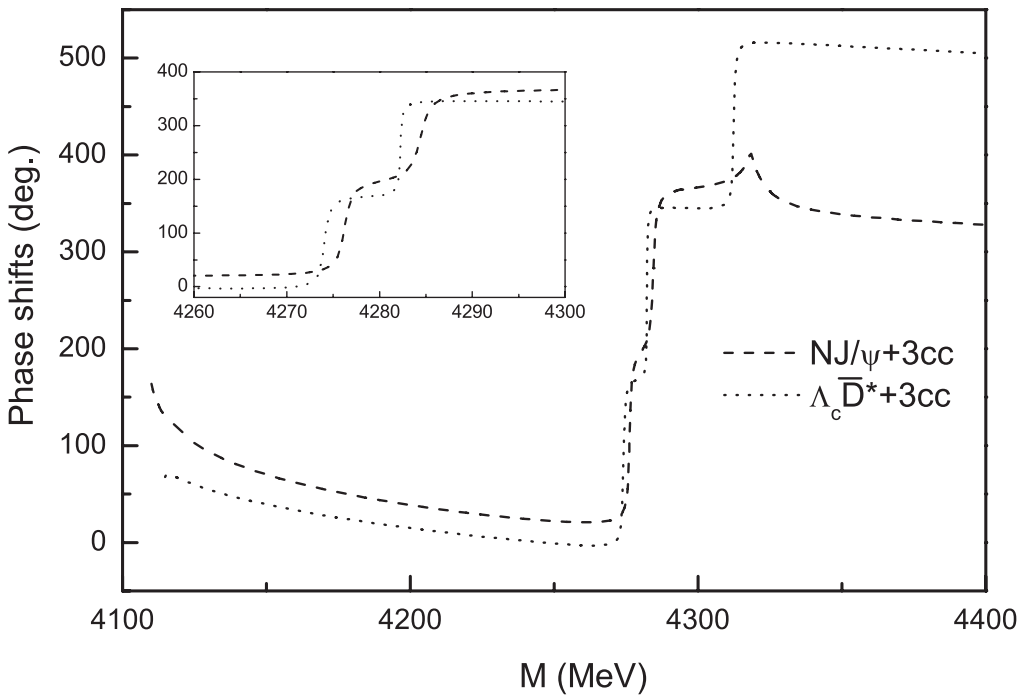

Figure 8. The NJ/ψ and $\Lambda_c\bar{D}^*$ S-wave phase shifts with four-channel coupling for the $I(J^P) = \frac{1}{2}(\frac{3}{2}^-)$ system. Taken from Ref. [48].

Table 3. The mass and decay width (in MeV) of the resonance states in the S-wave scattering channels.

$IJ^P = \frac{1}{2}\frac{1}{2}^-$						
	$\Sigma_c\bar{D}$		$\Sigma_c\bar{D}^*$		$\Sigma_c^*\bar{D}^*$	
	M'	Γ_i	M'	Γ_i	M'	Γ_i
$N\eta_c$	4311.3	4.5	4448.8	1.0	4525.8	4.0
NJ/ψ	4307.9	1.2	4459.7	3.9	nr	–
$\Lambda_c\bar{D}$	4306.7	0.02	4461.6	1.0	nr	–
$\Lambda_c\bar{D}^*$	4307.7	1.4	4449.0	0.3	nr	–
Γ_{total}		7.12		6.20		4.00
$IJ^P = \frac{1}{2}\frac{3}{2}^-$						
	$\Sigma_c^*\bar{D}$		$\Sigma_c\bar{D}^*$		$\Sigma_c^*\bar{D}^*$	
	M'	Γ_i	M'	Γ_i	M'	Γ_i
NJ/ψ	4376.4	1.5	4445.7	1.5	nr	–
$\Lambda_c\bar{D}^*$	4374.4	0.9	4444.0	0.3	4523.0	1.0
Γ_{total}		2.4		1.8		1.0

One can see that for the $J^P = \frac{1}{2}^-$ system, three molecular resonance states are obtained. The $\Sigma_c\bar{D}$ appears as a resonance state in the open channels $N\eta_c$, NJ/ψ, $\Lambda_c\bar{D}$, and $\Lambda_c\bar{D}^*$, with the resonance mass of 4307∼4311 MeV and decay width of 7 MeV (the first rising of each line in Figure 7). Both the mass and decay width are close to the subsequent experimental results of the $P_c(4312)$ state. The $\Sigma_c\bar{D}^*$ also behaves as a resonance state in the above four open channels with the resonance mass of 4449∼4462 MeV and decay width of 6.2 MeV (the second rising of each line in Figure 7). Both the mass and decay width are close to the reported $P_c(4457)$. Furthermore, there is also a resonance $\Sigma_c^*\bar{D}^*$ appearing in the $N\eta_c$ scattering phase shifts, with the resonance mass and decay width of 4526 MeV and 4 MeV, respectively. However, there is only a cusp around the threshold of $\Sigma_c^*\bar{D}^*$ in the NJ/ψ phase shifts. This is possible because the channel coupling may push the higher state above the threshold. Similar results were obtained for the $J^P = \frac{3}{2}^-$ system, where $\Sigma_c\bar{D}^*$ appears as a resonance state in NJ/ψ and $\Lambda_c\bar{D}^*$ scattering process (the first rising of each line in Figure 8), with the resonance mass of 4444.0∼4445.7 MeV and decay width of 1.8 MeV, which are close to the reported $P_c(4440)$. $\Sigma_c^*\bar{D}$ is also a resonance state in the NJ/ψ and $\Lambda_c\bar{D}^*$ phase shifts (the second rising of each line in Figure 8). Although the resonance mass 4374.4∼4376.4 MeV is close to the $P_c(4380)$, the decay width is only 2.4 MeV, much smaller than the experimental data. Furthermore, in the $\Lambda_c\bar{D}^*$ scattering process, the $\Sigma_c^*\bar{D}^*$ also behaves as a resonance state with the resonance mass and decay width of 4523.0 MeV and 1.0 MeV, respectively.

In short, the work of Refs. [48,78] indicates that the $P_c(4312)$ can be assigned as molecular resonance state $\Sigma_c\bar{D}$ with $J^P = \frac{1}{2}^-$; $P_c(4440)$ can be explained as $\Sigma_c\bar{D}^*$ with $J^P = \frac{3}{2}^-$; and $P_c(4457)$ is more likely to be $\Sigma_c\bar{D}^*$ with $\frac{1}{2}^-$. The theoretical study also shows that the $\Sigma_c^*\bar{D}$ with $\frac{3}{2}^-$ and $\Sigma_c^*\bar{D}^*$ with $\frac{1}{2}^-$, $\frac{3}{2}^-$, $\frac{5}{2}^-$ are all resonance states, but none of them have been verified by experiments. Besides the open channel NJ/ψ, other channels, such as $N\eta_c$, NJ/ψ, $\Lambda_c\bar{D}$, and $\Lambda_c\bar{D}^*$ with $\frac{1}{2}^-$, and $\Lambda_c\bar{D}^*$ with $\frac{3}{2}^-$, are possible decay channels for these resonances mentioned above. So the authors suggest the experiment to search for more heavy pentaquarks in more decay channels.

In ChQM, the hidden-charm pentaquark states were systematically investigated by the Gaussian expansion method (GEM) [236]. The structure of the states is not presupposed in this work, and it can be obtained by calculating the distance between any two quarks. The mass spectrum calculation in ChQM showed that $P_c(4380)$ can be identified as the $\Sigma_c^*\bar{D}$ with $J^P = \frac{1}{2}^-$; $P_c(4312)$, $P_c(4440)$, and $P_c(4457)$ can be explained as the states of $\frac{1}{2}^-$ $\Sigma_c\bar{D}$, $\frac{1}{2}^-$ $\Sigma_c\bar{D}^*$, and $\frac{3}{2}^-$ $\Sigma_c\bar{D}^*$, respectively. The distances between any two quarks are shown in Table 4. r_{qq}, r_{qQ}, $r_{q\bar{Q}}$, and $r_{Q\bar{Q}}$ represent the distance between $q-q$, $q-Q$, $q-\bar{Q}$, and $Q-\bar{Q}$, respectively. From Table 4, one can see that the distances are about 0.8∼0.9 fm between light quarks (u/d) and 0.7∼0.8 fm between the light quark and charm quark, whereas the distances between the quark (light or charm) and antiquark are much larger, that is, 2.0∼2.6 fm. This indicates the molecular nature of these pentaquark states. For the multiquark system, without assuming the structure of the system in advance, the GEM can be used to consider the relative motion between any two quarks, and the Gaussian wave function is used to expand the relative wave function so that the structure of the multiquark system can be obtained. This is the advantage of the GEM to study the structure of the multiquark states.

Table 4. Distances between any two quarks (unit: fm). $q = u/d$, $Q = c$.

J^P	Channel	r_{qq}	r_{qQ}	$r_{q\bar{Q}}$	$r_{Q\bar{Q}}$
$\frac{1}{2}^-$	$\Sigma_c\bar{D}$	0.8	0.7	2.1	2.1
	$\Sigma_c\bar{D}^*$	0.8	0.7	2.2	2.1
	$\Sigma_c^*\bar{D}^*$	0.9	0.8	2.1	2.0
$\frac{3}{2}^-$	$\Sigma_c\bar{D}^*$	0.8	0.7	2.4	2.3
	$\Sigma_c^*\bar{D}$	0.9	0.8	2.2	2.2
	$\Sigma_c^*\bar{D}^*$	0.9	0.8	2.6	2.4
$\frac{5}{2}^-$	$\Sigma_c^*\bar{D}^*$	0.9	0.8	2.4	2.3

4.1.2. Molecular Structure in Other Approaches

QCD sum rule techniques have proven to be a powerful and successful non-perturbative method over the past few decades. Various aspects of this formalism have been reviewed in Ref. [15]. It can also be applied in the framework of heavy quark effective theory to study heavy mesons and heavy baryons. In QCD sum rule, the authors of Ref. [240] systematically constructed all the possible local hidden-charm pentaquark currents with spins $J = \frac{1}{2}, \frac{3}{2}, \frac{5}{2}$ and quark contents $uudc\bar{c}$, through which they found that the internal structure of hidden-charm pentaquark states was quite complicated. They also obtained many mass predictions, some of which are consistent with the masses of the observed $P_c(4312)$, $P_c(4440)$, and $P_c(4457)$. Inspired by this coincidence, the authors gave the "molecular" picture explanation to these hidden-charm pentaquarks in Ref. [295]. They pointed out that a "molecular" current could be written as a combination of many diquark–diquark–antiquark currents by using the Fierz transformation, and showed that the molecular current was much more natural and simple. By extracting some useful information from the molecular currents being used, they suggested that the $P_c(4312)$ could be effectively explained as the $\Sigma_c^{++}\bar{D}^-$ bound state with $J^P = \frac{1}{2}^-$, while the $P_c(4440)$ and $P_c(4457)$ could be interpreted as the $\Sigma_c^+\bar{D}^0$ bound state with $\frac{1}{2}^-$, the $\Sigma_c^{*++}\bar{D}^-$ and $\Sigma_c^+\bar{D}^{*0}$ bound states with $\frac{3}{2}^-$, or the $\Sigma_c^{*+}\bar{D}^{*0}$ bound state with $\frac{5}{2}^-$. For this work, one may expect that the authors use the diquark–diquark–antiquark currents to perform the specific calculation, so as to obtain a corresponding molecular state, such as the $\Sigma_c^{++}\bar{D}^-$ bound state, which is also obtained by the molecular current. Nevertheless, it may be rather complicated work.

In the limit of infinitely heavy quarks, the spin of heavy quarks decouples from the system and is conserved individually. As a result, the total angular momentum of the light degrees of freedom becomes a good quantum number as well. This gives rise to the

so-called HQSS [296]. In the real world, quarks are not infinitely heavy; however, heavy quark effective field theory allows one to systematically include corrections that emerge from finite quark masses in a systematic expansion in Λ_{QCD}/M_Q, where M_Q denotes the heavy quark mass. One can refer to Ref. [297] for an extensive review. HQSS is the origin for the near degeneracy of D^* and D as well as B^* and B. Similarly, it also straightforwardly predicted multiplets of hadronic molecules made of a heavy hadron or heavy quarkonium and light hadrons [298,299].

The work of Ref. [261] showed that the three observed P_c states can be naturally accommodated in a contact-range effective field theory description that incorporates HQSS. This description leads to the prediction of seven possible S-wave heavy antimeson–baryon molecules, providing the first example of an HQSS molecular multiplet that is complete. In their work, the spectroscopic predictions of the contact-range effective field theory indicated a preference for identifying the $P_c(4440)$ and $P_c(4457)$ as the $J^P = \frac{1}{2}^-$ and $\frac{3}{2}^-$ molecules, respectively. Ref. [264] also studied the molecular picture $\Sigma_c^{(*)}\bar{D}^{(*)}$ in the coupled channels to $J/\psi p$ by using the constraints of HQSS and dynamics from the extension of the local hidden gauge approach. The $P_c(4312)$, $P_c(4440)$, and $P_c(4457)$ were replicated based on their mass and width and explained as the molecular structure $\Sigma_c\bar{D}$ with $\frac{1}{2}^-$, $\Sigma_c\bar{D}^*$ with $\frac{1}{2}^-$, and $\Sigma_c\bar{D}^*$ with $\frac{3}{2}^-$, respectively. Besides the three observed P_c states, another four states were also obtained in Ref. [264], which were the $\frac{3}{2}^-$ $\Sigma_c^*\bar{D}$ state around 4374 MeV, $\frac{1}{2}^-$, $\frac{3}{2}^-$, $\frac{5}{2}^-$ $\Sigma_c^*\bar{D}^*$ states around 4520 MeV.

In Ref. [267], the authors carried out a phenomenological study to decode the inner structure of three observed P_c states based on the OBE model by considering the channel-coupling effect and S-D wave mixing. They first assume that the structure of P_c states is the molecular one, and then verify this assumption by calculating the RMS radius. The masses of $P_c(4312)$ and $P_c(4440)$ were reproduced in the $J^P = \frac{1}{2}^-$ system with a reasonable cutoff value $\Lambda = 1.04$ GeV, and binding energies of -8.00 MeV and -19.27 MeV, respectively. Their corresponding RMS radii are 1.22 fm and 0.88 fm, respectively. The dominant channel of $P_c(4312)$ is the $\Sigma_c\bar{D}$ with the components around 84%, while the $P_c(4440)$ is mainly composed of $\Sigma_c\bar{D}^*$ with the probability over 94%. The mass of $P_c(4457)$ is also reproduced in the $J^P = \frac{3}{2}^-$ system with $\Lambda = 1.32$ GeV. Its binding energy and RMS radius are -4.38 MeV and 1.61 fm, respectively. The channel-coupling effect play an important role since the probabilities of the $\Sigma_c\bar{D}^*$ and $\Sigma_c^*\bar{D}^*$ components are around 75% and 25%, respectively. So the consistency of the LHCb observed hidden-charm pentaquarks with the baryon–meson configuration was demonstrated in the OBE model [267]. However, one should note that, to produce the experimental data well, different values of the cutoff parameter Λ are used for the different states.

In Ref. [278], the authors proposed that the structure of the $P_c(4457)$ can be diagnosed by using isospin-breaking decays. If $P_c(4457)^+$ is an S-wave $\Sigma_c\bar{D}^*$ hadronic molecule with $I = \frac{1}{2}$, it couples most strongly to the $\Sigma_c\bar{D}^*$ channels. Since its mass is closer to the $\Sigma_c^+\bar{D}^{*0}$ threshold than to the $\Sigma_c^{++}D^{*-}$ one, one expects large isospin-breaking effects in its decays. They gave a quantitative estimate of the ratio $B_r(P_c(4457) \to J/\psi\Delta^+)/B_r(P_c(4457) \to J/\psi p)$ at the level ranging from a few percent to about 30%. Such a large isospin-breaking decay ratio is two to three orders of magnitude larger than that for normal hadron resonances. It is a unique feature of the $\Sigma_c\bar{D}^*$ molecular model, and can be checked by LHCb.

Furthermore, after the release of measurements of $B_s^0 \to J/\psi p\bar{p}$, there have been numerous theoretical works discussing the nature of $P_c(4337)$ [300–305]. In Ref. [300], three possible theoretical explanations of $P_c(4337)$ were proposed: a bound state $\chi_{c0}(1P)p$, the $\bar{D}^*\Lambda_c$ and $\bar{D}\Sigma_c$ states close to threshold, and $\bar{D}^*\Lambda_c - \bar{D}\Sigma_c$ and $\bar{D}^*\Lambda_c - \bar{D}\Sigma_c^*$ coupled channel dynamics. Although the mass of $P_c(4337)$ might be explained in these configurations, it is still not clear why this structure is not observed in decay process $\Lambda_b^0 \to J/\psi K^- p$, even with a large number of reconstructed events. Ref. [305] performed a combined analysis for the three invariant mass spectra of $B_s^0 \to J/\psi p\bar{p}$ and found that the $J/\psi p$ structure near 4.34 GeV can correspond to the contributions from the $P_c(4380)$ state with the assumption

$J^P = \frac{3}{2}^-$. So this work provided possible evidence to support the existence of the pentaquark $P_c(4380)$ from the recent measurements of $B_s^0 \to J/\psi p\bar{p}$. The authors of Ref. [303] suggested that the $P_c(4312)$ and $P_c(4337)$ can be created by different interference patterns between the $\Sigma_c\bar{D}$ and $\Lambda_c\bar{D}^*$ threshold cusps, which can give a reasonable interpretation to the phenomenon that the $P_c(4312)$ and $P_c(4337)$ peaks appear in $\Lambda_b^0 \to J/\psi K^- p$ and $B_s^0 \to J/\psi p\bar{p}$, respectively.

4.2. Hidden-Charm Pentaquarks with Strangeness

The existence of the hidden-charm pentaquark states with strangeness was predicted in Refs. [224,306–309]. By using the OBE model, the author of Ref. [306] predicted the existence of several hidden-charm pentaquarks, including the $\Xi_c'\bar{D}^*$ with $I(J^P) = 0(\frac{1}{2}^-)$ and the $\Xi_c^*\bar{D}^*$ states with $0(\frac{1}{2}^-)$ and $0(\frac{3}{2}^-)$. Based on the results of the Ref. [224], the decay behavior of $\Lambda_{c\bar{c}}$ as an S-wave hadronic molecule state was investigated within the effective Lagrangian framework [307], which can provide guidance for searching for hidden charm pentaquark with strangeness. Furthermore, the author of Ref. [308] predicted several molecular states of the hidden-charm pentaquark with strangeness by studying the channel-coupling interaction. The spectrum of the strange hidden-charm molecular pentaquarks in chiral effective field theory was also calculated, and three new hadronic molecules were obtained in the isoscalar $[\Xi_c\bar{D}^*]_J$ systems ($J = \frac{1}{2}, \frac{3}{2}$) [309].

4.2.1. Experimental Progress

Experimentally, the P_{cs} state was reported by the LHCb Collaboration in 2020 in the $J/\psi\Lambda K^-$ decays [310]. The measured mass and width are

$$P_{cs}(4459) : M = 4458.8 \pm 2.9^{+4.7}_{-1.1}\ \text{MeV}, \quad \Gamma = 17.3 \pm 6.5^{+8.0}_{-5.7}\ \text{MeV}.$$

From the $J/\psi\Lambda$ decay mode, the new structure $P_{cs}(4459)$ contains at least five valence quarks. Furthermore, its spin-parity is not confirmed since the statistics are not large enough.

4.2.2. Molecular Explanation in ChQM

The discovery of the first strange hidden-charm pentaquark immediately instigated active discussions on its structure and nature. Since the mass of $P_{cs}(4459)$ is only 19 MeV below the threshold of $\Xi_c\bar{D}^*$, most works favored the $P_{cs}(4459)$ as the $\Xi_c\bar{D}^*$ molecular state [311–319]. Besides the molecular explanation, some works interpreted it as the compact pentaquark states [318,320–323]. The production, decays, and other properties were also observed [318,324–334]. Here, we mainly discuss the recent explanation of the molecular structure.

In ChQM, the strange hidden-charm pentaquark systems with $I(J^P) = 0(\frac{1}{2}^-)$, $0(\frac{3}{2}^-)$, $0(\frac{5}{2}^-)$, $1(\frac{1}{2}^-)$, $1(\frac{3}{2}^-)$ and $1(\frac{5}{2}^-)$ were investigated by using the GEM [319]. The single-channel calculation showed that the interaction between $\Xi_c/\Xi_c'/\Xi_c^*$ and $\bar{D}/\bar{D}^*$ is strong enough to form bound states. There exist weakly bound states $\Xi_c\bar{D}$, $\Xi_c\bar{D}^*$ and $\Xi_c'\bar{D}$ with $0(\frac{1}{2}^-)$, $\Xi_c\bar{D}^*$, $\Xi_c'\bar{D}^*$, and $\Xi_c^*\bar{D}$ with $0(\frac{3}{2}^-)$, and $\Xi_c^*\bar{D}^*$ with $IJ^P = 0(\frac{5}{2}^-)$. However, these bound states can decay to the corresponding open channels and become resonance states or scattering states. So the channel-coupling calculation between these bound states and open channels is necessary. The real-scaling method was used to find the genuine resonance states in Ref. [319]. In this method, the scaling factor α is used to adjust the Gaussian size parameter r_n of the basis functions between baryon and meson with $r_n \to \alpha r_n$. As a result, a genuine resonance will behave as avoid-crossing structures (see Figure 4) with the increase in α, while other continuum states will fall off towards its threshold. If the avoid-crossing structure is repeated periodically as α increases, then the avoid-crossing structure is a genuine resonance.

The results of Ref. [319] are shown in Figures 9–11. In these figures, the thresholds of all physical channels appear as horizontal lines and are marked with lines (red lines), tagged with their contents. As for genuine resonances, which appear as avoid-crossing structure, they are marked with blue lines. The continuum states fall off towards their respective threshold states (red horizontal lines). For $I(J^P) = 0(\frac{1}{2}^-)$ system, a resonance with the main component $\Xi_c\bar{D}^*$ is obtained, the mass of which is 4461 MeV, very close to $P_{cs}(4459)$, so it is a good candidate for the reported $P_{cs}(4459)$. Furthermore, another resonance with the main component $\Xi_c\bar{D}$ is obtained around the mass of 4301 MeV. For $0(\frac{3}{2}^-)$ system, three resonances were obtained, the masses of which are 4443 MeV, 4500 MeV, and 4601 Mev, and the main component is $\Xi_c\bar{D}^*$, $\Xi_c^*\bar{D}$, and $\Xi_c'\bar{D}^*$, respectively. For $0(\frac{5}{2}^-)$ system, there is only one bound state around 4671 MeV, marked horizontally under the threshold of $\Xi_c^*\bar{D}^*$, and it will turn to a narrow resonance state after coupling to $\Xi_c\bar{D}$ via tensor interaction. Furthermore, to explore the structure of the hidden-charm pentaquarks with strangeness, the distance between any two quarks was also calculated in Ref. [319]. The results show that the distances are about 0.6∼0.9 fm between two quarks which are in the same cluster, while the distances between two quarks that are in different clusters are much larger, reaching 1.7∼2.9 fm. This indicates that these P_{cs} states tend to be in the molecular structure.

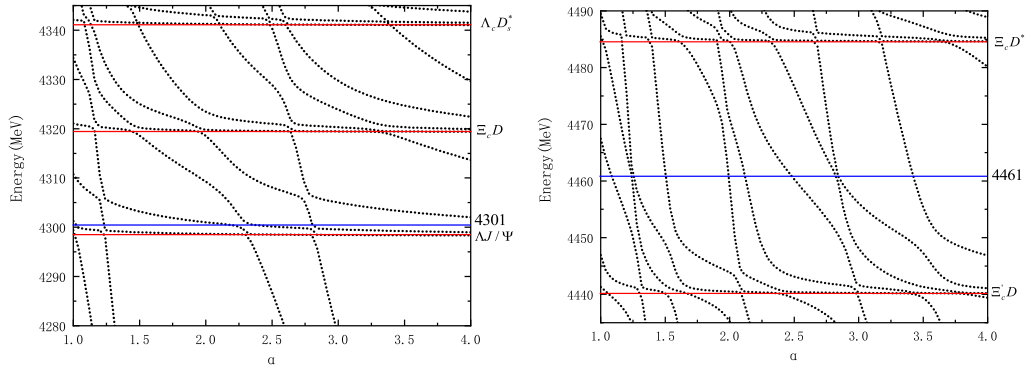

Figure 9. Energy spectrum of the $I(J^P) = 0(\frac{1}{2}^-)$ system. Taken from Ref. [319].

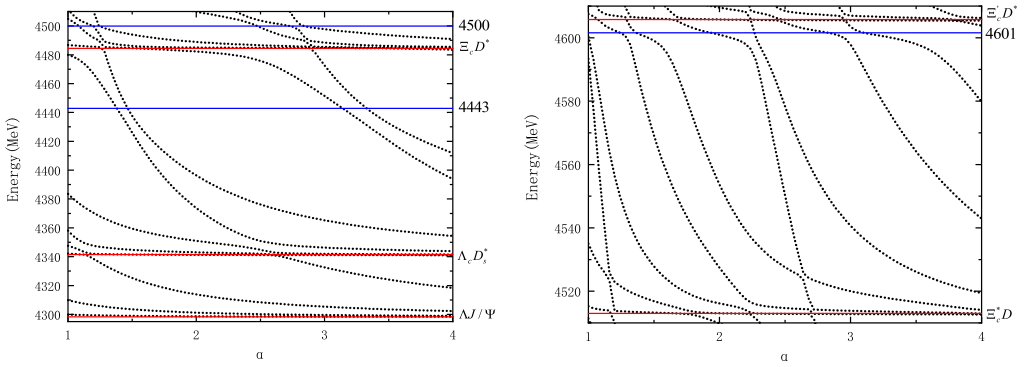

Figure 10. Energy spectrum of the $I(J^P) = 0(\frac{3}{2}^-)$ system. Taken from Ref. [319].

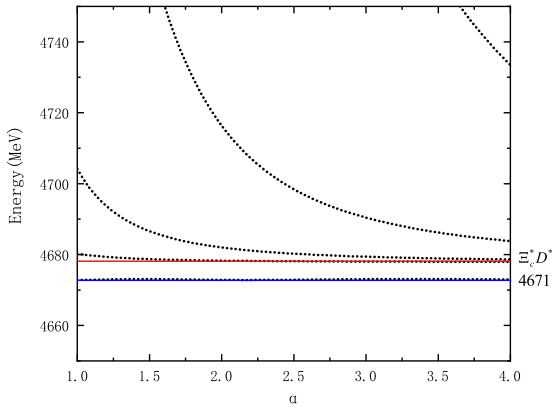

Figure 11. Energy spectrum of the $I(J^P) = 0(\frac{5}{2}^-)$ system. Taken from Ref. [319].

From the results of Ref. [319], one can see that the behaviors of P_{cs} systems are similar to that of P_c systems. It is worth noting that there are two resonances around 4443 and 4461 MeV in Ref. [319], which can form a two-peak structure composed of $\Xi_c\bar{D}^*$ with $J^P = \frac{3}{2}^-$ and $\frac{1}{2}^-$, respectively, similar to the two-peak structure of $P_c(4440)$ and $P_c(4457)$. The $\frac{1}{2}^-$ $\Xi_c\bar{D}$ molecular state around 4301 MeV is similar to the $P_c(4312)$. The $\frac{3}{2}^-$ $\Xi_c^*\bar{D}$ molecular state around 4500 MeV may correspond to the $\frac{3}{2}^-$ $\Sigma_c^*\bar{D}$ molecular state $P_c(4380)$. For the $\Xi_c^*\bar{D}^*$ state, although the $\frac{1}{2}^-$ and $\frac{3}{2}^-$ states are unbound in Ref. [319], the $\frac{5}{2}^-$ molecular state around 4671 MeV is obtained, corresponding to the $\frac{5}{2}^-$ $\Sigma_c^*\bar{D}^*$ molecular state. Furthermore, they also obtained a $\frac{3}{2}^-$ $\Xi_c^{'}\bar{D}^*$ molecular state with the mass of 4601 MeV. It is expected that all these possible resonances proposed above can be searched in future experiments.

4.2.3. Molecular Structure in Other Approaches

Ref. [311] studied the $P_{cs}(4459)$ by using the method of QCD sum rules. Since $P_{cs}(4459)$ is about 19 MeV below the $\Xi_c\bar{D}^*$ threshold, the authors investigated $\Xi_c\bar{D}^*$ molecular states with $J^P = \frac{1}{2}^-$ and $\frac{3}{2}^-$, and at the same time they also studied the $\Xi_c\bar{D}$ molecular state of $\frac{1}{2}^-$. They used the $\bar{c}$, c, s, u, and d quarks to construct the interpolating currents with molecular structure, and obtained masses of $\Xi_c\bar{D}^*$ molecular states, obtaining $4.46^{+0.16}_{-0.14}$ GeV for $\frac{1}{2}^-$ and $4.47^{+0.19}_{-0.15}$ GeV for $\frac{3}{2}^-$. These two values are both consistent with the experimental mass of the $P_{cs}(4459)$, supporting its interpretation as the $\Xi_c\bar{D}^*$ molecular state of either $\frac{1}{2}^-$ or $\frac{3}{2}^-$. Moreover, they also obtained the mass of the $\frac{1}{2}^-$ $\Xi_c\bar{D}$ molecular state, which is $4.29^{+0.13}_{-0.12}$ GeV.

Particularly, within the hadronic molecular picture, the three P_c and P_{cs} states observed by LHCb experiments were well-understood as a whole in Ref. [311]. Possible production mechanisms of the P_{cs}^0 and P_c^+ states in Ξ_b^-/Λ_b^0 decays are shown in Figure 12. The transition of $\Xi_b^- \to J/\psi K^-\Lambda$ is dominated by the Cabibbo-favored weak decay of $b \to c + \bar{c}s$ via the vector and axial $(V - A)$ current, which leads to an intuitive expectation that the sd pair in Ξ_b^- may exist as a spectator so that their total spin $S = 0$ is conserved. As a result, if this sd pair is combined with the c quark to form a charmed baryon, it will favor the baryon Ξ_c instead of the $\Xi_c^{'}$ and Ξ_c^* (the spin of sd pair in these two baryons is 1). Accordingly, the $P_{cs}(4459)$ is more likely to be $\Xi_c\bar{D}^*$ molecular state rather than $\Xi_c^{'}\bar{D}^*$ or $\Xi_c^*\bar{D}^*$ molecular states. From Figure 12b,c, the transition of $\Lambda_b^0 \to J/\psi K^- p$ can be similarly analyzed, which may favor the Λ_c instead of the Σ_c and Σ_c^*. However, the Λ_c is probably not bounded with $\bar{D}^{(*)0}$ due to the lack of π exchange. Nevertheless, the data sample for the $\Lambda_b^0 \to J/\psi K^- p$ decays is 680k, significantly larger than that for the $\Xi_b^- \to J/\psi K^-\Lambda$ decays, which is only 4k. So it is possible that the $P_c(4312)$, $P_c(4440)$, and $P_c(4457)$ are the $\Sigma_c\bar{D}$ and $\Sigma_c^*\bar{D}$ molecular states.

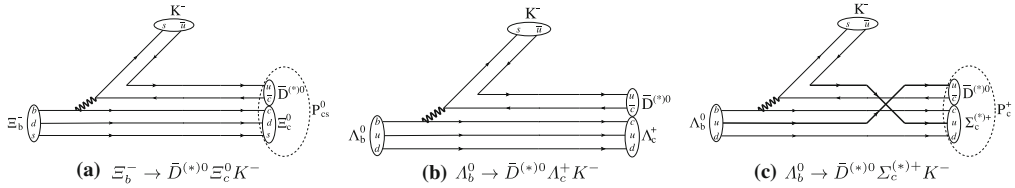

Figure 12. Possible production mechanisms of the P^0_{cs} and P^+_c states in Ξ_b^-/Λ_b^0 decays. Taken from Ref. [311].

The reported $P_{cs}(4459)$ was also deeply studied within the OBE model [316,318]. Ref. [316] performed a single $\Xi_c\bar{D}^*$ channel and a coupled channel ($\Xi_c\bar{D}^*/\Xi_c^*\bar{D}/\Xi_c^{'}\bar{D}^*/\Xi_c^*\bar{D}^*$) analysis by using the OBE model. In the single channel calculation, the mass of $P_{cs}(4459)$ with the experimental uncertainties can be effectively reproduced with the cutoff $3.6 < \Lambda < 5.25$ GeV, which is far away from the typical value 1.00 GeV in a loosely bound hadronic molecular state. So they concluded that the $P_{cs}(4459)$ cannot be a pure $\Xi_c\bar{D}^*$ molecule in the OBE method. When taken into the effect of the channel-coupling, the bound state solutions can be obtained with a cutoff around 1.00 GeV, which indicates that the channel-coupling effect is helpful to produce the bound state. For the $I(J^P) = 0(\frac{1}{2}^-)$ system, the mass range is 4476.32∼4456.33 MeV with the cutoff range value from 1.17 GeV to 1.20 GeV, and the $\Xi_c^{'}\bar{D}^*$ channel has a dominant contribution. However, the RMS radius is 1.39∼0.45 fm, which indicates that the molecular state picture with the $0(\frac{1}{2}^-)$ assignment to $P_{cs}(4459)$ is not favored. For the $0(\frac{3}{2}^-)$ system, with the cutoff range value from 0.99 GeV to 1.05 GeV, the corresponding mass range is 4476.49∼4458.67 MeV, and the RMS radius is 2.18∼0.65 fm. Nevertheless, they concluded that this coupled state with $I(J^P) = 0(\frac{3}{2}^-)$ can be a possible strange hidden-charm molecular candidate of the $P_{cs}(4459)$ with the dominant channels $\Xi_c\bar{D}^*$ and $\Xi_c^*\bar{D}$. From the results of Ref. [316], the RMS radius is very sensitive to the the cutoff value. By using the typical value of the cutoff, although the mass of $P_{cs}(4459)$ state can be obtained, the range of RMS radius is too large to regard this coupled $\Xi_c\bar{D}^*/\Xi_c^*\bar{D}/\Xi_c^{'}\bar{D}^*/\Xi_c^*\bar{D}^*$ system as the molecular structure.

In addition, the authors also studied the two-body strong decay behaviors for the $P_{cs}(4459)$ state by using the obtained bound state wave functions of the coupled $\Xi_c\bar{D}^*/\Xi_c^*\bar{D}/\Xi_c^{'}\bar{D}^*/\Xi_c^*\bar{D}^*$ system with $I(J^P) = 0(\frac{3}{2}^-)$ [318]. They took the binding energy from -0.75 MeV to -30 MeV, and obtained the total two-body strong decay width from 10 to 25 MeV, which is consistent with the experiment data $\Gamma = 17.3 \pm 6.5^{+8.0}_{-5.7}$ MeV. Although this phenomenological study is still model-dependent, the strong decay information can be a crucial test of the hadronic molecular state assignment to the P_{cs} state.

The pentaquark states $P_c(4312)$, $P_c(4440)$, and $P_c(4457)$ could be nicely arranged into a multiplet of seven molecules of $\Sigma_c^{(*)}\bar{D}^{(*)}$ dictated by HQSS. However, the spins of $P_c(4440)$ and $P_c(4457)$ are not yet fully determined. The work of Ref. [314] employed a contact-range effective field theory approach satisfying HQSS and $SU(3)$-flavor symmetry to search for the existence of the hidden-charm strange molecules and study the possibility of whether their discovery could help determine the spins of $P_c(4440)$ and $P_c(4457)$. In terms of HQSS, the contact-range potential between $\bar{D}^{(*)}$ and $\Xi_c^{\prime *}$ can be denoted as $F_{\frac{1}{2}}$ and $F_{\frac{3}{2}}$ via the coupling of the light quark spins, i.e., $\frac{1}{2} \otimes 1 = \frac{1}{2} \otimes \frac{3}{2}$. Applying the same approach to $\bar{D}^{(*)}$ and Ξ_c, the corresponding potential can be represented by one low-energy constant $F^{\prime}_{\frac{1}{2}}$, which is from the light quark spin coupling, $\frac{1}{2} \otimes 0 = \frac{1}{2}$. Two hypotheses were considered in this work. Case I assumed that the couplings $F_{\frac{1}{2}}$ and $F^{\prime}_{\frac{1}{2}}$ are the same, then the molecules $\Xi_c\bar{D}^{(*)}$ exist only if the spins of $P_c(4440)$ and $P_c(4457)$ are $\frac{1}{2}$ and $\frac{3}{2}$, respectively, indicating that the discovery of these states can help one to determine their spins. Case II employed the hidden-gauge approach to infer the coupling of $F^{\prime}_{\frac{1}{2}}$ and found that $\Xi_c\bar{D}^{(*)}$ molecules

exist irrespective of the spins of $P_c(4440)$ and $P_c(4457)$, meaning that the discovery of these states offers little help in determining the spins.

4.3. Other Heavy Pentaquark States

The discovery of the P_c states and the evidence of the P_{cs} also inspired the investigation of some other heavy pentaquark states, such as the hidden-bottom pentaquarks, the pentaquarks composed of $qqqq\bar{Q}$, $qq\bar{q}QQ$, $q\bar{q}QQQ$, $QQQQ\bar{Q}$, and so on.

4.3.1. Hidden-Bottom Pentaquarks

Because of the heavy flavor symmetry, the extension of the study from the hidden-charm pentaquarks (P_c) to the hidden-bottom pentaquarks (P_b) is natural. In the hidden-bottom sector, the larger mass of the bottom quark will reduce the kinetic energy of the system, which makes them easier to form bound states than in the hidden-charm sector. Therefore, one may wonder whether the P_b states exist or not. The P_b states were extensively studied in plenty of theoretical models. The molecular structure of P_b states is flavored by the QDCSM [48,78], the ChQM [335], the OBE model [227], the OPE model [239], the QCD sum rules [233], the heavy hadron chiral effective field theory [268], the coupled channel unitary approach [336–338], etc.

Refs. [48,78] investigated the hidden-bottom pentaquark states in the framework of the QDCSM. Two bound states, $J^P = \frac{1}{2}^-$ $N\eta_b$ and $\frac{3}{2}^-$ NY, and several narrow resonance states, $\Sigma_b B$, $\Sigma_b B^*$, $\Sigma_b^* B^*$ with $\frac{1}{2}^-$, $\Sigma_b^* B$, $\Sigma_b B^*$, $\Sigma_b^* B^*$ with $I(J^P) = \frac{3}{2}^-$, and $\Sigma_b^* B^*$ with $\frac{5}{2}^-$, are obtained. The masses of these P_b states are above 11 GeV. In Ref. [227], the hidden-bottom molecular pentaquarks composed of a bottom meson and a bottom baryon were studied extensively in the OBE model. Several hidden-bottom molecular pentaquarks are predicted; these are are the $\Sigma_b B$ with $\frac{3}{2}(\frac{1}{2}^-)$ and $\Sigma_b^* B^*$ with $\frac{1}{2}(\frac{1}{2}^-)$, $\frac{1}{2}(\frac{3}{2}^-)$, $\frac{3}{2}(\frac{1}{2}^-)$, $\frac{3}{2}(\frac{3}{2}^-)$. However, by using the OPE model, Ref. [239] obtained another molecular state $\Sigma_b B^*$ with $\frac{1}{2}(\frac{3}{2}^-)$ or $\frac{3}{2}(\frac{1}{2}^-)$. In Ref. [233], two hidden-bottom pentaquarks were predicted using the method of QCD sum rules as partners of the $P_c(4380)$ and $P_c(4450)$. Their masses are extracted as $11.55^{+0.23}_{-0.14}$ MeV and $11.66^{+0.28}_{-0.27}$ MeV, and spin-parity $\frac{3}{2}^-$ and $\frac{5}{2}^+$, respectively. In Ref. [268], the authors studied the hidden-bottom $\Sigma_b^* B^*$ systems and predicted their mass spectra in the framework of heavy hadron chiral effective field theory. The masses of the hidden-bottom molecular are all above 11 GeV, which may be observed in the $\Upsilon(1S)N$ and $\Upsilon(2S)N$ final states. Furthermore, the coupled channel unitary approach with the local hidden gauge formalism was applied to study the hidden-bottom pentaquarks in Refs. [336–338]. In Ref. [336], the authors studied possible resonances in the heavy meson–heavy baryon coupled-channel interactions. The $\bar{D}\Lambda_c$-$\bar{D}\Sigma_c$ interactions, as well as the $\bar{B}\Lambda_b$-$\bar{B}\Sigma_b$ interactions, were investigated. The results show that there are more resonances observed for $\bar{B}\Lambda_b$-$\bar{B}\Sigma_b$ interactions and they are more tightly bound because the b-quark is heavier than the c-quark. In Ref. [337], two $N^*_{b\bar{b}}$ states were predicted to be dynamically generated from coupled pseudoscalar-baryon (PB) and vector-baryon (VB) channels. The mass and width of these states are $(M, \Gamma) = (11052, 1.38)$ MeV and $(M, \Gamma) = (11100, 1.33)$ MeV, respectively. In Ref. [338], seven new states of N^* with hidden beauty were obtained with a mass around 11 GeV.

4.3.2. $qqqq\bar{Q}$

For the $qqqq\bar{Q}$ pentaquark states, all of them are explicit exotic states. If such pentaquark states are observed, their exotic nature can be easily identified. Actually, the existence of the pentaquark state ($uudu\bar{c}$) has been studied in the Fermilab experiment [339,340], but no evidence was found. Later, the signal for the pentaquark state ($uudu\bar{c}$) was observed in the DIS experiment by H1 Collaboration [341] and a peak was observed at $3099 \pm 3 \pm 5$ MeV with a Gaussian width of 12 ± 3 MeV in the distribution of D^*p. However, this resonance was not confirmed by other experiments [342–346]. Recently, the LHCb Collaboration reported the observation of the $\Lambda_b^0 \to DpK^-$ channel [347], where the

invariant mass spectrum of Dp was measured. However, more detailed analyses are still needed to identify the structures existing in the Dp invariant mass spectrum. So, whether there exist $qqqq\bar{Q}$ pentaquark states is still an open question.

Inspired by the experimental progress, many theoretical works were devoted to studying the $qqqq\bar{Q}$ pentaquark states [26,348–354]. In Refs. [26,348], the authors suggested that the $qqqq\bar{Q}$ states are stable in the quark model. In addition, the possible bound states were also discussed by the one-pion exchange interaction [349], the modified color-magnetic interaction model [350], the constituent quark model [351], and the QCD sum rule [352]. Moreover, the weak decay properties for the $qqqq\bar{Q}$ pentaquark system were discussed in Ref. [353]. In Ref. [354], the authors discussed the production of the singly charmed pentaquark, and the results suggest several golden channels for searching the singly charmed pentaquark in future experiments.

4.3.3. $qq\bar{q}QQ$

Aroused by the observation of the states Ξ_{cc} and T_{cc}, the existence of the doubly heavy pentaquark states $qq\bar{q}QQ$ was proposed. Various theoretical methods have been applied in this field, including various quark models [257,355–362], the chiral effective theory [363–365], the QCD sum rule [366], and the Bethe–Salpeter equation [367,368].

In the framework of the OBE model, the authors of Ref. [355] explored the intermediate and short-range forces and studied various hadron–hadron bound state problems. They found some S-wave molecules, such as $\Lambda_c D$, $\Lambda_c \bar{B}$, $\Lambda_b D$, $\Lambda_b \bar{B}$, and so on. In Refs. [356,357], a series of doubly heavy molecules were also obtained by using the same model as that of Ref. [355]. In Ref. [358], the mass spectra of doubly heavy pentaquark states were studied in the color-magnetic model. The results suggest several possible narrow states. Furthermore, to search for stable pentaquark states, the authors of Ref. [359] analyzed the color-flavor-spin structure of the heavy quark pentaquark system with the same method as that of Ref. [358]. The authors noticed that the $I(J^P) = 0(\frac{1}{2}^-)$ $ud\bar{s}cc$ state is perhaps the most stable one. The work of Ref. [360] predicted a bound state $\Xi_{cc}^* \pi$ with $\frac{1}{2}(\frac{3}{2}^-)$ and several resonance states in the chiral quark model. Moreover, in Ref. [361], the authors considered the coupled system $\Lambda_c D^*$-$\Sigma_c^* D^*$ in the $\frac{1}{2}(\frac{3}{2}^-)$ channel. The results indicate that there exists a doubly charmed molecule $qq\bar{q}cc$ named $\Xi_{cc}(4380)$.

4.3.4. $q\bar{q}QQQ$

The triply charmed pentaquark $q\bar{q}QQQ$ states were studied in many theoretical works [369–375]. In Ref. [369], a flavor singlet bound state with $I(J^P) = \frac{1}{2}(\frac{3}{2}^-)$ with mass around 4.3 GeV was proposed. In the systematic study of triply charmed dynamically generated baryons in Ref. [370], the authors found a $\frac{1}{2}^-$ bound state around 4.4 GeV and a $\frac{3}{2}^-$ bound state around 4.5 GeV by coupling ccc-$\bar{q}q$ and ccq-$c\bar{q}$ channels. By using the QCD sum rule, the triply charmed molecular states $\Xi_{cc}(3621)D^0$ with $\frac{1}{2}^\pm$ and $\Xi_{cc}(3621)D^{*0}$ with $\frac{3}{2}^\pm$ were obtained in Ref. [371]. Such molecular interpretation was also considered in Ref. [372], and two possible molecular pentaquark states were predicted in the OBE model. According to the results in Ref. [372], the authors in Ref. [373] studied the interactions between a doubly charmed baryon $\Xi_{cc}(3621)$ and a charmed meson in a T doublet, where the T doublet includes $D_1(2420)$ and $D_2^*(2460)$, respectively. The results show that several triply charmed molecular pentaquarks exist. In Ref. [374], the authors discussed whether the compact $q\bar{q}QQQ$ pentaquark states were possible within the CMI method by assuming that the QQQ was a color-octet state, and the results indicate that the compact pentaquarks should not be stable against their rearrangement decays, and its nature as a molecule would be preferred over a compact pentaquark. Furthermore, the work of Ref. [375] found the existence of a hadronic molecule $\Xi_{bb}^* \bar{B}^*$ with quantum numbers $1(\frac{1}{2}^-)$ and $1(\frac{3}{2}^-)$ within the effective field theory framework.

4.3.5. $QQQQ\bar{Q}$

There is no experimental report on the fully heavy pentaquarks so far. However, the discoveries of fully heavy tetraquark states and P_c states make one speculate that the fully heavy pentaquark $QQQQ\bar{Q}$ states may also exist.

In Ref. [376], a systematic study on the mass spectra and decay properties of the S-wave fully heavy pentaquarks $QQQQ\bar{Q}$ has been performed in the CMI model. A good stable candidate was found, the $P_{c^2b^2\bar{b}}(17416, 0, 3/2^-)$. It lies below the allowable decay channel $\Omega^*_{ccb}\eta_b$ by only 4 MeV and thus can decay only through electromagnetic or weak interactions. Meanwhile, the authors also found that $P_{c^2b^2\bar{b}}(17477, 0, 5/2^-)$ state is a relatively stable pentaquark. Although it is lower than all possible S-wave strong decay channels, it can still decay into the D-wave $\Omega_{ccb}\eta_b$ and $\Omega_{cbb}B_c$ final states. The fully heavy pentaquarks were also investigated by the QCD sum rule. The work of Ref. [377] studied the fully heavy pentaquark states and obtained the mass $7.41^{+0.27}_{-0.31}$ GeV for $ccccc\bar{c}$ and $21.60^{+0.73}_{-0.22}$ GeV for $bbbbb\bar{b}$, respectively. The work of Ref. [378] investigated this system of the diquark–diquark–antiquark type with $J^P = \frac{1}{2}^-$ and obtained the mass 7.93 ± 0.15 GeV for $ccccc\bar{c}$ and 23.91 ± 0.15 GeV for $bbbbb\bar{b}$, respectively. In addition, the $ccccc\bar{c}$ and $bbbbb\bar{b}$ were systematically investigated within the ChQM and QDCSM [379]. Three possible bound states are obtained, the $ccccc\bar{c}$ state with $J^P = \frac{1}{2}^-$ and the $bbbbb\bar{b}$ states with $J^P = \frac{1}{2}^-$ and $\frac{3}{2}^-$. The masses of these states are 7891.9∼7892.7 MeV, 23,810.1∼23,813.8 MeV, and 23,748.2∼23,752.3 MeV, respectively. The results are consistent in both of the models, and the effect of the channel coupling is crucial for forming a bound state of the fully heavy pentaquark system.

The $X(6900)$ is found in the invariant mass spectrum of J/ψ pairs, where two pairs of $c\bar{c}$ are produced. To produce the lowest fully heavy pentaquark state $ccccc\bar{c}$, one needs to simultaneously produce at least four pairs of $c\bar{c}$, and this seems to be a difficult task in experiments. Nevertheless, all of the fully heavy pentaquark states are worth searching for in future experiments.

4.4. Fully Strange Baryon $\Omega(2012)$

The discovery of the $\Omega(2012)$ by the Belle Collaboration [380] prompted a fast and diverse reaction on the theoretical side, looking at it from the quark model perspective as the low-lying P-wave excited baryon, or as a molecular state. The discovery of Ω baryons dates back to 1964 and yet until today, it is the least observed in experiments worldwide. As we know, the ground Ω hyperon is a member of the baryon decuplet in the quark model, which was unambiguously discovered in both production and decay at BNL about a half-century ago [381]. Three resonances, $\Omega(2250)$, $\Omega(2380)$, and $\Omega(2470)$, are also listed in the Particle Data Group (PDG) [382] with three- or two-star ratings and their nature still uncertain. So in experiments, there is only a little information on excited Ω baryons. There is much related work on excited states in the literature, which can be seen in the recent review on the strange baryon spectrum in Ref. [383]. Related work on new hadronic states can be found in the recent review of Ref. [19]. In this section, we mainly review the experimental progress and theoretical explanation of the $\Omega(2012)$ state.

4.4.1. Status of $\Omega(2012)$

In 2018, the Belle Collaboration reported the observation of a new resonance, which was identified as an excited Ω^- baryon [380]. It was found in the $\Xi^0 K^-$ and $\Xi^- K^0_s$ invariant mass distributions in data taken at the $\Upsilon(1S)$, $\Upsilon(2S)$, and $\Upsilon(3S)$ resonance energies. The measured mass and width of this resonance are

$$\Omega(2012): M = 2012.4 \pm 0.7(stat) \pm 0.6(syst)\ \text{MeV}, \qquad \Gamma = 6.4^{+2.5}_{-2.0}(stat) \pm 1.6(syst)\ \text{MeV}.$$

This new resonance has a mass 340 MeV higher than the ground state, and thus helps fill the large gap in the Ω^- spectrum between the ground state and the already observed

excited states. However, there is no information about the structure of this excited hyperon in this experiment.

Actually, various theoretical approaches [384–387] have investigated the Ω excited states in the molecular picture before the Belle Collaboration's report. The authors of Refs. [384,385] investigated the Ω excited states by using the chiral unitary approach where the coupled channel interactions of the $\Xi^*\bar{K}$ and $\Omega\eta$ were taken into account. In Ref [387], a dynamically generated Ω state with $J^P = \frac{3}{2}^-$ was obtained with the mass around 1800 MeV, which is in agreement with the predictions of the five-quark model. In addition, the Ω excited states were also investigated in classical quark models [388–391].

After the report of the $\Omega(2012)$ by the Belle collaboration, there were many theoretical studies on its mass, width, quantum numbers, and decay modes [392–409], which can be roughly divided into two types, the excited baryon state and the molecular state. Since the mass of the $\Omega(2012)$ state lies quite close to the threshold of the $\bar{K}\Xi^*$ channel with a binding energy of 15 MeV, it is quite natural to interpret $\Omega(2012)$ as a hadronic molecule composed of $\bar{K}\Xi^*$. Indeed, the hadronic molecule nature of the $\Omega(2012)$ was investigated in Refs. [400–402,408], and these calculations predicted a large decay width for $\Omega(2012) \to \bar{K}\Xi^* \to \pi\bar{K}\Xi$.

However, the molecular picture was challenged by Belle's report in 2019, where the Belle Collaboration searched for the three-body decay of $\Omega(2012) \to K\Xi(1530) \to K\pi\Xi$ by using data samples of e^+e^- collisions collected at the $\Upsilon(1S)$, $\Upsilon(2S)$, and $\Upsilon(3S)$ resonances with the Belle detector [410]. The measured ratio of the three-body decay $\Omega(2012) \to \pi\bar{K}\Xi$ width to the one of the two-body decay $\Omega(2012) \to \bar{K}\Xi$ is less than 11.9% at the 90% confidence level. Since the $\pi\bar{K}\Xi$ channel is associated with $\bar{K}\Xi^*$, such a small fraction is not in favor of the $\bar{K}\Xi^*$ component. So, no significant $\Omega(2012)$ signals were found in the studied channels, which indicated that the result disfavored the molecular interpretation of $\Omega(2012)$.

Yet, the phase space for this decay is very small, and in Refs.[406,407] the molecular picture was shown to be consistent with the experiment data. Ref. [406] investigated the $\Omega(2012)$ from the molecular perspective by using the coupled channel interactions of the $\bar{K}\Xi^*$ and $\eta\Omega$ in S-wave and $\bar{K}\Xi$ in D-wave. The study of Ref. [406] contains the $\bar{K}\Xi^*$, $\eta\Omega$, and $\bar{K}\Xi$ states as coupled channels in a unitary approach. The transition potential between $\bar{K}\Xi^*$ and $\eta\Omega$ is taken from the chiral Lagrangians but the transition potentials from $\bar{K}\Xi^*$ and $\eta\Omega$ in S-wave and $\bar{K}\Xi$ in D-wave are taken as free parameters. All data including the above Belle experiment data on $\Gamma_{\Omega^*\to\pi\bar{K}\Xi}/\Gamma_{\Omega^*\to\bar{K}\Xi}$ are compatible with the molecular picture stemming from meson–baryon interaction of these channels. The authors of Ref. [406] also pointed out that the molecular structure of $\Omega(2012)$ is rather peculiar, in the sense that it corresponds to mostly a $\bar{K}\Xi^*$ bound state; however, it requires the interaction with the $\eta\Omega$ and $\bar{K}\Xi$ channels to bind, while neither of them would be bound by themselves.

Ref. [407] also revisited the $\Omega(2012)$ state from the molecular perspective in which this resonance appears to be dynamically generated from the coupled channel interactions of the $\bar{K}\Xi^*$ and $\eta\Omega$ in S-wave and $\bar{K}\Xi$ in D-wave. In this scenario, the $\Omega(2012)$ is interpreted as a $J^P = \frac{3}{2}^-$ molecule state. The authors studied the two- and three-body strong decays of $\Omega(2012)$ within the model parameters for the D-wave interaction, and the result showed that the experimental properties of the $\Omega(2012)$ can be easily accommodated. A more precise measurement, providing the $\Gamma_{\Omega^*\to\pi\bar{K}\Xi}/\Gamma_{\Omega^*\to\bar{K}\Xi}$ ratio, or finding a much more stringent upper bound than the present one, is expected to settle the issue of the possible molecular picture for the $\Omega(2012)$ state.

The calculation of nonleptonic weak decays of charmed baryons is a useful tool to study hadron resonances [411]. The double strange baryon $\Xi^*(1620)^0$ was first observed in its decay mode to $\pi^+\Xi^-$ via $\Xi_c^+ \to \pi^+\pi^+\Xi^-$ process by the Belle Collaboration [412]. Taking advantage of this idea, Ref. [403] studied the nonleptonic weak decays of $\Omega(2012)$ resonance in the $\Omega_c^0 \to \pi^+\bar{K}\Xi^*(\eta\Omega) \to \pi^+(\bar{K}\Xi)^-$ decays, showing that they provided a good filter for $I = 0$ and strangeness $S = -3$ resonances, which can be used to probe the nature of the Ω excited states. The authors found that the $\Omega_c^0 \to \pi^+(\bar{K}\pi\Xi)^-$ decay

was not well-suited to study the $\Omega(2012)$ because the dominant contribution is from the $\Omega_c^0 \to \pi^+(\bar{K}\Xi^*)^-$ decay at tree level, and this will not contribute to production of the $\Omega(2012)$. On the other hand, they predicted that the $\Omega(2012)$ would be visible in the $(\bar{K}\Xi)^-$ invariant mass spectrum of the $\Omega_c^0 \to \pi^+(\bar{K}\Xi)^-$ decay. It is obvious that observing the $\Omega(2012)$ in different production mechanisms can not only further confirm its existence but also yield important information that can increase the understanding of its internal structure.

In 2021, by using the entire data sample of 980 fb^{-1} integrated luminosity collected with the Belle detector, the Belle Collaboration searched for the $\Omega(2012)^-$ resonance in $\Omega_c^0 \to \pi^+\Omega(2012)^- \to \pi^+(\bar{K}\Xi)^-$ and $\Omega_c^0 \to \pi^+\Omega(2012)^- \to \pi^+K_S^0\Xi^-$. In $\Omega_c^0 \to \pi^+\Omega(2012)^- \to \pi^+K^-\Xi^0$, they found the evidence for the $\Omega(2012)^-$ in the $K^-\Xi^0$ invariant mass spectrum with a statistical significance of 4.0σ. In $\Omega_c^0 \to \pi^+\Omega(2012)^- \to \pi^+K_S^0\Xi^-$, a marginal $\Omega(2012)^-$ signal could be seen in the $K_S^0\Xi^-$ invariant mass spectrum with a statistical significance of 2.3σ [413].

In 2022, the Belle Collaboration discovered a new resonant three-body decay $\Omega(2012) \to \Xi(1530)^0K^- \to \Xi^-\pi^+K^-$ with a significance of 5.2σ by using the $\Upsilon(1S)$, $\Upsilon(2S)$, and $\Upsilon(3S)$ data [414]. The mass of the observed $\Omega(2012)^-$ is $(2012.5 \pm 0.7 \pm 0.5)$ MeV. The branching fraction ration $\mathcal{R}_{\Xi\bar{K}}^{\Xi(1530)\bar{K}}$ is $0.97 \pm 0.24 \pm 0.07$, consistent with the molecular interpretation for the $\Omega(2012)$ proposed in Refs. [400,401,405,408], which predicts similar branching fractions for $\Omega(2012)$ decays to $\Xi(1530)\bar{K}$ and $\Xi\bar{K}$.

After the new experiment, Ref. [415] investigated the interpretation of the $\Omega_c \to \pi^+\Omega(2012) \to \pi^+(\bar{K}\Xi)$ relative to $\Omega_c \to \pi^+\bar{K}\Xi$ from the $\Omega(2012)$ molecular perspective. The authors presented a mechanism for the production of $\Omega_c \to \pi^+\Omega(2012)$ through an external emission Cabibbo favored weak decay mode, where the $\Omega(2012)$ is dynamically generated from the interaction of $\bar{K}\Xi^*$ and $\eta\Omega$, with $\bar{K}\Xi$ as the main decay channel. The $\Omega(2012)$ can decay later to $\bar{K}\Xi$ in this picture, and the results are compatible with the Belle data [410]. Then, one can evaluate the decays $\Omega_c^0 \to \pi^+K^-\Xi^0$ and $\Omega_c^0 \to \pi^+\bar{K}\Xi^*$, $\pi^+\eta\Omega$ with couplings of $\bar{K}\Xi^*$ and $\eta\Omega$ to $K^-\Xi^0$. The authors found that within uncertainties all three channels account for about 12%∼20% of the total $\Omega_c^0 \to \pi^+K^-\Xi^0$ decay rate by using data from a recent Belle measurement [410]. The consistency of the molecular picture with all the data is established by showing that $\Omega_c \to \bar{K}^{*0}\Xi^0 \to \pi^+K^-\Xi^0$ and $\Omega_c \to \pi^+\Omega^* \to \pi^+K^-\Xi^0$ account for about 85% of the total $\Omega_c \to \pi^+K^-\Xi^0$. They also pointed out that the data from the Belle experiment in Ref. [413] has been very useful to establish a new test for the nature of the $\Omega(2012)$. Further measurements are expected to constrain the picture of the $\Omega(2012)$.

4.4.2. Molecular Picture Support from ChQM

The quark model study also supports the molecular picture for the $\Omega(2012)$ state. In Ref. [416], the $\Omega(2012)$ is investigated by means of the GEM and the real-scaling method in the framework of the chiral quark model. Although all low-lying states of $sss\bar{q}q$ ($q = u,\ d$) systems were considered, only the explanation of $\Omega(2012)$ is reviewed here. In that work, the single channel calculation of $\Xi^*\bar{K}$ with $I(J^P) = 0(\frac{3}{2}^-)$ is unbound. However, the bound state can be formed by the coupling of all color singlet–singlet channels, which include $\Xi\bar{K}^*$, $\Xi^*\bar{K}^*$, $\Omega\eta$, and $\Omega\omega$. The study of the component of this system shows that the main channel is still the $\Xi^*\bar{K}$, with a percentage of about 94%. Furthermore, after coupling the hidden-color channels, the binding energy increased by a few MeVs, and the corrected energy of the bound state was 2018 MeV, which is close to the mass of reported $\Omega(2012)$. This indicates that the $\Xi^*\bar{K}$ system with $I(J^P) = 0(\frac{3}{2}^-)$ is a good candidate for $\Omega(2012)$.

In order to explore the structure of $\Omega(2012)$, the work of Ref. [416] also calculated the RMS distances between any two quarks by using the GEM. From the distances, the size of Ξ^* is $0.7 \sim 0.8$ fm, the size of $\bar{K}$ is about 0.5 fm, and the distance between two clusters is about 2.3 fm. This feature obviously supports the molecular picture. Therefore, in the chiral quark model calculation, the reported $\Omega(2012)$ can be explained as a $I(J^P) = 0(\frac{3}{2}^-)$ molecular state with the main component of $\Xi^*\bar{K}$. The effect of the channel coupling cannot

be ignored for forming the bound state, although the percentages of other channels are not very large.

4.5. Short Summary

Note that all of the measurements of P_c and P_{cs} states have been made by LHCb. The only independent evidence for P_c states to date comes from the D0 Collaboration, which observes events consistent with the unresolved $P_c(4440) \to J/\psi p$ structure at 3.2σ [417]. The P_c search in the GlueX $\gamma p \to J/\psi p$ cross-section measurement ended up with a null result [289]. Much about the pentaquark states remains unknown. Higher statistics data and more theoretical works in the future might provide more information for the hidden-heavy flavor pentaquark states. The CLAS12 at Jefferson Lab (JLab) may be a possible place to observe the P_c states in J/ψ photoproduction [418,419]. Its spin and photocouplings may be measured with future data, too. Now, the search for the LHCb pentaquark in the photo-production process in Hall C at JLab has been approved [420,421]. In future, the P_c, P_{cs}, and P_b states can also be searched for by PANDA/FAIR [422], EIC, JPARC, etc.

The discovery of the $\Omega(2012)$ state offers a great opportunity to study the hadron spectrum and understand the strong interactions. The explanation of the structure of the $\Omega(2012)$ has always been controversial. Another possibility is that this state may be a mixture state of the three-quark system and the five-quark system. An unquenched quark model can be used to investigate this state, which deserves further study. Furthermore, it is clear that observing the $\Omega(2012)$ in different production mechanisms can not only further confirm its existence but also yield important information that can increase the understanding of its internal structure. From the experimental and theoretical research process of $\Omega(2012)$ state, theoretical research can provide effective information for experiments, and experimental research can also promote the development of theoretical research. The upcoming experimental facility at FAIR, PANDA-GSI is expected to be a dedicated study of hyperons at a low energy regime [423–428].

In order to delve deeper into the study of the multiquark states, we need to consider the influence of channel coupling. Coupling the closed channels to the open channels will shift the mass of the resonance and give the decay width to the resonance or destroy the resonance. The RGM, a well-established method for studying a bound-state problem or a scattering one, is used to calculate the hadron–hadron scattering phase shifts and cross-sections and investigate the resonance states. Furthermore, a stabilization method, for example, the real-scaling method, has been invented to pick up genuine resonance states from the states with discrete energies. These two approaches are widely employed to identify genuine resonances.

The structure is one of the important properties of exotic hadrons. The GEM can be used not only to calculate the mass spectrum, but also to study the structure of hadronic states. The distance between any two quarks obtained by GEM can be used to explore the structure of the multiquark.

5. Color Structure Resonances

In the long-distance region, the hadron–hadron interaction is dominated by the colorless configuration due to the color confinement, such as the deuteron, while the hidden color configurations can be ignored completely. In the intermediate- and short-distance region, especially in the range of confinement (around 1 fm), various hidden color configurations can occur because of the flux-tube fluctuations. The hidden color configurations may dominante the properties of the compact multiquark states because their number is larger than the color singlet configuration.

The multiquark states with hidden color configurations have compact spatial structures [25,31,47], in which the multibody confinement potential based on the color flux tubes plays an important role. As a collective degree of freedom, the color flux-tube binds all quarks together to establish compact multiquark states [88]. In general, the mass of the hidden color configurations is higher than that of colorless configuration in the mul-

tiquark states except for the doubly heavy tetraquark states [28,31,47]. The hidden color configurations cannot directly decay into several colored subclusters because of the color confinement. They must transform back into color singlets before decaying through the collapse and arrangement of the color flux tubes. Such a process is similar to compound nucleus formation and therefore should induce a resonance around the energies of these hidden color states in the hadron–hadron interactions. Those states were named as "color confined, multiquark resonance" [31] and they are different from all of the microscopic resonances discussed by S. Weinberg [429]. In this section, we will take several tetraquark states as an example to discuss the theoretical study of color structure resonances in detail.

5.1. Fully Charm Tetraquark States

In 2020, the LHCb Collaboration researched the invariant mass spectrum of J/ψ pairs using proton–proton collision data at center-of-mass energies of $\sqrt{s} = 7$, 8 and 13 TeV. The narrow structure, denoted as $X(6900)$, was assumed to be a resonance with the Breit–Wigner lineshape. The LHCb found a broad structure ranging from 6.2 GeV to 6.8 GeV and a narrow structure around 6.9 GeV. The central value of the broad structure ranging locates at around 6490 MeV [11]. The mass and width of the structure $X(6900)$ are

$$X(6900): M = 6905 \pm 11 \pm 7 \text{ MeV}, \ \Gamma = 80 \pm 19 \pm 33 \text{ MeV}$$

assuming no interference with the nonresonant single-parton scattering continuum [11]. The mass and width are changed to

$$X(6900): M = 6886 \pm 11 \pm 11 \text{ MeV}, \ \Gamma \quad = \quad 168 \pm 33 \pm 69 \text{ MeV}$$

when assuming the nonresonant single-parton scattering continuum interferes with the broad structure [11]. Besides the above two structures, there exists a hint of another structure around 7.2 GeV. LHCb also performed a fit with an additional Breit–Wigner function introduced to describe this structure. However, their properties and spin-parity quantum numbers are not completely clear so far.

In 2022, the CMS Collaboration reported three structures in the $J/\psi J/\psi$ mass spectrum produced by proton–proton collisions at $\sqrt{s} = 13$ TeV [12]. Two structures were observed with local significance well above 5 standard deviations at masses of $6927 \pm 9(\text{stat}) \pm 5(\text{syst})$ and $6552 \pm 10(\text{stat}) \pm 12(\text{syst})$ MeV. The first one is consistent with the LHCb observed $X(6900)$. Evidence for a third structure was found at a mass of $7287 \pm 19(\text{stat}) \pm 5(\text{syst})$ MeV with a local significance of 4.1 standard deviations. The states are the first to be made up of four heavy quarks of the same type. This is a very important step in the exploration of heavy hadrons, after the charmonium $c\bar{c}$ in 1974, the charmed hadrons $c\bar{q}$ and cqq in the following years, the bottomonium $b\bar{b}$ in 1977, and then the mesons and baryons carrying beauty, the $b\bar{c}$ in 1996 at Fermilab, and the double-charm baryons Ξ_{cc}^{++} in 2017 by the LHCb [430].

The states provided an extreme and yet theoretically fairly simple case to explore the strong interaction and to test various phenomenological methods that can be used to explain the nature of ordinary hadrons. The structures also revitalized the investigations of multiquark resonances made of heavy quarks and heavy antiquarks [430–439].

There is no threshold channel near the observed fully charm tetraquark $X(6900)$. This narrow structure around 6.9 GeV lies well above the thresholds of $\eta_c\eta_c$, $J/\psi J/\psi$, $\eta_c(2S)J/\psi$, and $\eta_c\psi(2S)$. At the same time, it is much lower than the thresholds of $\eta_c(2S)\eta_c(2S)$ and $\psi(2S)\psi(2S)$. The molecular states composed of a pair of the doubly charm baryon and anti-baryon lie above (or around) 7.2 GeV. Therefore, $X(6900)$ is unlikely to be the hadronic molecule, which is usually formed by light meson exchanges with small binding energies. The situation of the structure around 6.6 GeV is similar to $X(6900)$, while another structure around 7.2 GeV can possibly be explained as a molecular state, because the energy is near the thresholds of $\eta_c(2S)\eta_c(2S)$ and $\psi(2S)\psi(2S)$. In order to understand the structure and properties of the fully charm tetraquark states, diquark–antidiquark

configuration [24,81,432,434,440–454], threshold effect [436,455–461], color octet configuration [462,463], Higgs-like boson [464], and hybrid state [465] were proposed in various theoretical frameworks, in which the diquark–antidiquark configuration is the most popular one. In this subsection, we mainly concentrate on the work related to the diquark–antidiquark picture and the color octet configuration explanation. More investigations on the fully charm tetraquark states can be found in Ref. [17].

5.1.1. Diquark–Antidiquark Configuration

Since the interaction between two charmonia may not be strong enough to form a traditional molecular state due to the absence of meson exchange interactions, many theoretical studies on the fully charm tetraquark states adopted the compact diquark–antidiquark configuration.

At present, many quark models are devoted to researching the fully charm tetraquark states. In the framework of the ChQM and the QDCSM, the authors of Ref. [81] systematically investigated the fully charm tetraquark system $cc\bar{c}\bar{c}$. Two structures, meson–meson and diquark–antidiquark, are considered. The dynamic bound-state calculation shows that the energy of both configurations is above the corresponding theoretical threshold in both models. So no stable state under the threshold of $\eta_c\eta_c$ is obtained. However, it is possible to obtain resonance states, because the colorful subclusters diquark and antidiquark cannot fall apart directly due to the color confinement. To check the possibility, an adiabatic calculation of the effective potentials for the $cc\bar{c}\bar{c}$ system with diquark–antidiquark structure was performed, the results of which are shown in Figure 13. In both models, the minimum of the potential of each channel appears at the separation of 0.3∼0.5 fm, which indicates that the two subclusters $[cc]$ and $[\bar{c}\bar{c}]$ are not willing to huddle together or fall apart. Furthermore, the energy of each channel is higher than the corresponding threshold. So each state with diquark–antidiquark structure is possibly a resonance state. Moreover, the minimum of the potential appears at the separation of 0.3∼0.5 fm indicating that these two subclusters are close to each other. Therefore, these resonance states may be compact resonance states.

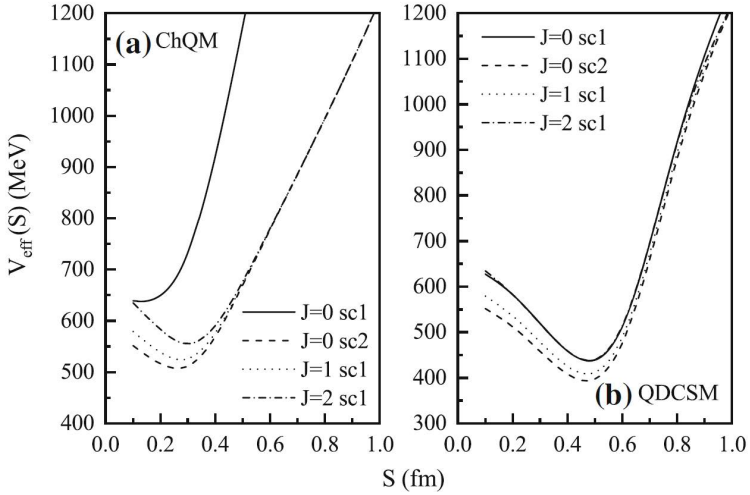

Figure 13. The effective potentials for the diquark–antidiquark $[cc][\bar{c}\bar{c}]$ systems in two quark models. Taken from Ref. [81].

To check whether these resonance states can survive by coupling to the open channels, a channel-coupling calculation of all channels with both meson–meson and diquark–antidiquark structures was carried out, and the real-scaling method was used. The distance between two clusters is labeled as S_i, and the largest one is S_m. With the increase in S_m, an unbound state will fall off toward its threshold, but a resonance state will appear as avoid-crossing structure. In Ref. [81], two quark models with three different sets of parameters are used. Here, the result of one set in ChQM is taken as an example; see Figure 14. It shows that the first horizontal line is the threshold of $J/\psi J/\psi$, and another horizontal line is

possibly a resonance state with $J^P = 2^+$, and the energy is around 6970 MeV. The numerical results in Ref. [81] show that there are four possible resonance states with 0^+, and the energy ranges are 6205∼6270, 6825∼6975, 7140∼7170, and 7210∼7260 MeV, respectively. The possible decay channels are $\eta_c\eta_c$ and $J/\psi J/\psi$. Furthermore, two resonance states with 1^+ are obtained. The energies are 6740∼7150 and 7250∼7280 MeV, respectively. The possible decay channel is $\eta_c J/\psi$. Moreover, a resonance state with $I(J^P) = 0(2^+)$ is also obtained. The energy is 6725∼7050 MeV. The possible decay channel is $\eta_c\eta_c$. The reported state $X(6900)$ can be explained as a compact resonance state with 0^+, and the reported structure around 7200 MeV can be explained as a compact resonance state with 0^+ or 1^+. All these fully charm resonance states are worth searching for in future experiments.

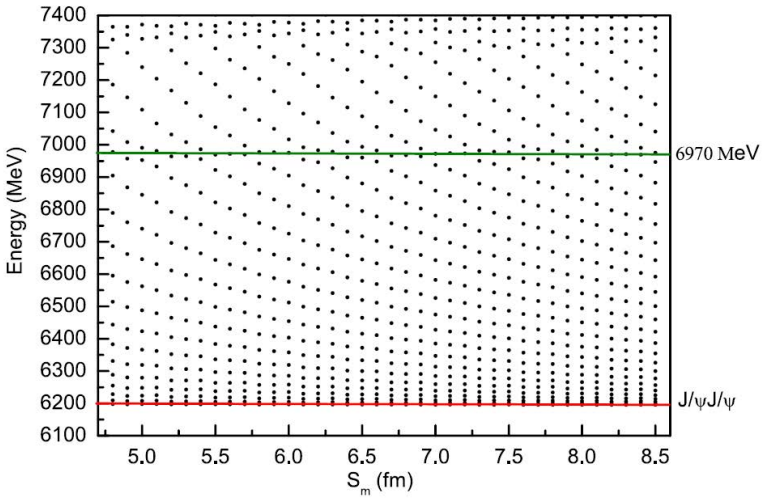

Figure 14. The stabilization plots of the energies of the $cc\bar{c}\bar{c}$ system with $J^P = 2^+$. Taken from Ref. [81].

The work of Ref. [24] used a CMI model, a traditional constituent quark model (CQM), and a multiquark color flux-tube model (CFTM) to systematically investigate the properties of the fully charm tetraquark states $[cc][\bar{c}\bar{c}]$ with the diquark–antidiquark structure, including two color combinations: $\left[[cc]_{\bar{\mathbf{3}}_c}[\bar{c}\bar{c}]_{\mathbf{3}_c}\right]_{\mathbf{1}_c}$ and $\left[[cc]_{\mathbf{6}_c}[\bar{c}\bar{c}]_{\bar{\mathbf{6}}_c}\right]_{\mathbf{1}_c}$. In CMI model, the masses of the ground states $[cc][\bar{c}\bar{c}]$ are close to the thresholds of corresponding two heavy mesons, which are much lower, about hundreds of MeVs, than the masses predicted by the models with QCD dynamic effects. This conclusion is consistent with that of other versions of CMI model. Berezhnoy et al. applied a CMI model, in which the tetraquark mass can be determined by solving a two-particle Schrödinger equation with the point-like diquark (antidiquark) in color $\bar{\mathbf{3}}_c$ ($\mathbf{3}_c$), to research the state $[cc][\bar{c}\bar{c}]$ [466]. The mass of the lowest states is below the threshold of the corresponding two mesons. Karliner et al. studied the $[cc][\bar{c}\bar{c}]$ state with the CMI model motivated by the QCD-string junction picture [467], in which the mass 6192 ± 25 MeV was obtained [467]. One should note that all CMI models ignore the spatial degree of freedom so that everything in the models depends only on the color-spin algebra. The generalization of the CMI model from the conventional hadrons to the multiquark states is implemented under the assumption that the spatial configurations of each QQ, $Q\bar{Q}$, and $\bar{Q}\bar{Q}$ pairs are the same in the multiquark states as in the ordinary hadrons. The CMI of the state $[cc][\bar{c}\bar{c}]$ in the CMI model are overestimated relative to that in the dynamical models due to the spatial assumption, which leads to the much lower energy [24].

In Ref. [24], the masses predicted by the CFTM are 30∼120 MeV lower than those by the CQM. The authors found that the Coulomb interaction plays a critical role in the dynamical model calculations on the heavy hadrons. The color configuration $\left[[cc]_{\mathbf{6}_c}[\bar{c}\bar{c}]_{\bar{\mathbf{6}}_c}\right]_{\mathbf{1}_c}$ should be taken seriously in the ground states due to the strong Coulomb attraction between the $[cc]_{\mathbf{6}_c}$ and $[\bar{c}\bar{c}]_{\bar{\mathbf{6}}_c}$, which is supported by Ref. [442]. The color configuration $\left[[cc]_{\bar{\mathbf{3}}_c}[\bar{c}\bar{c}]_{\mathbf{3}_c}\right]_{\mathbf{1}_c}$

is absolutely dominant in the excited states because of the strong Coulomb attraction within the $[cc]_{\bar{\mathbf{3}}_c}$ and $[\bar{c}\bar{c}]_{\mathbf{3}_c}$. The broad structure ranging from 6.2 to 6.8 GeV can be described as the ground tetraquark state $[cc][\bar{c}\bar{c}]$ in the models. The narrow structure $X(6900)$ can be identified as the excited state $[cc][\bar{c}\bar{c}]$ with $L = 1$ ($L = 2$) in the CQM (CFTM). It is worth mentioning that the CFTM is not a completely new model but the updated version of the traditional CQM based on the color flux-tube picture of hadrons in the lattice QCD. In fact, it merely modifies the two-body confinement potential into the multibody one to describe multiquark states with multibody interaction. The CFTM reduces to the CQM in the mesons while the CFTM can obtain different results from the CQM in the multiquark states.

There is also a lot of work using the QCD sum rule approach to study fully charm tetraquark states within the diquark–antidiquark configuration [432,453,468,469]. Most of them prefer the quantum number of the broad structure around 6.2∼6.8 GeV and the narrow structure around 6.9 GeV to be both $J^{PC} = 0^{++}$. Ref. [453] considered four types of currents, namely scalar–scalar, pseudoscalar–pseudoscalar, axial–axial, and vector–vector. By calculating the mass spectra of these four currents individually, it was found that all the results are numerically consistent with the LHCb's experimental data 6.2∼6.8 GeV for the broad structure, which could support its internal structure as a 0^+ $[cc][\bar{c}\bar{c}]$ tetraquark state. Unlike the treatment in Ref. [453], Refs. [468,469] calculated the mass spectrum of the ground state, first, second, and third radial excited fully charm tetraquark states in the diquark–antidiquark configuration with the QCD sum rules plus Regge trajectories. The authors took the vector diquark operator as the basic constituent, and constructed the scalar and tensor local four-quark currents to explore the scalar, axialvector, and tensor fully charm tetraquark states. By taking account of the CMS and ATLAS experimental data and preforming a self-consistent analysis, they attempted to make possible assignments of the $X(6600)$, $X(6900)$, and $X(7300)$ in the picture of tetraquark states with the 0^{++} or 1^{+-}.

In addition, the decay property of the fully charm tetraquarks was investigated by Chen et al. [432]. They studied strong decays of the possible fully charm tetraquarks observed by LHCb and calculated their relative branching ratios in the framework of the QCD sum rule approach. In this work, the authors assumed the two structures observed by LHCb to be compact diquark–antidiquark $[cc][\bar{c}\bar{c}]$ states, and used the Fierz rearrangement of the Dirac and color indices to transform diquark–antidiquark ($[cc][\bar{c}\bar{c}]$) currents into meson–meson ($[c\bar{c}][c\bar{c}]$) currents, based on which they studied the possible fall-apart decays within the naive factorization scheme, and all possible relative branching ratios are obtained. Together with their previous QCD sum rule study, their results suggested that the broad structure around 6.2∼6.8 GeV can be interpreted as an S-wave $[cc][\bar{c}\bar{c}]$ tetraquark state with $J^{PC} = 0^{++}$ or 2^{++}, and the narrow structure around 6.9 GeV can be interpreted as a P-wave one with 0^{-+} or 1^{-+}. They also proposed to search for their partner states having the negative charge-conjugation parity in the $J/\psi\eta_c$, $J/\psi\chi_{c0}$, $J/\psi\chi_{c1}$, and $\eta_c h_c$ channels.

5.1.2. Color Octet Configuration

For the compact tetraquark state, the hidden color component may also be the color configuration $[[c\bar{c}]_{\mathbf{8}_c}[c\bar{c}]_{\mathbf{8}_c}]_{\mathbf{1}_c}$ in addition to the diquark–antidiquark configuration $\left[[cc]_{\mathbf{6}_c}[\bar{c}\bar{c}]_{\bar{\mathbf{6}}_c}\right]_{\mathbf{1}_c}$ and $\left[[cc]_{\bar{\mathbf{3}}_c}[\bar{c}\bar{c}]_{\mathbf{3}_c}\right]_{\mathbf{1}_c}$. In Ref. [462], Wang et al. systematically calculated the mass spectra for S-wave and P-wave tetraquark state with color configuration $[[c\bar{c}]_{\mathbf{8}_c}[c\bar{c}]_{\mathbf{8}_c}]_{\mathbf{1}_c}$, by using the moment QCD sum rule. The masses for the tetraquark states are predicted to be about 6.3∼6.5 GeV for S-wave channels and 7.0∼7.2 GeV for P-wave channels. These results suggested the possibility that there are some $[[c\bar{c}]_{\mathbf{8}_c}[c\bar{c}]_{\mathbf{8}_c}]_{\mathbf{1}_c}$ components in LHCb's di-J/ψ structures. In Ref. [463], Yang et al. constructed four scalar ($J^{PC} = 0^{++}$) $[[c\bar{c}]_{\mathbf{8}_c}[c\bar{c}]_{\mathbf{8}_c}]_{\mathbf{1}_c}$ type currents to investigate the fully charm tetraquark state in the framework of QCD sum rules. Their results suggested that the broad structure around 6.2 ∼ 6.8 GeV can be interpreted as the 0^{++} states $[[c\bar{c}]_{\mathbf{8}_c}[c\bar{c}]_{\mathbf{8}_c}]_{\mathbf{1}_c}$ with masses 6.44 ± 0.11 GeV and 6.52 ± 0.10 GeV. The narrow structure around 6.9 GeV can be interpreted as the 0^{++} states $[[c\bar{c}]_{\mathbf{8}_c}[c\bar{c}]_{\mathbf{8}_C}]_{\mathbf{1}_c}$ with masses 6.87 ± 0.11 GeV and 6.96 ± 0.11 GeV, respectively.

The authors of Ref. [454] considered the coupling of all structures, which is different from the above work. The authors studied the mass spectra of the fully charm tetraquark systems in QCD sum rules with the complete next-to-leading order contribution to the perturbative QCD part of the correlation functions. Furthermore, the diagonalized current under operator renormalization was used instead of meson–meson or diquark–antidiquark currents. The results indicated that the three obtained $J^{PC} = 0^{++}$ states can be explained as a broad structure around 6.2∼6.8 GeV and the narrow resonance $X(6900)$ state, respectively. Furthermore, another state around 7.25 GeV with 2^{++} was also obtained in Ref. [454]. Their numerical results show that the next-to-leading order corrections are very important for the fully heavy system, because they not only give significant contributions but also reduce the scheme and scale dependence and make Borel platform more distinct.

5.2. Fully Bottom Tetraquark States

In 2016, the CMS Collaboration reported the first observation of the $\Upsilon(1S)$ pair production in pp collision at $\sqrt{s} = 8$ TeV [470]. In 2018, the LHCb Collaboration investigated the $\Upsilon\mu^+\mu^-$ invariant mass distribution to search for a possible fully heavy tetraquark state $[bb][\bar{b}\bar{b}]$, but no significant results were found [471]. However, the fully bottom tetraquark states are also studied in various theoretical frameworks after the discovery of the fully charm tetraquark states.

Some theoretical studies have found that the nature of the fully bottom states is similar to that of the fully charm states. The masses of the $[bb][\bar{b}\bar{b}]$ states are much higher than the thresholds of corresponding channels, so the $[bb][\bar{b}\bar{b}]$ states are identified as the color structure resonances. In QDCSM, the $[bb][\bar{b}\bar{b}]$ systems were systematically investigated in both meson–meson and diquark–antidiquark configurations [81]. The resonances with masses around 19.1∼19.4 GeV and $J^P = 0^+$, 1^+, and 2^+ are possible by considering the channel coupling of two structures. The authors also found that the results are very sensitive to the model parameters, especially the parameter b in the Gaussian describing the size of baryons/mesons. If they use the set of parameters which describes light baryons well, $b = 0.6$ fm, the deeply bound $[bb][\bar{b}\bar{b}]$ states can be obtained. However, when extending to the heavy flavor system, the parameter b needs to be readjusted according to the size of heavy baryons/mesons, which is determined by GEM. They found that the size of η_b or Υ is less than 0.2 fm. By using such a small value of b, they obtained the masses of the $[bb][\bar{b}\bar{b}]$ systems, which are higher than the thresholds of $\eta_b\eta_b$ and $\Upsilon\Upsilon$. Therefore, some theoretical results often depend on model parameters, and it is extremely important to use reasonable model parameters to study exotic hadrons. Liu et al. systematically calculated the mass spectra of the tetraquark states $[bb][\bar{b}\bar{b}]$ in a nonrelativistic potential quark model [444]. The ground states with 0^+, 1^+, and 2^+ have masses of about 19.3 GeV, which are qualitatively consistent with those of Ref. [24]. The nonrelativistic model is also used to study the $[bb][\bar{b}\bar{b}]$ system by assuming it as a compact state consisting of diquark–antidiquark pairs [472]. It was found that predicted masses 19.6∼20.0 GeV of ground state $[bb][\bar{b}\bar{b}]$ are significantly higher than the thresholds of the fall-apart decays to the lowest allowed two-meson states. In addition, Li et al. studied the states $[bb][\bar{b}\bar{b}]$ within the Bethe–Salpeter framework [450]. Their results showed that the three ground states $[bb][\bar{b}\bar{b}]$ are also in the mass range of 19.2∼19.3 GeV.

Some researchers obtained the masses of the fully bottom tetraquark states, which are lower than the thresholds of corresponding channels, so stable $[bb][\bar{b}\bar{b}]$ states are possible. The authors of Ref. [473] calculated the mass-spectra of the state $[bb][\bar{b}\bar{b}]$ in a non-relativistic framework that includes the Cornell-like potential along with the relativistic correction term to the potential and spin-dependent interaction. They found that the masses of S- and P-wave states are between 18.7 and 19.4 GeV, in which the masses of S-wave states are less than the $\eta_b(1S)\eta_b(1S)$, $\eta_b(1S)\Upsilon(1S)$, and $\Upsilon(1S)\Upsilon(1S)$ thresholds. In Ref. [448], the authors studied the mass of the ground state $[bb][\bar{b}\bar{b}]$ by solving the nonrelativistic four-body Schroedinger equation. The mass of the state measured with the flip-flop is about 18.440 GeV, which is in good agreement with the experimental mass of pair $\Upsilon(1S)$

mesons. In Ref. [462], Wang et al. systematically calculated the mass spectra for S-wave and P-wave states in the $[b\bar{b}]_{\mathbf{8}} \otimes [b\bar{b}]_{\mathbf{8}}$ color configuration by using the moment QCD sum rule method. Their masses are around 18.2 GeV for the S-wave states, while they are 18.4∼18.8 GeV for the P-wave ones, which is below the $\eta_b\eta_b$ and $\Upsilon(1S)\Upsilon(1S)$ two-meson decay thresholds. Chen et al. studied the existence of exotic doubly hidden-charm/bottom tetraquark states in a moment QCD sum rule method and discovered that the masses of the $[bb][\bar{b}\bar{b}]$ tetraquarks are all below or very close to the thresholds of $\Upsilon(1S)\Upsilon(1S)$ and $\eta_b(1S)\eta_b(1S)$, except one current of $J^{PC} = 0^{++}$. However, the masses of the fully charm tetraquarks are all above the threshold in Ref. [474]. Therefore, the properties of the fully bottom tetraquark states are still uncertain, which is worthy of further study by experiment and theory.

5.3. Hidden-Charm and Hidden-Strange Tetraquark States

5.3.1. Experimental Progress

Inspired by the recent results of LHCb experiment about the resonances $X(4140)$, $X(4274)$, $X(4500)$, $X(4700)$, $X(4630)$, and $X(4685)$ [475], people have shown great interest in studying the tetraquark system composed of $cs\bar{c}\bar{s}$. In 2009, the CDF Collaboration announced a measurement of a new resonance $X(4140)$ in the $J/\psi\phi$ invariant mass distribution of $B^+ \longrightarrow J/\psi\phi K^+$ [476]. The mass and width of this state are

$$X(4140): M = 4143.0 \pm 2.9 \pm 1.2 \text{ MeV}, \quad \Gamma = 11.7^{+8.3}_{-5.0} \pm 3.7 \text{ MeV}.$$

With the passage of time, this resonance state was also successively found by other experimental collaborations, such as LHCb, D0, CMS, and BABAR [477–480]. Furthermore, the BABAR Collaboration performed a study of the decays $B^{+,0} \longrightarrow J/\psi K^+ K^- K^{+,0}$ and $B^{+0} \longrightarrow J/\psi\phi K^{+0}$, and two resonances, $X(4140)$ and $X(4274)$, were obtained in the $J/\psi\phi$ mass spectrum [480]. In 2017, the CDF Collaboration observed the resonance state $X(4274)$ in the $B^+ \longrightarrow J/\psi\phi K^+$ decay with 3.1σ significance [481], and the LHCb Collaboration confirmed the existence of the $X(4140)$ and $X(4274)$ in the $B^+ \longrightarrow J/\psi\phi K^+$ decay [482]. Their quantum numbers were determined to be $J^{PC} = 1^{++}$. In the same process, the Collaboration observed two higher resonances, $X(4500)$ and $X(4700)$ with $J^{PC} = 0^{++}$ [483].

5.3.2. Diquark–Antidiquark Explanation

The experimental information on resonances $X(4140)$, $X(4274)$, $X(4500)$, and $X(4700)$ stimulated the appearance of different approaches to account for their properties. These states were considered as meson–meson molecules in Refs. [484–492], and the diquark–antidiquark picture was discussed in Refs. [493,494]. There are also competing approaches which consider them as dynamically generated resonances [495,496] or channel-coupling effects [497]. However, after the precise measurements, the situation of $X(4140)$, $X(4274)$, $X(4500)$, $X(4700)$ became clearer, especially that of $X(4140)$ and $X(4274)$. The new experimental results removed an explanation of $X(4140)$ as 0^{++} or 2^{++} $D_s^{*+}D_s^{*-}$ molecular states from the agenda and also excluded interpretation of $X(4274)$ as a molecular bound state and as a cusp [482]. So many theorists attempt to interpret X resonances as excited charmonium or as color structure resonances [498–503]. Based on various models, many theoretical researches have explored the nature of X states in the context of color resonance picture [504]. In this section, we review some typical work, which explains these X states as the color structure resonance states. In Ref. [504], the $cs\bar{c}\bar{s}$ systems with $J^{PC} = 0^{++}$, 1^{++}, 1^{+-}, and 2^{++} were systemically investigated by using the RGM in the QDCSM. Two structures, the meson–meson and diquark–antidiquark structures, are taken into account.

Although the energy of the diquark–antidiquark structure is higher than the meson–meson threshold, it is still possible for the states to be resonances because the colorful subcluster diquark and antidiquark cannot fall apart directly due to the color confinement. By using the real-scaling method, the authors carried out the calculation of all channels coupling of both the meson–meson and diquark–antidiquark structures, and several resonances were obtained. There are four $J^{PC} = 0^{++}$ states with masses around

4028∼4033, 4378∼4401, 4500∼4530, and 4630∼4648 MeV, respectively, one $J^{PC} = 1^{++}$ state with the resonance mass around 4307∼4341 MeV and two $J^{PC} = 2^{++}$ states with the resonance masses around 4394∼4448 and 4526∼4536 MeV, respectively. Compared with the experimental data, people tend to interpret the exotic states $X(4350)$, $X(4500)$, and $X(4700)$ as the compact tetraquark states with 0^{++}. The $X(4274)$ is a possible candidate of the compact tetraquark state with 1^{++}. Furthermore, the 0^{++} resonance state with an energy range 4028∼4033 MeV, the two $J^{PC} = 2^{++}$ resonance states with an energy range of 4394∼4448 MeV and 4526∼4536 MeV are possible exotic states which are worthy of attention.

By using the method of QCD sum rule, Ref. [499] investigated $X(4500)$ and $X(4700)$ based on the diquark–antidiquark configuration. The results show that $X(4500)$ can be assigned as a D-wave tetraquark with the color structure $\left[[cs]_{\bar{\mathbf{3}}_c}[\bar{c}\bar{s}]_{\mathbf{3}_c}\right]_{\mathbf{1}}$, while $X(4700)$ is a D-wave tetraquark with $\left[[cs]_{\mathbf{6}_c}[\bar{c}\bar{s}]_{\bar{\mathbf{6}}_c}\right]_{\mathbf{1}}$. Furthermore, the conclusion of Ref. [498] is relatively similar to that of Ref. [499], in which $X(4140)$ and $X(4274)$ can be both interpreted as S-wave $cs\bar{c}\bar{s}$ tetraquark states of $J^P = 0^+$, but with opposite color structures. In Refs. [505,506], five types of tetraquark states with $J^{PC} = 1^{++}$ were investigated, and these are $[sc]_S[\bar{s}\bar{c}]_A \pm [sc]_A[\bar{s}\bar{c}]_S$, $[sc]_P[\bar{s}\bar{c}]_V \mp [sc]_V[\bar{s}\bar{c}]_P$, $[sc]_T[\bar{s}\bar{c}]_A - [sc]_A[\bar{s}\bar{c}]_T$, $[sc]_T[\bar{s}\bar{c}]_V - [sc]_V[\bar{s}\bar{c}]_P$, and $[sc]_A[\bar{s}\bar{c}]_V \pm [sc]_V[\bar{s}\bar{c}]_A$, respectively. The subscripts S, P, A, V, and T denote the scalar, pseudoscalar, axialvector, vector, and tensor diquark, respectively. The $X(4140)$ and $X(4274)$ cannot be described as the tetraquarks with $[sc]_S[\bar{s}\bar{c}]_A \pm [sc]_A[\bar{s}\bar{c}]_S$ and $[sc]_P[\bar{s}\bar{c}]_V \mp [sc]_V[\bar{s}\bar{c}]_P$. However, $X(4140)$ can be regarded as the $[sc]_T[\bar{s}\bar{c}]_V - [sc]_V[\bar{s}\bar{c}]_T$ axialvector tetraquark state, and $X(4274)$ can be explained as the $[sc]_A[\bar{s}\bar{c}]_V \pm [sc]_V[\bar{s}\bar{c}]_A$ tetraquark state with a relative P-wave between the diquark and antidiquark constituents.

Based on a diquark–antidiquark model, the hidden-charm with flavor octet and singlet tetraquarks with different spin parties in diquark–antidiquark configuration were studied [507]. The diquark and antidiquark are regarded as constituents in this work, and a similar assumption was also adopted in Refs. [508,509]. The results show that the $X(4500)$ and $X(4700)$ may be explained as the radial excitation of $J^P = 0^+$ tetraquark, while $X(4140)$ and $X(4274)$ may be explained as $J^P = 1^+$ tetraquarks.

In Ref. [510], the masses of all possible hidden-charm tetraquarks were also calculated in the diquark–antidiquark structure. However, the diquark and antidiquark appear dynamically as a clustering in the wave function, which is different from Ref. [507]. There was no mass that can match the $X(4500)$, $X(4700)$, and $X(4140)$ in the work of Ref. [510]. However, $X(4274)$ is interpreted as the $J^{PC} = 1^{++}$ state in this work. The mass of this state is 4373 MeV and 4280 MeV with two sets of parameters, respectively.

In the simple color-magnetic interaction model, the authors adopted the diquark–antidiquark structure to analyze the S-wave $cs\bar{c}\bar{s}$ system with the effective quark mass method and the reference parameter method [511]. The numerical results show that the $X(4140)$, $X(4274)$, and $X(4350)$ are assumed to be the tetraquark assignment, and they may be found in the $J/\psi\phi$ or $\eta_c\phi$ channel. In Refs. [88,512], the state $cs\bar{c}\bar{s}$ was studied with the diquark–antidiquark picture in the multiquark color flux-tube model, where the D-wave and P-wave angular excitation were also considered. From the analysis of the calculation results, the masses of the fourth and fifth S-wave radial excited state are, respectively, 4466 MeV and 4699 MeV, which match with those of the states $X(4500)$ and $X(4700)$. Furthermore, the lowest energy of $cs\bar{c}\bar{s}$ with $J^{PC} = 1^{++}$ was 4330 MeV, which was close to the mass of the $X(4274)$ but far from $X(4140)$. This indicates that the main component of the state $X(4274)$ may be the state $cs\bar{c}\bar{s}$ with $J^{PC} = 1^{++}$.

In the relativistic quark model [513], the $X(4140)$ was regarded as the $cs\bar{c}\bar{s}$ tetraquark ground state, the $X(4700)$ was assigned as the $2S$ excited tetraquark state, and the $X(4500)$ was explained as the tetraquark composed of $2S$ scalar diquark and scalar antidiquark by considering the internal excitation of diquark. However, in Ref. [514], although the same method was used, the conclusions were different. The calculated lowest mass with 1^{++} was 4159 MeV, which is close to the experimental data of $X(4140)$, so this state can be deemed as $X(4140)$. In addition, the masses of axial–vector diquark–antidiquark and scalar

diquark–antidiquark in the $J^{PC} = 0^{++}$ system were 4509 MeV and 4653 MeV, respectively. Compared to the experimental data, $X(4500)$ and $X(4700)$ were interpreted as 0^{++} radial excitations of S-wave axial–vector diquark–antidiquark and scalar diquark–antidiquark, respectively. However, $X(4274)$ cannot be effectively explained in the relativistic quark model.

In addition, we gather the conclusions from the diquark–antidiquark explanation and summarize them in Table 5.

Table 5. The conclusions of $X(4140)$, $X(4274)$, $X(4500)$, and $X(4700)$ are summarized as follows for the diquark–antidiquark structure.

	J^P	
X(4140)	1^+	[498,505–509,511,513]
X(4274)	1^+	[88,498,504–512]
X(4500)	0^+	[499,504,507–509,513]
X(4700)	0^+	[499,504,507–509,513]

5.4. Alternative QCD Isomers for P_c and P_{cs}

In chemistry, isomers consist of the same atoms but have different chemical bonds. Similarly, the multiquark states made of the same quark contents but possessing different color flux-tube structures can be named as QCD isomers, which is a kind of novel strong interaction phenomenon that may exist. The observation of the hidden charm pentaquark states P_c and P_{cs} presents an extremely interesting spectrum, which provides a good platform to explore the effect of the QCD isomers.

Ref. [47] investigated the QCD isomers in the pentaquark states. Numerical results indicate that the QCD isomers, pentagon, diquark, and octet configurations, have close masses. The mass order is $E_o > E_d > E_p$, where E_o, E_d, and E_p represent the mass of the octet, diquark, and pentagon structure, respectively. The mass difference between the two adjacent items is several tens of MeV, which mainly comes from the different types of confinement potential determined by the color structure. The confinement potential of the octet structure is bigger than that of the diquark structure because there is one piece of stronger color **8**-dimension color flux-tube than **3**-dimension one. That of the ring-like pentagon structure is lowest because the structure is easier to shrink into a compact multiquark state relative to the octet and diquark structures, which is held for the hexaquark states [31]. Like the color-magnetic interaction, such a color structure effect can also induce mass splitting in the spectrum and make the hadron world more fantastic.

The hidden charm pentaquark states P_c and P_{cs} were widely described as the meson–baryon molecular states. The multibody confinement potential based on the color flux-tube picture provides an alternative mechanism for their structures. The states $P_c(4312)^+$, $P_c(4337)^+$, $P_c(4380)^+$, $P_c(4440)^+$, $P_c(4457)^+$, and $P_{cs}(4459)^0$ are pentagon, diquark, pentagon, diquark, octet, and pentagon structures, respectively. The fact enlarges the insights into the hadron structure and low-energy strong interaction.

5.5. Short Summary

For some reported structures, if there is no threshold channel near the observed energies, it will be difficult to explain these structures with molecular states. Resonance states with multiple color structures may be a good explanation. In addition, these resonance states can be coupled with molecular states, and the coupling to the open channels will shift the mass of the resonance and give the decay width to the resonance, or destroy the resonance. Therefore, the coupling effect of these color structure resonance states and scattering states should be considered.

The fully charm tetraquark states observed by LHCb and CMS experiments in the J/ψ-pair mass spectrum may open up a new testing ground for the genuine compact tetraquark states arising from the quark–gluon interaction in QCD, aside from the molecular hadrons

that are loosely bound by light meson exchanges. These significant signals clearly await the confirmation of other experiments. Furthermore, the hidden-charm and hidden-strange tetraquark states are also worth exploring in other experiments. It will be very helpful to determine the quantum numbers of these resonances and investigate the structures of these states. With more progress in the investigation of the fully heavy tetraquark states, as well as the hidden-charm and hidden-strange tetraquark states in the future, we may gain new insight into the confinement mechanism and the short-range interaction of QCD.

In the study of exotic hadrons, different treatments are usually used in the same theoretical methods, such as different confinement interactions used in various quark models, a variety of currents used in QCD sum rules, multi-channel coupling with diverse configurations included in calculations, and so on, which will lead to significantly disparate results. A thorough study of the differences between these methods will help to study the multi-quark system and understand the nature of exotic hadrons.

6. The Exotic States in Unquenched Quark Model

The unquenched quark model can be utilized to understand the properties of the second type of exotic hadrons, whose quantum numbers can be created using quark–antiquark or three-quark configurations but whose properties cannot be explained by the valence quark model. In principle, all the hadron states are linear combinations of valence quark term, multi-quark, and hybrid terms. For the ordinary hadrons, the valence quark term is the dominating one, whereas the multiquark terms may dominate for the exotic hadrons. For some exotic states, the valence quark term and the multiquark terms contribute comparably. For example, $X(3872)$, now named $\chi_{c1}(2P)$, is taken as a typical state in the unquenched quark model. The multiquark terms $D^{(*)}\bar{D}^{(*)}$ are the important components in the state. For the P_c family, they can be treated as pure pentaquark states, although the quantum numbers of states are the same as that of the excited state of the nucleon. The three-quark term will make an ignorable contribution to the states due to the high energy. For the ground states of hadrons, the contribution from multiquark terms can be neglected. In the following, several typical states in the unquenched quark model are picked up to illustrate the main features of the model.

6.1. $X(3872)$

In 2003, the Belle Collaboration reported the discovery of the $X(3872)$ state [2]. Since then, extensive research has been conducted to study its properties, which has been reviewed in Refs. [515,516]. In this article, we primarily focus on the latest experimental findings. Recently, the LHCb Collaboration reported the mass splitting between the $X(3872)$ and the $\psi(2S)$ to be $\Delta m = 185.598 \pm 0.067 \pm 0.068$ MeV, along with a decay width of $1.39 \pm 0.24 \pm 0.10$ MeV [517]. Utilizing the known mass of the $\psi(2S)$, the mass of the $X(3872)$ was determined to be $3871.695 \pm 0.067 \pm 0.068 \pm 0.010$ MeV, where the uncertainties are attributed to statistical, systematic, and $\psi(2S)$ mass knowledge, respectively. Through an examination of the Flatte amplitude structure obtained by fitting the state's lineshape, Aaij et al. discovered a pole structure that is consistent with a quasi-bound $D\bar{D}^*$ state, although the possibility of a quasi-virtual state is still allowed at a 2 standard deviation level. Notably, the width of the state in the Flatte model is approximately five times smaller than the Breit–Wigner width. Furthermore, by studying the decay of $B^+ \to \psi_2(3823)K^+$ with $\psi_2(3823) \to J/\psi\pi^+\pi^-$, the Breit–Wigner width in the $X(3872)$ was measured to be $\Gamma^{BW}_{X(3872)} = 0.96^{+0.19}_{-0.18} \pm 0.21$ MeV [518]. The width of the $X(3872)$ state, as determined by the LHCb Collaboration, is highly consistent with the result reported by Belle, $\Gamma_{X(3872)} < 1.2$ MeV [519]. To gain insights into the nature of the $X(3872)$ state, Dubynskiy and Voloshin pointed out that if it is a pure charmonium $\chi_{c1}(2P)$ state, the dominant decay process would be $X(3872) \to \pi\pi\chi_{c1}$. Conversely, if the $X(3872)$ is a pure molecular $D\bar{D}^*$ state with a significant isovector component, the single-pion transitions would be substantially enhanced, leading to comparable rates for all three χ_{cJ} resonances in the final state [520]. Building upon this observation, BESIII recently conducted searches

for the decays $X(3872) \to \pi^0\chi_{c0}$ and $X(3872) \to \pi\pi\chi_{c0}$ [521]. Their findings revealed suppression in both decay modes, indicating that the $X(3872)$ may not be a pure charmonium state or a pure molecular state. As a result, the unquenched effects on $X(3872)$ will be emphasized in this review.

The contribution of virtual decay loops of charmed meson pair to the charmonium states in $^3P_0$ model was first discussed by Barnes [522]. In the calculation, the accumulating approach was adopted and the orbital wavefunctions of all the involved mesons were taken as the same Gaussian; the relative motion wavefunction between the charmed meson pair was fixed to a plane wave function. The mass shifts for the charmonia below $D\bar{D}$ threshold were found to be surprising large, -386 MeV to -537 MeV, and the probability of $c\bar{c}$ component is not dominant, 43%∼71%. A systematical study of the charmonium spectrum was performed by Kalashnikova in the framework of the quark model considering the contributions of hadron loops, which is calculated by invoking the $^3P_0$ model [96]. The same approximations as that of Ref. [522] are introduced but Gaussians with different sizes are employed for different mesons. For orbital excited states, the simple harmonic oscillator (SHO) wave functions (they are Gaussians for ground states) are employed. In addition, different quark pair creation strength γ in $^3P_0$ model is used. The results showed that most lower charmonium states, such as η_c, J/ψ, $\chi_{cJ}(1P)$, $J = 0, 1, 2$, and so on, can be described well with more than 80% of $c\bar{c}$ structure, and the mass shifts due to the hadron loops are around 200 MeV. As for $2P$ levels, $\chi_{cJ}(2P)$, $J = 0, 1, 2$, the mass shifts are still about 200 MeV, and even the bare masses of states are above the threshold of charmed meson pairs. The calculated masses of unquenched states are higher than experimental data, about 100 MeV. For example, the original 2^3P_1 $c\bar{c}$ with a bare mass of 4180 MeV can be shifted down to 3990 MeV by hadronic loop of $D\bar{D}^*$. In addition, the coupling between $c\bar{c}$ and charmed meson pairs generated a virtual state very close to the $D\bar{D}^*$ threshold. It is possible to assign the virtual state to $X(3872)$. The author also concluded that for $2P$ levels, the opening of strong S-wave channels leads to pronounced threshold effects. Similarly, Santopinto et al. [97] also used $^3P_0$ model to investigate the spectrum of $c\bar{c}$. The $c\bar{c}$ spectrum was calculated by Godfrey–Isgur relativized quark model. The coupling effect of the meson–meson continuum is considered using the $^3P_0$ model, but the transition operator is modified by introducing a damping factor $\exp(-2r_q\boldsymbol{p}^2/3)$ with $\boldsymbol{p}$ being the relative momentum between the created quark and antiquark and r_q being the parameter, and the created quark–antiquark pairs from vacuum are extended to include $c\bar{c}$ and $b\bar{b}$. The wave functions of the involved meson are approximated by the SHO wave function with fixed oscillator parameters by assuming good flavor symmetry. The calculated mass shifts of charmonium states under 4 GeV are in the range of 80 MeV to 190 MeV, especially for the ground states of $c\bar{c}$; the mass shifts are less than 100 MeV. As expected, the contributions from heavier meson–meson interactions are very small, 1 MeV to 3 MeV or less. For $X(3872)$, they tried to assign it to charmonium $\chi_{c1}(2P)$ but include extra components of charmed meson pairs, which induces a 117 MeV mass shift downward. The unquenched mass of $\chi_{c1}(2P)$ is 3908 MeV, 36 MeV higher than the experimental value. Two open flavor channels $D\bar{D}^*$, $D^*\bar{D}^*$ contribute near 100 MeV mass shift to 2^3P_1 $c\bar{c}$, while the other mesonic channels only contribute 21 MeV mass shift. The largest contribution comes from $D^*\bar{D}^*$ channel, -66 MeV mass shift, which is twice that of $D\bar{D}^*$ ($D^*\bar{D}$). The reason is that the bare mass of 2^3P_1 $c\bar{c}$ is 4025 MeV close to the threshold $D^*\bar{D}^*$. Based on this fact, Ferretti et al. proposed the following hypotheses to converge the Fock expansion of a meson state [105]: (1) Only the closest complete set of accessible $SU^F(N)\otimes SU^\sigma(2)$ open flavor meson–meson intermediate states can influence multiple structures, while the other meson–meson states are supposed to give a background contribution; (2) The presence of a certain complete set of open-flavor intermediate states does not affect the properties of a single resonance, but it influences those of all the multiple members.

In Ref. [523], the refined Cornell coupled-channel model was employed to consider the coupling between $c\bar{c}$ levels and two-meson states. The similar Hamiltonian and eigenvalue equation as Equations (15) and (16) are used to obtain the energy of the charmonium

state. To simplify the calculation, the Gaussian is also used for the orbital wave function of charmed mesons. The calculated results showed that the mass shifts for the low-lying $1S$ and $1P$ levels are small, and the coupled-channel effects are noticeable for other states. For $\chi_{c1}(2P)$ state, the unquenched mass is 3920.5 MeV, 48 MeV above the experimental mass of $X(3872)$. The percentage of $c\bar{c}$ in the $\chi_{c1}(2P)$ state is 50%, $D\bar{D}^* + D^*\bar{D}$ fraction is around 40%, and $D^*\bar{D}^*$ fraction is 6%. The further calculation of the E1 radiative transition to $\gamma J/\psi$ and strong transition to $D\bar{D}^*$ of $\chi_{c1}(2P)$ unfavored the interpretation of $X(3872)$ as $\chi_{c1}(2P)$.

Instead of using the SHO wave function, Ortega et al. [98] took the GEM to perform coupled channel calculation of 1^{++} $c\bar{c}$ sector including $c\bar{c}$ and $D\bar{D}^*$ molecular configuration. This calculation was based on the constituent quark model, which contains screening confinement potential and $^3P_0$ model. For the $1P$ state, the $c\bar{c}$ component dominates the state, over 95%. For the $2P$ state, the situation is different. The state with a large $c\bar{c}$ component has higher energy than the state with large $D\bar{D}^* + D^*\bar{D}$ component. One of the unquenched masses of 2^3P_1 $c\bar{c}$ is 3865 MeV, which is very close to the mass of $X(3872)$ if the quark–antiquark pair creation strength γ is fixed by the decay width of $\psi(3770) \to D\bar{D}$, $\gamma = 0.26$. The main component of this state is the charmed meson pair, 67%. To reproduce the experimental properties of $X(3872)$, the parameter γ is set to 0.19, and the isospin breaking is taken into consideration by using the charge basis instead of the isospin symmetric one, then the calculated mass of the $2P$ state is 3871 MeV, the percentage of $c\bar{c}$ in the $2P$ state is only 7%, state $D\bar{D}^* + D^*\bar{D}$ with isospin 0 dominates with 70% percentage and the probability of the state with isospin 1 is 10%.

The modified transition operator of $^3P_0$ model Equation (18) was used in an unquenched quark model to investigate the properties of $X(3872)$ in Ref. [90]. In the calculation, the GEM was employed to deal with the orbital wave functions of mesons and relative motion between mesons, and the diagonalization of the full Hamiltonian matrix is performed. In this way, the systematic error of neglecting the coupling among different channels of two charmed mesons can be amended. Applied to ground states of charmonium, η_c and J/ψ, the mass shifts are around -70 MeV, and the $c\bar{c}$ component dominates the ground states, 94% and 93%, respectively. Applied to $\chi_{c1}(2P)$ state, the mass shift is -150 MeV, which induces the unquenched mass reaching the experimental value of $X(3872)$. The probability of finding $c\bar{c}$ component in the unquenched $\chi_{c1}(2P)$ state is 30%, $D\bar{D}^* + \bar{D}D^*$ is 22.5%, $D^*\bar{D}^*$ is 5.6%, and $D_s^{(*)}\bar{D}_s^{(*)}$ is 2.4%.

The unquenched nature of $X(3872)$ can explain not only its relatively lower mass but also its isospin violation decay process. According to the fact that the BESIII Collaboration searched for $X(3872)$ signals in $e^+e^- \to \gamma\chi_{cJ}\pi^0$ $(J = 0, 1, 2)$ process and reported an observation of $X(3872) \to \chi_{c1}\pi^0$ with a ratio of branching fractions $B_r(X(3872) \to \chi_{c1}\pi^0)/B_r(X(3872) \to J/\psi\pi^+\pi^-) = 0.88^{+0.33}_{-0.27} \pm 0.10$ [524], there may be a large $D\bar{D}^*$ component in $X(3872)$. In Ref. [520], the author found that the relative rates for the transitions of $X(3872)$ to χ_{cJ} with different J significantly depend on the internal structure of the $X(3872)$. If the resonance is dominantly a charmonium $^3P_1$ state, the pionic transitions are quite weak, with the process $X(3872) \to \pi\pi\chi_{c1}$ being dominant. If $X(3872)$ is a molecular state with a significant iso-vector part in its wave function, the considered single pion transitions should be greatly enhanced and exhibit comparable rates for all three χ_{cJ} resonances in the final state. The ratios of decay rates are estimated to be Γ_0:Γ_1:Γ_2 = 0:2.7:1 when assuming the $X(3872)$ as a traditional charmonium state or Γ_0:Γ_1:Γ_2 = 2.88:0.97:1 as a meson–meson state.

Zhou systematically investigated the properties of the $X(3872)$ state within the extended Friedrichs scheme, considering the coupling between the bare 2^3P_1 $c\bar{c}$ state and the continuum $D\bar{D}^*$, $D^*\bar{D}$, and $D^*\bar{D}^*$ [525]. In this framework, the decay rates of $X(3872)$ into $\chi_{c0}\pi^0$, $\chi_{c1}\pi^0$, $\chi_{c2}\pi^0$, $J/\psi\pi^+\pi^-$, and $J/\psi\pi^+\pi^-\pi^0$ were calculated, yielding relative ratios of 1.5:1.3:1.0:16:26. Notably, although the decay rate of $X(3872) \to \chi_{c1}\pi^0$ is smaller than that of $X(3872) \to J/\psi\pi^+\pi^-$, it remains consistent with the measurements from BESIII within the margin of error. Guo et al. explored the influence of intermediate charmed

meson pairs on charmonium transitions involving the emission of one π or η, using a non-relativistic effective field theory [526]. They observed that charmed meson loops are enhanced compared to the corresponding tree-level contributions for both S-wave and P-wave charmonium transitions. Similar calculations were conducted by Fleming et al. in Ref. [527], where they studied the decays of $X(3872)$ by matching heavy hadron chiral perturbation theory amplitudes for $D^0\bar{D}^{*0} \to \chi_{cJ}(\pi^0, \pi\pi)$ onto local operators. The analysis revealed that decays to final states with two pions are predominantly governed by the $\chi_{c1}\pi^0\pi^0$ final state.

The radiative decays of the $X(3872)$ have attracted interest in studying its properties. The ratio of branching fractions into final states with a photon and a J/ψ or a $\psi(2S)$ has been measured as $B_r(X \to \psi(2S)\gamma)/B_r(X \to J/\psi\gamma) = 2.46 \pm 0.64 \pm 0.29$. In Ref. [528], a coupled-channel approach was employed to investigate the radiative decays of the $X(3872)$. The $c\bar{c}$ states were described using a relativistic string Hamiltonian, while for the decay channels involving $D\bar{D}^*$, a string breaking mechanism was incorporated. The coupling effect was found to shift the 2^3P_1 charmonium state down to the $D\bar{D}^*$ threshold, and the mixing angle between the 2^3P_1 and $^1P_1$ states was estimated to be 8.8°. As a result of this mixing, the transition rate $\Gamma_1(X(3872) \to J/\psi\gamma)$ was predicted to increase several times, reaching a value in the range of 45∼80 keV. Conversely, the transition rate $\Gamma_2(X(3872) \to \psi'\gamma)$ was predicted to decrease by 15%. Dong et al. also studied the $X(3872)$ as a composite state containing both molecular hadronic and a $c\bar{c}$ component in Ref. [529]. Their analysis revealed that a nontrivial interplay between a possible charmonium and the molecular components in the $X(3872)$ is necessary to explain the observed ratio $B_r(X(3872) \to \psi(2S)\gamma)/B_r(X(3872) \to J\psi\gamma)$ of radiative decay modes.

In the framework of HQSS [530], the authors systematically investigated $2P$ charmonium $c\bar{c}$ with the $D\bar{D}^*$ coupling effect. They have shown that the interplay of the charmonium components in the $X(3872)$ produces an extra attraction, while such an attraction does not appear in the $J^{PC} = 2^{++}$ sector, where one should expect instead some repulsion from the charmonium degrees of freedom. They also indicated that around a 10%∼30% charmonium probability in the $X(3872)$ might explain the experimental value of the ratio $R_{\psi\gamma}$, confirming that this ratio is not in conflict with a predominantly molecular nature of the $X(3872)$.

6.2. $D^*_{s0}(2317)$ and $D_{s1}(2460)$

Just before the observation of $X(3872)$, the BaBar Collaboration claimed a narrow charm-strange meson, named $D^*_{s0}(2317)$, and the mass is near 2320 MeV [1]. The observation of the state in the inclusive $D_s^+\pi^0$ mass distribution and the mass almost 40 MeV below the DK threshold make this state quite different from those predicted by the quark model. The decay of $c\bar{s}$ state to $D_s\pi$ violates isospin conservation, so the decay width must be small. The favored spin-parity assignment is $J^P = 0^+$. The state was soon confirmed by the CLEO Collaboration in the same final state [531]. In addition, a new state, $D_{s1}(2460)$ was also observed in the $D_s^{*+}\pi^0$ final state. Belle Collaboration also confirmed the existence of these two states [532]. The tentative quantum number assignment is $J^P = 1^+$. The upper limits of the natural widths of $D^*_{s0}(2317)$ and $D_{s1}(2460)$ are found to be $\Gamma < 7$ MeV. The absolute branching fraction $B_r(D^*_{s0}(2317) \to \pi^0 D_s) = 1.00^{+0.00}_{-0.14} \pm 0.14$ was reported recently by the BESIII Collaboration [533].

There is much theoretical research which has investigated the exotic properties of $D^*_{s0}(2317)$ and $D_{s1}(2460)$ [16,23]. The popular explanation of $D^*_{s0}(2317)$ and $D_{s1}(2460)$ is that both of them are hadronic molecules because they lie just below the thresholds of DK and D^*K, respectively. In fact, the quantum numbers of them are normal, i.e., they can be reached by $c\bar{s}$, so it is natural to explain them as unquenched states in unquenched quark model. In this review, we only focus on the mixing nature of these two D_s states.

In 2003, Browder et al. proposed an explanation for the $D^*_{s0}(2317)$ and $D_{s1}(2460)$ states by considering the mixing between conventional P-wave excited D_s^+ mesons and four-quark states [534]. They argued that the coupling effects between the P-wave $c\bar{s}$ state

and the meson–meson channel could shift the high mass of the P-wave charm-strange meson, predicted to be around 2480 MeV in potential models, down to the experimentally observed values. To describe the coupling between the $c\bar{s}$ and DK states, Browder et al. introduced a phenomenological parameter δ, representing the off-diagonal matrix element in the mass matrix. They set the bare mass of the DK state to the threshold of DK and chose a suitable value of δ (92 MeV) to obtain the masses of the mixed states, which turned out to be 2319.4 MeV and 2537.5 MeV. The lower state, below the DK threshold but above the $D\pi$ threshold, was identified as the $D_{s0}^*(2317)$ state. The higher state, above the DK threshold, can decay rapidly into D and K mesons, resulting in its broad width. Regarding the $D_{s1}(2460)$ state, Browder et al. suggested that a similar mixing mechanism could be applied. However, they did not perform a detailed fit due to the complexity arising from the multi-channel coupling. They also noted that if the mixing angle between the $c\bar{s}$ state and the DK state is small, the radiative transition would be suppressed.

To consolidate the coupling between $q\bar{q}$ and two-meson states, the transition operator in the C^3 model or $^3P_0$ model can be invoked [90,96–101,106,107]. For example, Hwang et al. also took coupled channel effect into consideration in calculating the mass of 1^3P_0 state of charm-strange meson [535]. Unlike Browder's approach [534], the transition operator in the C^3 model was employed to calculate the off-diagonal matrix element. The author emphasized that the linear confinement and Coulomb terms in the charmonium potential are important in the calculation of transition amplitude between two-quark state and two-meson continuum states. In the calculation, the Gaussians are used to describe the radial wave functions of mesons. Finally, they showed that the unquenched mass of 1^3P_0 state can be lowered to the experimental value of $D_{s0}^*(2317)$; the probability of $c\bar{s}$ state is around 70% and the results are stable against to the Gaussian size. A similar method was used by Zhou [536]. Instead of C^3 model, they took $^3P_0$ model to consider the transition between $c\bar{s}$ states and two-meson states. Again, the Gaussians with different sizes are employed to denote the radial wave functions of different mesons. The strength of quark–antiquark pair creation γ was fine-tuned to 5.5, and an overall fitting of experimental data of $1S$, $1P$, and $3P$ charm-strange mesons can be achieved. For 1^3P_0 and 1^1P_1 states, the bare mass 2480 MeV and 2530 MeV are shifted to 2358 MeV and 2470 MeV, respectively. The authors also suggested that the coupling between two bare states 1^1P_1 and 1^3P_1 is responsible for the low mass of 1^1P_1 state.

In their study, Ortega et al. investigated the molecular components in P-wave charm-strange mesons using the $^3P_0$ model with a modified transition operator that includes an energy damping factor $\exp(-\frac{P^2}{2\Lambda^2})$ and the chromomagnetic quark model [537]. The parameters of the model were constrained by various hadron observables. They solved the coupled channel equation numerically using the GEM without making the plane wave assumption for the relative motion between the mesons. They used a smaller quark–antiquark pair creation strength $\gamma = 0.38$ compared to other studies. For the $D_{s0}^*(2317)$ state, the authors obtained a dressed mass of 2323.7 MeV for the 1^3P_0 $c\bar{s}$ state with a percentage of 66.3% $c\bar{s}$ component. Regarding the $D_{s1}(2460)$ state, in addition to the coupling to meson–meson states, the coupling between the 1^1P_1 and 1^3P_1 states was also considered. The unquenched mass obtained was 2484 MeV with a percentage of 54.3% D^*K component. It is worth noting that the study includes the introduction of the one-loop correction to the one-gluon exchange potential and the use of a screened confinement potential, which suggests that quark–antiquark excitations are taken into account. The question of whether there is a double counting between the quark–antiquark excitation in the quark–quark interaction and the high Fock components in the wave function is raised by the authors, indicating that further research is necessary to clarify this aspect.

In most calculations of unquenched masses of $D_{s0}^*(2317)$ and $D_{s1}(2460)$, only the two-meson states DK or D^*K are considered. Do other high Fock components, $D_s\eta$, $D_s\phi$, make negligible contributions? Torres et al. [538] investigated the channel coupling effect of $D_s\eta$ on the DK phase shifts and the position of the $D_{s0}^*(2317)$. In the SU(4) extrapolation of the chiral unitary theory, a channel coupling of DK and $D_s\eta$ calculation showed that the

accurate DK phase shifts and the position of the $D_{s0}^*(2317)$ can be obtained. The position is not affected by the coupling and the phase shifts in the high-energy part need the channel coupling. In this calculation, $D_{s0}^*(2317)$ is taken as DK molecular state. In Ref. [539], a systematic calculation of D_s states is carried on in the framework of the unquenched quark model with the help of GEM. In this approach, the modified transition operator of $^3P_0$ model (Equation (18)) is invoked to couple the $c\bar{s}$ states to all possible two-meson states, DK, D^*K^*, $D_s\eta$, and $D_s\phi$, and a full matrix diagonalization is performed. The results showed that the $c\bar{s}$ component dominates the ground states D_s and D_s^*; the mass shifts are in the range of $-30\sim-36$ MeV. For $1P$ states, $c\bar{s}$ component is not the main component, reaching 45% for 1^3P_0, and 40% for 1^1P_1; and mass shifts are about -60 MeV. The unquenched masses for these states are 1926.9, 2073, 2358.1, and 2456.6 MeV. The contribution of $D_s\eta$, $D_s\phi$ to the mass shifts of $c\bar{s}$ mesons is small, less than 10 MeV, and the probabilities of them in the unquenched states are less than 1%. The results are expected due to the Okubo–Zweig–Iizuka rule violation. It is worth mentioning that the D-wave $D^{(*)}K^{(*)}$ make a comparable contribution to mass shifts of $1P$ states with S-wave $D^{(*)}K^{(*)}$. This result may lead to a convergence problem. It is also interesting to see whether the model can give a better description of charm-strange mesons after fine-tuning the model parameters.

Lattice QCD is a nonperturbative framework to calculate hadron properties, and it has been applied to D_s spectroscopy. The early quenched calculations obtained large masses for the 1^3P_0 states, for example, 2358$\sim$2404 MeV in Ref. [540]. The dynamical lattice QCD simulations do not lower the mass of the state below the DK threshold [541]. Because the state is close to the threshold of DK, the two-meson scattering operator should be included in the simulation. In Ref. [542], $1P$ states of D_s mesons are studied using lattice QCD. In the simulation, $N_f = 2 + 1$ gauge configuration with $m_\pi = 156$ MeV is used. In addition to $q\bar{q}$ operators, the meson–meson interpolators are also included in the correlation functions. The results show that all the $1P$ states are described well. In $J^P = 0^+$ channel, the energy of the state is just above the DK threshold if only $q\bar{q}$ operator is used. When DK scattering operator was included, there are two states; one is a scattering state with energy above DK threshold, and the other is a bound state, which can be identified with the $D_{s0}^*(2317)$. In 1^+ channel, the coupling between 1^1P_1 and 1^3P_1 leads to the energy of the lower state below D^*K threshold if only $q\bar{q}$ operator is used. The inclusion of D^*K scattering operator moves the energy of the state to the experimental value of $D_{s1}(2460)$. Although the analysis shows that there are considerable meson–meson components in $D_{s0}^*(2317)$ and $D_{s1}(2460)$, a quantitative result is expected to verify the outcome of the unquenched quark model.

The unquenched properties of $D_{s0}^*(2317)$ and $D_{s1}(2460)$ are also investigated in other approaches. Simonov et al. calculated the mass shift of 1^1P_1 of $c\bar{s}$ meson using a QCD string model and the chiral Lagrangian [543]. In dealing with two-channel coupling problem, the Feshbach approach is adopted [544], then the problem is reduced to a one-channel one, called the Feshback equation. The results show that the original $c\bar{s}$ mass, 2390 MeV, is shifted to a value of 2317 MeV by coupling to DK channel. Their result is supported by Ref. [545]. The author studied the mass shifts of the $D_s^*(0^+)$ and $D_s(1^{+'})$ and $B_s^*(0^+)$ and $B_s(1^{+'})$ due to the strong coupling to decay channels DK, D^*K, BK, and B^*K based on chiral quark–pion Lagrangian without fitting parameters.

6.3. $N^*(1440)$ *and* $N^*(1535)$

The lightest excited state of nucleon $N^*(1440)$, which was discovered in 1963, also called Roper resonance, has puzzled physicists for decades. Since Gell-Mann proposed the quark model in 1964 [51], the quark model has successfully explained the properties of hadron states by assuming baryons consist of three valence quarks, while mesons are made up of valence quark–antiquark. However, Roper resonance $N^*(1440)$ has defied the efforts of putting the state in the quark model for over fifty years [546]. According to the quark model, the lightest excited state of nucleon should be the angular momentum excitation, i.e., $L = 1$, so the parity should be negative. The radial excitation, which has positive parity, will have higher energy. This statement is correct for a broad class of phenomenological

potentials [547,548]. Experimentally, the lowest resonance N^* with negative parity was found to be $N^*(1535)$, which is heavier than the positive parity Roper resonance $N^*(1440)$. To solve the conflict between experiment and theory, various conjectures are proposed [546]. It is interesting to see that a constituent quark model with only Goldstone-boson exchange (GBE) potential in addition to the confinement potential, which is called the GBE model, can invert the excited state levels [549]. Nevertheless, the validity of the GBE model was questioned by Isgur [550]. In the ChQM, both one-gluon exchange and Goldstone-boson exchange are considered in addition to the confinement potential; Yang et al. carried out a precise numerical calculation with the help of GEM [551]. The order of energy levels of $1P$ and $2S$ can be reversed by using suitable parameters.

So far there is no systematic work to study the baryon spectrum in the unquenched quark model. To solve the "Proton spin crisis", $5q$ components have to be included [552]. By assuming $N^*(1440)$ is the lowest radial excited $3q$ state with a large admixture of $(qqqq\bar{q})$ pentaquark component and $N^*(1535)$ is the lowest $L = 1$ orbital excited $3q$ with a large admixture of $(qqqs\bar{s})$ pentaquark component, the mass difference between $uuds\bar{s}$ and $uudu\bar{u}$ may be responsible for the mass reversion of $N^*(1440)$ and $N^*(1535)$ [553]. The large component $uuds\bar{s}$ in $N^*(1535)$ can naturally explain its large couplings to the channels with strangeness. This point of view is partly supported by the work of Ref. [554]. In a non-relativistic quark model, the authors studied the $qqqq\bar{q}$ component of $N^*(1440)$ by considering the pion and electromagnetic decays and transition form factors. The results showed that by explicitly introducing a sizable, 30%, $qqqq\bar{q}$ component in the low-lying broad $N^*(1440)$ resonance and a smaller such component in the proton, the empirical width for $N^*(1440) \to N\pi$ decay can be explained with the same set of quark model parameters. In the calculation, not only the $qqqq\bar{q}$ component of $N^*(1440)$ but also $qqq(q\bar{q})^2$ component are considered. Actually, their result was confirmed by S. G. Yuan et al. [555] within a constituent quark model. They predict a unity axial charge for $N^*(1440)$ with 30 % $qqqq\bar{q}$ components constrained by the strong and electromagnetic decays.

There is a warning from the work of Morel et al. [556]: stable self energies of low-lying nucleons can be obtained only when the sum over intermediate states runs from ground state of baryons ($N = 0$), lowest-lying negative-parity states ($N = 1$), excited positive-parity states ($N = 2$), to the highly excited negative-parity state ($N = 3$) of baryons. In Ref. [556], the authors studied the masses of non-strange baryons with the corrections from baryon–meson loops. The transition operator of $^3P_0$ model is employed to couple the qqq state to baryon–meson states, and a form factor $\exp(-f^2\boldsymbol{p}^2)$, $\boldsymbol{p}$, the relative momentum between created quark and antiquark, is added to the operator. The calculation takes into account a full set of spin-flavor symmetry-related baryon–meson states,

$$M \in \{\pi, K, \eta, \eta', \rho, \omega, K^*\}, \quad B \in \{N, \Delta, N^*, \Delta^*, \Lambda, \Sigma, \Lambda^*, \Sigma^*\},$$

all excitations of all of the intermediate baryon states up to and including $N = 3$ states. The wave functions of baryons and mesons are obtained from the naïve quark model. The results show that the self energy correction of nucleon and Δ resonance can reach thousands of MeVs. For example, the bare mass of ground state nucleon, 2375 MeV, is shifted to 1087 MeV. This work proposed a question: Does the unquenched quark model converge if the transition operator (even with a form factor) of $^3P_0$ model is employed? In calculating the unquenched mass of a meson, generally, only the ground meson–meson states are included. Is it stable? Further calculations are needed.

6.4. Short Summary

The unquenched quark model is an important step to unify the description of the ordinary and exotic hadrons, at least the q^3 baryons, $q\bar{q}$ mesons, and multiquark states. To incorporate the high Fock components into the valence part, the transition operator to link them has to be introduced. Due to the success of describing strong decay of hadrons, the operator in $^3P_0$ model is commonly invoked. Another reason for using the operator is its simplicity. Another transition operator to use is the one in C^3 model. Its advantage is that

there is no new parameter introduced and there are dynamics. In the direct application of the transition to charmonium states, the mass shifts will be as high as several hundreds of MeVs. It is acceptable for charmonium, although mass shifts are large. Applying this to light meson leads to a diaster; the mass shifts will be thousands MeVs. Although the large mass shifts can be absorbed by renormalizing model parameters, it really destroys the validity of the valence quark model as a zeroth-order approximation. The transition operator has to be modified. For the calculations above, one can see that the percentages of high Fock components are very small, several percents, for the ground states of hadrons by using modified operator. For some exotic hadrons, a large percentage of high Fock component is obtained and the exotic hadrons can be effectively described. So the possibility of unifying the description of hadrons is apparent.

So far, the high Fock component is limited to two hadrons. For multiquark system, the states with two low-lying hadrons cannot establish a complete set; all the excitations of hadrons have to be added to arrive at a complete set. The job is too difficult to be done. Another economic way is to include the low-lying hidden color channels, for example, color octet–octet, to enlarge the model space. Considering that some exotic hadrons can be described as color structure resonances, including multiquark states with various structures in the unquenched quark model is expected.

7. Summary and Perspective

The quark model was formulated in 1964 to classify mesons and baryons. However, QCD does not deny the existence of more complex structures, generically called exotic hadrons, which include four-quark states (tetraquarks), five-quark states (pentaquarks), six-quark states (dibaryons), and states with active gluonic degrees of freedom (hybrids), and even states of pure glue (glueballs). Although only a few of the exotic hadrons are now confirmed by experiment, more and more theoretical work has been devoted to investigate the exotic hadrons. Searching for exotic hadrons is one of the most significant research topics in hadron physics. In this paper, we review the recent experimental and theoretical progress on the tetraquarks and pentaquarks from the perspective of the quark model. By giving this review, we also learn some valuable lessons and gain great inspirations.

(1) Theoretical approaches

QCD is believed to be the fundamental theory of the strong interaction. However, the low-energy phenomena are much harder to calculate directly from QCD. Thus, many theoretical approaches have been developed, such as lattice QCD, effective field theories (EFTs), various phenomenological models, and so on.

Lattice QCD is the non-perturbative theoretical framework to study the hadron spectroscopy starting from first principles. It has provided valuable information on quark confinement between two static colored quarks, preliminary pictures of the QCD vacuum, internal structures of hadrons, phase transitions of strongly interacting matter, and so on. In the past few years, tremendous results calculated by lattice QCD were accurate enough to be compared with both the phenomenological results and the experimental data. Lattice QCD studies of the $X(3872)$ and T_{cc}^{+} states, as well as baryon–baryon interactions, are some of the successful examples which provide an explicit picture of the underlying structures of the exotic states. However, lattice QCD calculations cannot describe all hadron properties well. Furthermore, lattice QCD calculations of exotic hadrons adopt approximations, which reduces their reliability. For instance, lattice QCD studied the $\eta_c N$ and $J/\psi N$ scattering processes for the hidden-charm pentaquark systems, but no resonance or bound state was obtained in Ref. [253]

EFTs are a theoretical tool to investigate exotic states with a clear connection to QCD. In particular, under certain conditions, EFTs are able to describe the systems characterized by several energy scales just on the basis of a few relevant degrees of freedom. However, they are limited by their specific ranges of applicability and need to be supplemented by experimental data or lattice QCD results. Another non-perturbative approach often applied to exotic hadrons is the QCD sum rule method. It is a useful analytical tool aimed

at exploring the properties of the hadronic states by studying directly with intrinsic features of the QCD vacuum encoded in various local condensates. The QCD sum rule has been widely applied to study the mass spectra and decay properties of various exotic hadrons. However, the method depends on the additional assumptions and approximations that make systematic improvements and uncertainty estimations difficult, especially for exotic near-threshold states.

In addition, the QCD-inspired constituent quark model is another successful approach, which has been quite effective in understanding hadron spectroscopy and hadron–hadron interactions even though it cannot be derived from QCD directly. As we know, the quark model plays an important role in the development of hadron physics. The discovery of Ω^- is based on the quark concept proposed by Gell-Mann-Zweig. The naïve quark model of Isgur-Karl gave an extraordinary description of the properties of ground state hadrons. To study the hadron–hadron interaction, multiquark systems, as well as the excited hadrons, extensions to the naïve quark model have to be made. The application of the extended quark model to multiquark systems predicts some bound states or resonances. The prediction of dibaryons d^* and $N\Omega$ were supported by experiments [557,558]. Three hidden-charm resonance states, $\Sigma_c D$ with $J^P = \frac{1}{2}^-$, $\Sigma_c D^*$ with $\frac{3}{2}^-$ and $\frac{1}{2}^-$, were predicted in the model accurately, and finally they were consistent with the experimental report of $P_c(4312)$, $P_c(4440)$, and $P_c(4457)$, respectively. The predictions and confirmation of these states witnessed the success of quark models.

Although various theoretical approaches have achieved some successes in describing exotic hadrons, they often cannot give a consistent explanation for the same hadron state. More efforts are needed to improve these theoretical methods. The discovery of more and more exotic hadronic states will pose great challenges and opportunities to the theoretical development.

(2) Structure of exotic hadrons

The structure is one of the important properties of exotic hadrons. In the theoretical study of $D_{s0}^*(2317)$, one found that the structure of the state has important effect on branching ratio of $B_r(D_{s0}^*(2317) \to \gamma D_s) : B_r(D_{s0}^*(2317) \to \pi^0 D_s)$. If $D_{s0}^*(2317)$ is assumed as a $c\bar{s}$ state, the ratio is not very small, 0.19 [559], while as a DK molecular state, the ratio very small, 10^{-2} [215]. The latest results of BESIII Collaboration showed the absolute branching fraction $B_r(D_{s0}^*(2317) \to \pi^0 D_s)$ is around 1 [533], which means that the DK molecular component dominates $D_{s0}^*(2317)$. The traditional constituent quark model has been very successful in explaining the static properties, such as mass and magnetic moment, of the orbital ground states of the flavor $SU(3)$ octet and decuplet baryons. The predicted Ω baryon with mass around 1670 MeV was discovered by later experiments. However, its predictions for the orbital excited baryons are not so successful. For instance, the lowest excited state $\Lambda^*(1405)$ should be about 130 MeV heavier than $N^*(1535)$ if they have one quark in orbital angular momentum $L = 1$. In addition, if the $N^*(1440)$ is the first radial excited state of the nucleon, it should be heavier than the first angular momentum excited state $N^*(1535)$ because of the energy formula $(2n + L + \frac{3}{2})\hbar\omega$ for a simple harmonic-oscillator potential. However, experimentally, the lowest negative parity state $N^*(1535)$ is heavier than $\Lambda^*(1405)$ and $N^*(1440)$. To explain these phenomena, pentaquark structure is proposed. The authors of Ref. [560] proposed that the $N^*(1535)$ might be the lowest $L = 1$ excited $|uud\rangle$ state with a large admixture of $|uuds\bar{s}\rangle$ pentaquark components and the $N^*(1440)$ is probably the lowest radial excited $|uud\rangle$ state with a large component of $|uudd\bar{d}\rangle$ pentaquarks having two ud diquarks in the relative P-wave. Similarly, the lighter $\Lambda^*(1405)$ has a dominant pentaquark component $|uuds\bar{u}\rangle$ [560].

In the past decade, many new excited heavy baryon and meson states have been discovered by experiments. Plenty of work has been devoted to identify their properties and structures. However, it is still difficult to determine the structure of these states. Some precautions about the proliferation of quark model bound states have to be posed. For a particular multiquark state, there exist different points of view. The unquenched quark model may be a vitally important development of the quark model, where the

valence quarks and real/virtual quark pair are treated equally. The application of the unquenched quark model to $X(3872)$ may be a good test, as it pointed out that $X(3872)$ was a mixture state of $c\bar{c}$ and $D\bar{D}^*$ [90]. By considering the multi-quark coupling effect, the phenomenological quark model is expected to give a unified description of ordinary and exotic hadrons, and important progress may be achieved in the study of the structure of exotic hadrons.

Furthermore, there has been huge controversy on whether the exotic states observed in experiments are molecular states or compact multiquark states. Moreover, some of them were proposed to be caused by the kinematical effects, such as the triangle singularities. These different perspectives have been tremendously improving our understanding of the nature of exotic hadrons and the non-perturbative behaviors of the strong interaction in the low energy region.

(3) Resonances

It is widely known that the most exotic hadrons reported are resonance states. The resonance states lie above the threshold of some strong decay channels and they will decay strongly to other states. So the coupling between the resonance states and the decay channels is important for the observation of the resonance states. For the multiquark system, various structures are obtained by arranging quarks/antiquarks into sub-clusters, and different channels are obtained due to different color, spin, and flavor coupling schemes for each structure. It is easy to obtain stable states for the colorful sub-clusters structure. However, the existence of these states depends on the coupling to open channels. The coupling of bound channels and open channels can shift the energy of the resonance, give the width to the resonance, or even destroy the resonance.

Generally, there always exists many different theoretical interpretations to each experimental observation. In order to provide useful information for the experimental search for exotic hadrons, mass spectrum calculations alone are not enough. The coupling calculation between the bound channels and open channels is inevitable. The study of the scattering process may be an effective way to look for the resonances. Furthermore, the real-scaling method and the complex scaling method are also the valid approaches to investigate the genuine resonances. However, it is still very difficult to confirm the existence of the exotic hadrons and distinguish the various explanations, which requires the joint efforts of both experimentalists and theorists.

Author Contributions: Conceptualization, H.H., C.D. and J.P.; methodology, H.H., C.D. and J.P.; software, J.P.; validation, H.H., C.D., X.L. and Y.T.; formal analysis, H.H. and C.D.; investigation, H.H., C.D., X.L. and Y.T.; resources, J.P.; data curation, J.P.; writing—original draft preparation, H.H., C.D., X.L. and Y.T.; writing—review and editing, J.P.; visualization, H.H. and C.D.; supervision, J.P.; project administration, J.P.; funding acquisition, H.H., C.D., X.L. and J.P. All authors have read and agreed to the published version of the manuscript.

Funding: This work is supported partly by the National Natural Science Foundation of China under Contract Nos. 11675080, 11775118, 11535005 and 12205249. Chongqing Natural Science Foundation under Project No. cstc2019jcyj-msxmX0409 and Fundamental Research Funds for the Central Universities under Contracts No. SWU118111. The China Postdoctoral Science Foundation No. 2021M690626.

Institutional Review Board Statement: Not applicable.

Informed Consent Statement: Not applicable.

Data Availability Statement: Not applicable.

Acknowledgments: We are grateful to Fan Wang for valuable discussions.

Conflicts of Interest: The authors declare no conflicts of interest. Moreover, the funders had no role in the design of the study; in the collection, analyses, or interpretation of data; in the writing of the manuscript; or in the decision to publish the results.

Abbreviations

The following abbreviations are used in this manuscript:

ChQM	Chiral quark model
CMI	Chromomagnetic interaction
CFTM	Color flux-tube model
CQM	Constituent quark Model
C^3	Cornell coupled-channel
EFT	Effective Field Theory
GEM	Gaussian expansion method
GBE	Goldstone boson exchange
HQSS	Heavy-quark spin symmetry
NN	Nucleon–nucleon
OZI	Okubo–Zweig–Iizuka
OBE	One-boson exchange
OGE	One-gluon exchange
OPE	One-pion exchange
PDG	Particle data group
QDCSM	Quark delocalization and color screening model
RGM	Resonating group method
SHO	Simple harmonic oscillator

References

1. Aubert, B. [BaBar Collaboration]. Observation of a narrow meson decaying to $D_s^+\pi^0$ at a mass of 2.32-GeV/c^2. *Phys. Rev. Lett.* **2003**, *90*, 242001. [CrossRef] [PubMed]
2. Choi, S.K. [Belle Collaboration]. Observation of a narrow charmonium-like state in exclusive $B^\pm \to K^\pm\pi^+\pi^- J/\psi$ decays. *Phys. Rev. Lett.* **2003**, *91*, 262001. [CrossRef] [PubMed]
3. Ablikim, M. [BESIII Collaboration]. Observation of a Charged Charmoniumlike Structure in $e^+e^- \to \pi^+\pi^- J/\psi$ at $\sqrt{s}$ =4.26 GeV. *Phys. Rev. Lett.* **2013**, *110*, 252001. [CrossRef]
4. Ablikim, M. [BESIII Collaboration]. Observation of a Charged Charmoniumlike Structure $Z_c(4020)$ and Search for the $Z_c(3900)$ in $e^+e^- \to \pi^+\pi^- h_c$. *Phys. Rev. Lett.* **2013**, *111*, 242001. [CrossRef] [PubMed]
5. Ablikim, M. [BESIII Collaboration]. Observation of a charged charmoniumlike structure in $e^+e^- \to (D^*\bar{D}^*)^\pm\pi^\mp$ at $\sqrt{s} = 4.26$ GeV. *Phys. Rev. Lett.* **2014**, *112*, 132001. [CrossRef]
6. Bondar, A. [Belle Collaboration]. Observation of two charged bottomonium-like resonances in $\Upsilon(5S)$ decays. *Phys. Rev. Lett.* **2012**, *108*, 122001. [CrossRef]
7. Garmash, A. [Belle Collaboration]. Observation of $Z_b(10610)$ and $Z_b(10650)$ Decaying to B Mesons. *Phys. Rev. Lett.* **2016**, *116*, 212001. [CrossRef]
8. Ablikim, M. [BESIII Collaboration]. Observation of a Near-Threshold Structure in the K^+ Recoil-Mass Spectra in $e^+e^- \to K^+(D_s^-D^{*0} + D_s^{*-}D^0)$. *Phys. Rev. Lett.* **2021**, *126*, 102001. [CrossRef]
9. Aaij, R. [LHCb Collaboration]. Observation of $J/\psi p$ Resonances Consistent with Pentaquark States in $\Lambda_b^0 \to J/\psi K^- p$ Decays. *Phys. Rev. Lett.* **2015**, *115*, 072001. [CrossRef]
10. Aaij, R. [LHCb Collaboration]. Observation of a narrow pentaquark state, $P_c(4312)^+$, and of two-peak structure of the $P_c(4450)^+$. *Phys. Rev. Lett.* **2019**, *122*, 222001. [CrossRef]
11. Aaij, R. [LHCb Collaboration]. Observation of structure in the J/ψ -pair mass spectrum. *Sci. Bull.* **2020**, *65*, 1983–1993. [CrossRef]
12. CMS Collaboration. Observation of new structures in the $J/\psi J/\psi$ mass spectrum in pp collisions at $\sqrt{s} = 13$ TeV. *arXiv* **2022**, arXiv:2306.07164.
13. Aaij, R. [LHCb Collaboration]. A model-independent study of resonant structure in $B^+ \to D^+D^-K^+$ decays. *Phys. Rev. Lett.* **2020**, *125*, 242001. [CrossRef] [PubMed]
14. Aaij, R. Observation of an exotic narrow doubly charmed tetraquark. *Nat. Phys.* **2022**, *18*, 751–754. [CrossRef]
15. Chen, H.X.; Chen, W.; Liu, X.; Zhu, S.L. The hidden-charm pentaquark and tetraquark states. *Phys. Rept.* **2016**, *639*, 1–121. [CrossRef]
16. Chen, H.X.; Chen, W.; Liu, X.; Liu, Y.R.; Zhu, S.L. A review of the open charm and open bottom systems. *Rept. Prog. Phys.* **2017**, *80*, 076201. [CrossRef] [PubMed]
17. Liu, Y.R.; Chen, H.X.; Chen, W.; Liu, X.; Zhu, S.L. Pentaquark and Tetraquark states. *Prog. Part. Nucl. Phys.* **2019**, *107*, 237–320. [CrossRef]
18. Brambilla, N.; Eidelman, S.; Hanhart, C.; Nefediev, A.; Shen, C.P.; Thomas, C.E.; Vairo, A.; Yuan, C.Z. The XYZ states: Experimental and theoretical status and perspectives. *Phys. Rept.* **2020**, *873*, 1–154. [CrossRef]
19. Chen, H.X.; Chen, W.; Liu, X.; Liu, Y.R.; Zhu, S.L. An updated review of the new hadron states. *Rept. Prog. Phys.* **2023**, *86*, 026201. [CrossRef]

20. Meng, L.; Wang, B.; Wang, G.J.; Zhu, S.L. Chiral perturbation theory for heavy hadrons and chiral effective field theory for heavy hadronic molecules. *Phys. Rept.* **2023**, *1019*, 1–149. [CrossRef]
21. Isgur, N.; Paton, J.E. A Flux Tube Model for Hadrons in QCD. *Phys. Rev. D* **1985**, *31*, 2910. [CrossRef] [PubMed]
22. Bissey, F.; Cao, F.G.; Kitson, A.R.; Signal, A.I.; Leinweber, D.B.; Lasscock, B.G.; Williams, A.G. Gluon flux-tube distribution and linear confinement in baryons. *Phys. Rev. D* **2007**, *76*, 114512. [CrossRef]
23. Guo, F.K.; Hanhart, C.; Meißner, U.G.; Wang, Q.; Zhao, Q.; Zou, B.S. Hadronic molecules. *Rev. Mod. Phys.* **2018**, *90*, 015004. [CrossRef]
24. Deng, C.; Chen, H.; Ping, J. Towards the understanding of fully-heavy tetraquark states from various models. *Phys. Rev. D* **2021**, *103*, 014001. [CrossRef]
25. Wei, J.; Wang, Y.H.; An, C.S.; Deng, C.R. Color flux-tube nature of the states $T_{cs}(2900)$ and $T^a_{cs}(2900)$. *Phys. Rev. D* **2022**, *106*, 096023. [CrossRef]
26. Jaffe, R.L.; Wilczek, F. Diquarks and exotic spectroscopy. *Phys. Rev. Lett.* **2003**, *91*, 232003. [CrossRef]
27. Huang, H.; Deng, C.; Ping, J. The various configurations of pentaquark in quark models. *J. Phys. G* **2007**, *34*, 1917–1926. [CrossRef]
28. Deng, C.R.; Zhu, S.L. Decoding the double heavy tetraquark state T^+_{cc}. *Sci. Bull.* **2022**, *67*, 1522. [CrossRef]
29. Deng, C.; Ping, J.; Wang, H.; Zhou, P.; Wang, F. QCD quark cyclobutadiene and light tetraquark spectra. *Phys. Rev. D* **2012**, *86*, 114035. [CrossRef]
30. Deng, C.; Ping, J.; Huang, H.; Wang, F. Heavy pentaquark states and a novel color structure. *Phys. Rev. D* **2017**, *95*, 014031. [CrossRef]
31. Ping, J.L.; Deng, C.R.; Wang, F. Quantum chromodynamics quark benzene. *Phys. Lett. B* **2008**, *659*, 607–611. [CrossRef]
32. Richard, J.M. An introduction to the quark model. *arXiv* **2012**, arXiv:1205.4326.
33. Stanley, D.P.; Robson, D. Instability of colored baryons in quark potential models. *Phys. Rev. D* **1981**, *23*, 2776–2778. [CrossRef]
34. Bali, G.S. Casimir scaling of SU(3) static potentials. *Phys. Rev. D* **2000**, *62*, 114503. [CrossRef]
35. Feinberg, G.; Sucher, J. Is There a Strong Van Der Waals Force Between Hadrons? *Phys. Rev. D* **1979**, *20*, 1717. [CrossRef]
36. Greenberg, O.W.; Lipkin, H.J. The Potential Model of Colored Quarks: Success for Single Hadron States, Failure for Hadron-Hadron Interactions. *Nucl. Phys. A* **1981**, *370*, 349–364. [CrossRef]
37. Greenberg, O.W.; Hietarinta, J. Permanent quark confinement without van der Waals forces. *Phys. Lett. B* **1979**, *86*, 309–312. [CrossRef]
38. Lipkin, H.J. Why Explicit Gluonic Components Are Needed in Multi-Quark Wave Functions. *Phys. Lett. B* **1982**, *113*, 490–494. [CrossRef]
39. Dmitrasinovic, V. Color SU(3) symmetry, confinement, stability, and clustering in the q^2 q^2 system. *Phys. Rev. D* **2003**, *67*, 114007. [CrossRef]
40. Okiharu, F.; Suganuma, H.; Takahashi, T.T. First study for the pentaquark potential in SU(3) lattice QCD. *Phys. Rev. Lett.* **2005**, *94*, 192001. [CrossRef]
41. Okiharu, F.; Suganuma, H.; Takahashi, T.T. Detailed analysis of the tetraquark potential and flip-flop in SU(3) lattice QCD. *Phys. Rev. D* **2005**, *72*, 014505. [CrossRef]
42. Takahashi, T.T.; Matsufuru, H.; Nemoto, Y.; Suganuma, H. The Three quark potential in the SU(3) lattice QCD. *Phys. Rev. Lett.* **2001**, *86*, 18–21. [CrossRef] [PubMed]
43. Deng, C.; Ping, J.; Yang, Y.; Wang, F. X(1835), X(2120) and X(2370) in a flux tube model. *Phys. Rev. D* **2012**, *86*, 014008. [CrossRef]
44. Lucha, W.; Schoberl, F.F.; Gromes, D. Bound states of quarks. *Phys. Rept.* **1991**, *200*, 127–240. [CrossRef]
45. Deng, C.; Ping, J.; Wang, F.; Goldman, T. Tetraquark state and multibody interaction. *Phys. Rev. D* **2010**, *82*, 074001. [CrossRef]
46. Deng, C.; Ping, J.; Wang, F. Interpreting $Z_c(3900)$ and $Z_c(4025)/Z_c(4020)$ as charged tetraquark states. *Phys. Rev. D* **2014**, *90*, 054009. [CrossRef]
47. Deng, C.R. Compact hidden charm pentaquark states and QCD isomers. *Phys. Rev. D* **2022**, *105*, 116021. [CrossRef]
48. Huang, H.; Ping, J. Investigating the hidden-charm and hidden-bottom pentaquark resonances in scattering process. *Phys. Rev. D* **2019**, *99*, 014010. [CrossRef]
49. Ping, J.L.; Huang, H.X.; Pang, H.R.; Wang, F.; Wong, C.W. Quark models of dibaryon resonances in nucleon-nucleon scattering. *Phys. Rev. C* **2009**, *79*, 024001. [CrossRef]
50. Godfrey, S.; Napolitano, J. Light meson spectroscopy. *Rev. Mod. Phys.* **1999**, *71*, 1411–1462. [CrossRef]
51. Gell-Mann, M. A Schematic Model of Baryons and Mesons. *Phys. Lett.* **1964**, *8*, 214–215. [CrossRef]
52. Zweig, G. *An SU(3) Model for Strong Interaction Symmetry and Its Breaking, Version 1*; CERN-TH-401; CERN: Geneva, Switzerland, 1964. [CrossRef]
53. Greenberg, O.W. Spin and Unitary Spin Independence in a Paraquark Model of Baryons and Mesons. *Phys. Rev. Lett.* **1964**, *13*, 598–602. [CrossRef]
54. Han, M.Y.; Nambu, Y. Three Triplet Model with Double SU(3) Symmetry. *Phys. Rev.* **1965**, *139*, B1006–B1010. [CrossRef]
55. De Rujula, A.; Georgi, H.; Glashow, S.L. Hadron Masses in a Gauge Theory. *Phys. Rev. D* **1975**, *12*, 147–162. [CrossRef]
56. Appelquist, T.; De Rujula, A.; Politzer, H.D.; Glashow, S.L. Charmonium Spectroscopy. *Phys. Rev. Lett.* **1975**, *34*, 365. [CrossRef]
57. Eichten, E.; Gottfried, K.; Kinoshita, T.; Kogut, J.B.; Lane, K.D.; Yan, T.M. The Spectrum of Charmonium. *Phys. Rev. Lett.* **1975**, *34*, 369–372; Erratum in *Phys. Rev. Lett.* **1976**, *36*, 1276. [CrossRef]
58. Isgur, N.; Karl, G. P Wave Baryons in the Quark Model. *Phys. Rev. D* **1978**, *18*, 4187. [CrossRef]

59. Isgur, N.; Karl, G. Positive Parity Excited Baryons in a Quark Model with Hyperfine Interactions. *Phys. Rev. D* **1979**, *19*, 2653; Erratum in *Phys. Rev. D* **1981**, *23*, 817. [CrossRef]
60. Isgur, N.; Karl, G. Ground State Baryons in a Quark Model with Hyperfine Interactions. *Phys. Rev. D* **1979**, *20*, 1191–1194. [CrossRef]
61. Neudachin, V.G.; Smirnov, Y.F.; Tamagaki, R. An Explanation of n n Repulsive Core in Terms of Forbidden States Based on the Quark Model. *Prog. Theor. Phys.* **1977**, *58*, 1072. [CrossRef]
62. Oka, M.; Yazaki, K. Short Range Part of Nuclear Force and Deuteron in a Quark Model. *Nucl. Phys. A* **1983**, *402*, 477–490; Erratum in *Nucl. Phys. A* **1986**, *458*, 773. [CrossRef]
63. Manohar, A.; Georgi, H. Chiral Quarks and the Nonrelativistic Quark Model. *Nucl. Phys. B* **1984**, *234*, 189–212. [CrossRef]
64. Diakonov, D.; Petrov, V.Y. Instanton Based Vacuum from Feynman Variational Principle. *Nucl. Phys. B* **1984**, *245*, 259–292. [CrossRef]
65. Diakonov, D.; Petrov, V.Y. A Theory of Light Quarks in the Instanton Vacuum. *Nucl. Phys. B* **1986**, *272*, 457–489. [CrossRef]
66. Obukhovsky, I.T.; Kusainov, A.M. The Nucleon nucleon scattering and the baryon spectrum in the quark cluster model with two scales of interaction. *Phys. Lett. B* **1990**, *238*, 142–148. [CrossRef]
67. Fernandez, F.; Valcarce, A.; Straub, U.; Faessler, A. The Nucleon-nucleon interaction in terms of quark degrees of freedom. *J. Phys. G* **1993**, *19*, 2013–2026. [CrossRef]
68. Valcarce, A.; Fernandez, F.; Gonzalez, P.; Vento, V. Chiral quark cluster model study of the low-energy baryon spectrum. *Phys. Lett. B* **1996**, *367*, 35–39. [CrossRef]
69. Glozman, L.Y.; Riska, D.O. The Spectrum of the nucleons and the strange hyperons and chiral dynamics. *Phys. Rept.* **1996**, *268*, 263–303. [CrossRef]
70. Vijande, J.; Fernandez, F.; Valcarce, A. Constituent quark model study of the meson spectra. *J. Phys. G* **2005**, *31*, 481. [CrossRef]
71. Fujiwara, Y.; Nakamoto, C.; Suzuki, Y. Effective meson exchange potentials in the SU(6) quark model for N N and Y N interactions. *Phys. Rev. C* **1996**, *54*, 2180–2200. [CrossRef]
72. Fujiwara, Y.; Fujita, T.; Kohno, M.; Nakamoto, C.; Suzuki, Y. Resonating group study of baryon baryon interactions for the complete baryon octet: N N interaction. *Phys. Rev. C* **2001**, *65*, 014002. [CrossRef]
73. Fujiwara, Y.; Miyagawa, K.; Kohno, M.; Suzuki, Y.; Nakamoto, C. A realistic baryon-baryon interaction in the SU(6) quark model and its applications to few-baryon systems. *Nucl. Phys. A* **2004**, *737*, 243–247. [CrossRef]
74. Fujiwara, Y.; Kohno, M.; Nakamoto, C.; Suzuki, Y. Interactions between octet baryons in the SU(6) quark model. *Phys. Rev. C* **2001**, *64*, 054001. [CrossRef]
75. Wang, F.; Wu, G.H.; Teng, L.J.; Goldman, J.T. Quark delocalization, color screening, and nuclear intermediate range attraction. *Phys. Rev. Lett.* **1992**, *69*, 2901–2904. [CrossRef]
76. Wang, F.; Ping, J.L.; Wu, G.H.; Teng, L.J.; Goldman, J.T. Quark delocalization, color screening and dibaryons. *Phys. Rev. C* **1995**, *51*, 3411. [CrossRef]
77. Huang, H.; Ping, J.; Wang, F. Prediction of $N\Omega$-like dibaryons with heavy quarks. *Phys. Rev. C* **2020**, *101*, 015204. [CrossRef]
78. Huang, H.; Deng, C.; Ping, J.; Wang, F. Possible pentaquarks with heavy quarks. *Eur. Phys. J. C* **2016**, *76*, 624. [CrossRef]
79. Ping, J.L.; Wang, F.; Goldman, J.T. The d* dibaryon in the extended quark delocalization, color screening model. *Phys. Rev. C* **2002**, *65*, 044003. [CrossRef]
80. Ping, J.L.; Wang, F.; Goldman, J.T. Effective baryon baryon potentials in the quark delocalization and color screening model. *Nucl. Phys. A* **1999**, *657*, 95–109. [CrossRef]
81. Jin, X.; Xue, Y.; Huang, H.; Ping, J. Full-heavy tetraquarks in constituent quark models. *Eur. Phys. J. C* **2020**, *80*, 1083. [CrossRef]
82. Kondo, K.I.; Kato, S.; Shibata, A.; Shinohara, T. Quark confinement: Dual superconductor picture based on a non-Abelian Stokes theorem and reformulations of Yang–Mills theory. *Phys. Rept.* **2015**, *579*, 1–226. [CrossRef]
83. Weinstein, J.D.; Isgur, N. Do Multi-Quark Hadrons Exist? *Phys. Rev. Lett.* **1982**, *48*, 659. [CrossRef]
84. Weinstein, J.D.; Isgur, N. K anti-K Molecules. *Phys. Rev. D* **1990**, *41*, 2236. [CrossRef] [PubMed]
85. Robson, D. Hadron Hadron Interactions with Orthogonal Lattice Gauge Field Configurations. 1. General Outlook. *Phys. Rev. D* **1987**, *35*, 1018–1028. [CrossRef]
86. Alexandrou, C.; De Forcrand, P.; Tsapalis, A. The Static three quark SU(3) and four quark SU(4) potentials. *Phys. Rev. D* **2002**, *65*, 054503. [CrossRef]
87. Takahashi, T.T.; Suganuma, H.; Nemoto, Y.; Matsufuru, H. Detailed analysis of the three quark potential in SU(3) lattice QCD. *Phys. Rev. D* **2002**, *65*, 114509. [CrossRef]
88. Deng, C.; Ping, J.; Huang, H.; Wang, F. Hidden charmed states and multibody color flux-tube dynamics. *Phys. Rev. D* **2018**, *98*, 014026. [CrossRef]
89. Tornqvist, N.A. The Meson Mass Spectrum and Unitarity. *Ann. Phys.* **1979**, *123*, 1. [CrossRef]
90. Tan, Y.; Ping, J. X(3872) in an unquenched quark model. *Phys. Rev. D* **2019**, *100*, 034022. [CrossRef]
91. Micu, L. Decay rates of meson resonances in a quark model. *Nucl. Phys. B* **1969**, *10*, 521–526. [CrossRef]
92. Le Yaouanc, A.; Oliver, L.; Pene, O.; Raynal, J.C. Naive quark pair creation model of strong interaction vertices. *Phys. Rev. D* **1973**, *8*, 2223–2234. [CrossRef]
93. Le Yaouanc, A.; Oliver, L.; Pene, O.; Raynal, J.C. Naive quark pair creation model and baryon decays. *Phys. Rev. D* **1974**, *9*, 1415–1419. [CrossRef]

94. Le Yaouanc, A.; Oliver, L.; Pene, O.; Raynal, J.C. Resonant Partial Wave Amplitudes in $\pi N \to \pi\pi N$ According to the Naive Quark Pair Creation Model. *Phys. Rev. D* **1975**, *11*, 1272. [CrossRef]
95. Roberts, W.; Silvestre-Brac, B. General method of calculation of any hadronic decay in the $^3P_0$ model. *Few Body Syst.* **1992**, *11*, 171–193. [CrossRef]
96. Kalashnikova, Y.S. Coupled-channel model for charmonium levels and an option for X(3872). *Phys. Rev. D* **2005**, *72*, 034010. [CrossRef]
97. Ferretti, J.; Galatà, G.; Santopinto, E. Interpretation of the X(3872) as a charmonium state plus an extra component due to the coupling to the meson-meson continuum. *Phys. Rev. C* **2013**, *88*, 015207. [CrossRef]
98. Ortega, P.G.; Segovia, J.; Entem, D.R.; Fernandez, F. Coupled channel approach to the structure of the X(3872). *Phys. Rev. D* **2010**, *81*, 054023. [CrossRef]
99. Hwang, D.S.; Kim, D.W. Mass shift of $D_{sj}^*(2317)$ by coupled channel effect. *J. Phys. Conf. Ser.* **2005**, *9*, 63–66. [CrossRef]
100. Mohler, D.; Lang, C.B.; Leskovec, L.; Prelovsek, S.; Woloshyn, R.M. $D_{s0}^*(2317)$ Meson and D-Meson-Kaon Scattering from Lattice QCD. *Phys. Rev. Lett.* **2013**, *111*, 222001. [CrossRef]
101. Bali, G.S.; Collins, S.; Cox, A.; Schäfer, A. Masses and decay constants of the $D_{s0}^*(2317)$ and $D_{s1}(2460)$ from $N_f = 2$ lattice QCD close to the physical point. *Phys. Rev. D* **2017**, *96*, 074501. [CrossRef]
102. Chen, X.; Ping, J.; Roberts, C.D.; Segovia, J. Light-meson masses in an unquenched quark model. *Phys. Rev. D* **2018**, *97*, 094016. [CrossRef]
103. Barnes, T.; Swanson, E.S. Hadron loops: General theorems and application to charmonium. *Phys. Rev. C* **2008**, *77*, 055206. [CrossRef]
104. Ping, J.; Deng, C.; Huang, H.; Dong, F.F.; Wang, F. Quark models for mesons. *EPJ Web Conf.* **2012**, *20*, 01007. [CrossRef]
105. Ferretti, J.; Santopinto, E. Threshold corrections of $\chi_c(2P)$ and $\chi_b(3P)$ states and $J\psi\rho$ and $J/\psi\omega$ transitions of the $\chi(3872)$ in a coupled-channel model. *Phys. Lett. B* **2019**, *789*, 550–555. [CrossRef]
106. Eichten, E.; Gottfried, K.; Kinoshita, T.; Lane, K.D.; Yan, T.M. The Interplay of Confinement and Decay in the Spectrum of Charmonium. *Phys. Rev. Lett.* **1976**, *36*, 500. [CrossRef]
107. Eichten, E.; Gottfried, K.; Kinoshita, T.; Lane, K.D.; Yan, T.M. Charmonium: Comparison with Experiment. *Phys. Rev. D* **1980**, *21*, 203. [CrossRef]
108. Briceno, R.A.; Dudek, J.J.; Young, R.D. Scattering processes and resonances from lattice QCD. *Rev. Mod. Phys.* **2018**, *90*, 025001. [CrossRef]
109. Kondo, Y.; Morimatsu, O.; Nishikawa, T. Two-hadron-irreducible QCD sum rule for pentaquark baryon. *Phys. Lett. B* **2005**, *611*, 93–101. [CrossRef]
110. Lee, S.H.; Kim, H.; Kwon, Y. Parity of $\Theta^+(1540)$ from QCD sum rules. *Phys. Lett. B* **2005**, *609*, 252–258. [CrossRef]
111. Lee, H.J.; Kochelev, N.I. On the $\pi\pi$ contribution to the QCD sum rules for the light tetraquark. *Phys. Rev. D* **2008**, *78*, 076005. [CrossRef]
112. Chen, H.X.; Hosaka, A.; Toki, H.; Zhu, S.L. Light Scalar Meson $\sigma(600)$ in QCD Sum Rule with Continuum. *Phys. Rev. D* **2010**, *81*, 114034. [CrossRef]
113. Albuquerque, R.M.; Dias, J.M.; Khemchandani, K.P.; Martínez Torres, A.; Navarra, F.S.; Nielsen, M.; Zanetti, C.M. QCD sum rules approach to the X, Y and Z states. *J. Phys. G* **2019**, *46*, 093002. [CrossRef]
114. Feshbach, H. A Unified theory of nuclear reactions. 2. *Ann. Phys.* **1962**, *19*, 287–313. [CrossRef]
115. Tang, Y.C.; Lemere, M.; Thompson, D.R. Resonating-group method for nuclear many-body problems. *Phys. Rept.* **1978**, *47*, 167–223. [CrossRef]
116. Kamimura, M. Chapter V. A Coupled Channel Variational Method for Microscopic Study of Reactions between Complex Nuclei. *Prog. Theor. Phys. Suppl.* **1977**, *62*, 236–294. [CrossRef]
117. Simons, J. Resonance state lifetimes from stabilization graphs. *J. Chem. Phys.* **1981**, *75*, 2465. [CrossRef]
118. Aguilar, J.; Combes, J.M. A class of analytic perturbations for one-body schroedinger hamiltonians. *Commun. Math. Phys.* **1971**, *22*, 269–279. [CrossRef]
119. Balslev, E.; Combes, J.M. Spectral properties of many-body schroedinger operators with dilatation-analytic interactions. *Commun. Math. Phys.* **1971**, *22*, 280–294. [CrossRef]
120. Ho, Y. The method of complex coordinate rotation and its applications to atomic collision processes. *Phys. Rep.* **1983**, *99*, 1–68. [CrossRef]
121. Moiseyev, N. Quantum theory of resonances: Calculating energies, widths and cross-sections by complex scaling. *Phys. Rep.* **1998**, *302*, 212–293. [CrossRef]
122. Myo, T.; Kikuchi, Y.; Masui, H.; Katō, K. Recent development of complex scaling method for many-body resonances and continua in light nuclei. *Prog. Part. Nucl. Phys.* **2014**, *79*, 1–56. [CrossRef]
123. Yang, G.; Ping, J.; Segovia, J. Doubly-heavy tetraquarks. *Phys. Rev. D* **2020**, *101*, 014001. [CrossRef]
124. Ader, J.P.; Richard, J.M.; Taxil, P. Do narrow heavy multiquark states exist? *Phys. Rev. D* **1982**, *25*, 2370. [CrossRef]
125. Ballot, J.l.; Richard, J.M. Four quark states in additive potentials. *Phys. Lett. B* **1983**, *123*, 449–451. [CrossRef]
126. Carlson, J.; Heller, L.; Tjon, J.A. Stability of Dimesons. *Phys. Rev. D* **1988**, *37*, 744. [CrossRef]
127. Zouzou, S.; Silvestre-Brac, B.; Gignoux, C.; Richard, J.M. Four quark bound states. *Z. Phys. C* **1986**, *30*, 457. [CrossRef]
128. Silvestre-Brac, B.; Semay, C. Spectrum and decay properties of diquonia. *Z. Phys. C* **1993**, *59*, 457–470. [CrossRef]

129. Brink, D.M.; Stancu, F. Tetraquarks with heavy flavors. *Phys. Rev. D* **1998**, *57*, 6778–6787. [CrossRef]
130. Vijande, J.; Valcarce, A.; Tsushima, K. Dynamical study of QQ-$\bar{u}\bar{d}$ mesons. *Phys. Rev. D* **2006**, *74*, 054018. [CrossRef]
131. Yang, Y.; Deng, C.; Ping, J.; Goldman, T. S-wave $QQ\bar{q}\bar{q}$ state in the constituent quark model. *Phys. Rev. D* **2009**, *80*, 114023. [CrossRef]
132. Manohar, A.V.; Wise, M.B. Exotic $QQ\bar{q}\bar{q}$ states in QCD. *Nucl. Phys. B* **1993**, *399*, 17–33. [CrossRef]
133. Vijande, J.; Valcarce, A.; Richard, J.M. Stability of multiquarks in a simple string model. *Phys. Rev. D* **2007**, *76*, 114013. [CrossRef]
134. Ay, C.; Richard, J.M.; Rubinstein, J.H. Stability of asymmetric tetraquarks in the minimal-path linear potential. *Phys. Lett. B* **2009**, *674*, 227–231. [CrossRef]
135. Bicudo, P.; Wagner, M. Lattice QCD signal for a bottom-bottom tetraquark. *Phys. Rev. D* **2013**, *87*, 114511. [CrossRef]
136. Ikeda, Y.; Charron, B.; Aoki, S.; Doi, T.; Hatsuda, T.; Inoue, T.; Ishii, N.; Murano, K.; Nemura, H.; Sasaki, K. Charmed tetraquarks T_{cc} and T_{cs} from dynamical lattice QCD simulations. *Phys. Lett. B* **2014**, *729*, 85–90. [CrossRef]
137. Du, M.L.; Chen, W.; Chen, X.L.; Zhu, S.L. Exotic $QQ\bar{q}\bar{q}$, $QQ\bar{q}\bar{s}$ and $QQ\bar{s}\bar{s}$ states. *Phys. Rev. D* **2013**, *87*, 014003. [CrossRef]
138. Chen, W.; Steele, T.G.; Zhu, S.L. Exotic open-flavor $bc\bar{q}\bar{q}$, $bc\bar{s}\bar{s}$ and $qc\bar{q}\bar{b}$, $sc\bar{s}\bar{b}$ tetraquark states. *Phys. Rev. D* **2014**, *89*, 054037. [CrossRef]
139. Aaij, R. Observation of the doubly charmed baryon Ξ_{cc}^{++}. *Phys. Rev. Lett.* **2017**, *119*, 112001. [CrossRef]
140. Deng, C.; Chen, H.; Ping, J. Systematical investigation on the stability of doubly heavy tetraquark states. *Eur. Phys. J. A* **2020**, *56*, 9. [CrossRef]
141. Karliner, M.; Rosner, J.L. Discovery of doubly-charmed Ξ_{cc} baryon implies a stable $(bb\bar{u}\bar{d})$ tetraquark. *Phys. Rev. Lett.* **2017**, *119*, 202001. [CrossRef]
142. Eichten, E.J.; Quigg, C. Heavy-quark symmetry implies stable heavy tetraquark mesons $Q_iQ_j\bar{q}_k\bar{q}_l$. *Phys. Rev. Lett.* **2017**, *119*, 202002. [CrossRef] [PubMed]
143. Francis, A.; Hudspith, R.J.; Lewis, R.; Maltman, K. Lattice Prediction for Deeply Bound Doubly Heavy Tetraquarks. *Phys. Rev. Lett.* **2017**, *118*, 142001. [CrossRef] [PubMed]
144. Bicudo, P.; Scheunert, J.; Wagner, M. Including heavy spin effects in the prediction of a $b\bar{b}ud$ tetraquark with lattice QCD potentials. *Phys. Rev. D* **2017**, *95*, 034502. [CrossRef]
145. Czarnecki, A.; Leng, B.; Voloshin, M.B. Stability of tetrons. *Phys. Lett. B* **2018**, *778*, 233–238. [CrossRef]
146. Agaev, S.S.; Azizi, K.; Barsbay, B.; Sundu, H. Weak decays of the axial-vector tetraquark $T^-_{bb;\bar{u}\bar{d}}$. *Phys. Rev. D* **2019**, *99*, 033002. [CrossRef]
147. Francis, A.; Hudspith, R.J.; Lewis, R.; Maltman, K. Evidence for charm-bottom tetraquarks and the mass dependence of heavy-light tetraquark states from lattice QCD. *Phys. Rev. D* **2019**, *99*, 054505. [CrossRef]
148. Lü, Q.F.; Chen, D.Y.; Dong, Y.B. Masses of doubly heavy tetraquarks $T_{QQ'}$ in a relativized quark model. *Phys. Rev. D* **2020**, *102*, 034012. [CrossRef]
149. Braaten, E.; He, L.P.; Mohapatra, A. Masses of doubly heavy tetraquarks with error bars. *Phys. Rev. D* **2021**, *103*, 016001. [CrossRef]
150. Aaij, R. Study of the doubly charmed tetraquark T_{cc}^+. *Nat. Commun.* **2022**, *13*, 3351. [CrossRef]
151. Li, N.; Sun, Z.F.; Liu, X.; Zhu, S.L. Coupled-channel analysis of the possible $D^{(*)}D^{(*)}$, $\overline{B}^{(*)}\overline{B}^{(*)}$ and $D^{(*)}\overline{B}^{(*)}$ molecular states. *Phys. Rev. D* **2013**, *88*, 114008. [CrossRef]
152. Meng, L.; Wang, G.J.; Wang, B.; Zhu, S.L. Probing the long-range structure of the T_{cc}^+ with the strong and electromagnetic decays. *Phys. Rev. D* **2021**, *104*, 051502. [CrossRef]
153. Weng, X.Z.; Deng, W.Z.; Zhu, S.L. Doubly heavy tetraquarks in an extended chromomagnetic model. *Chin. Phys. C* **2022**, *46*, 013102. [CrossRef]
154. Deng, C.; Zhu, S.L. T_{cc}^+ and its partners. *Phys. Rev. D* **2022**, *105*, 054015. [CrossRef]
155. Feijoo, A.; Liang, W.H.; Oset, E. $D_0D_0\pi^+$ mass distribution in the production of the T_{cc} exotic state. *Phys. Rev. D* **2021**, *104*, 114015. [CrossRef]
156. Yan, M.J.; Valderrama, M.P. Subleading contributions to the decay width of the T_{cc}^+ tetraquark. *Phys. Rev. D* **2022**, *105*, 014007. [CrossRef]
157. Fleming, S.; Hodges, R.; Mehen, T. T_{cc}^+ decays: Differential spectra and two-body final states. *Phys. Rev. D* **2021**, *104*, 116010. [CrossRef]
158. Li, N.; Sun, Z.F.; Liu, X.; Zhu, S.L. Perfect DD^* molecular prediction matching the T_{cc} observation at LHCb. *Chin. Phys. Lett.* **2021**, *38*, 092001. [CrossRef]
159. Wu, T.W.; Pan, Y.W.; Liu, M.Z.; Luo, S.Q.; Geng, L.S.; Liu, X. Discovery of the doubly charmed Tcc+ state implies a triply charmed Hccc hexaquark state. *Phys. Rev. D* **2022**, *105*, L031505. [CrossRef]
160. Ling, X.Z.; Liu, M.Z.; Geng, L.S.; Wang, E.; Xie, J.J. Can we understand the decay width of the T_{cc}^+ state? *Phys. Lett. B* **2022**, *826*, 136897. [CrossRef]
161. Chen, R.; Huang, Q.; Liu, X.; Zhu, S.L. Predicting another doubly charmed molecular resonance $T_{cc}^+(3876)$. *Phys. Rev. D* **2021**, *104*, 114042. [CrossRef]
162. Dai, L.Y.; Sun, X.; Kang, X.W.; Szczepaniak, A.P.; Yu, J.S. Pole analysis on the doubly charmed meson in D0D0π+ mass spectrum. *Phys. Rev. D* **2022**, *105*, L051507. [CrossRef]

163. Xin, Q.; Wang, Z.G. Analysis of the doubly-charmed tetraquark molecular states with the QCD sum rules. *Eur. Phys. J. A* **2022**, *58*, 110. [CrossRef]
164. Guo, T.; Li, J.; Zhao, J.; He, L. Mass spectra of doubly heavy tetraquarks in an improved chromomagnetic interaction model. *Phys. Rev. D* **2022**, *105*, 014021. [CrossRef]
165. Kim, Y.; Oka, M.; Suzuki, K. Doubly heavy tetraquarks in a chiral-diquark picture. *Phys. Rev. D* **2022**, *105*, 074021. [CrossRef]
166. Agaev, S.S.; Azizi, K.; Sundu, H. Newly observed exotic doubly charmed meson T_{cc}^{+}. *Nucl. Phys. B* **2022**, *975*, 115650. [CrossRef]
167. Agaev, S.S.; Azizi, K.; Sundu, H. Hadronic molecule model for the doubly charmed state T_{cc}^{+}. *J. High Energy Phys.* **2022**, *6*, 57. [CrossRef]
168. Jaffe, R.L. Exotica. *Phys. Rept.* **2005**, *409*, 1–45. [CrossRef]
169. Anselmino, M.; Predazzi, E.; Ekelin, S.; Fredriksson, S.; Lichtenberg, D.B. Diquarks. *Rev. Mod. Phys.* **1993**, *65*, 1199–1234. [CrossRef]
170. Barabanov, M.Y. Diquark correlations in hadron physics: Origin, impact and evidence. *Prog. Part. Nucl. Phys.* **2021**, *116*, 103835. [CrossRef]
171. Zhang, J.; Wang, J.B.; Li, G.; An, C.S.; Deng, C.R.; Xie, J.J. Spectrum of the S-wave fully-heavy tetraquark states. *Eur. Phys. J. C* **2022**, *82*, 1126. [CrossRef]
172. Ohkoda, S.; Yamaguchi, Y.; Yasui, S.; Sudoh, K.; Hosaka, A. Exotic Mesons with Hidden Bottom near Thresholds. *Phys. Rev. D* **2012**, *86*, 014004. [CrossRef]
173. Bali, G.; Hetzenegger, M. Static-light meson-meson potentials. *PoS* **2011**, *105*, 142. [CrossRef]
174. Dias, J.M.; Narison, S.; Navarra, F.S.; Nielsen, M.; Richard, J.M. Relation between $T_{cc,bb}$ and $X_{c,b}$ from QCD. *Phys. Lett. B* **2011**, *703*, 274–280. [CrossRef]
175. Bicudo, P.; Peters, A.; Velten, S.; Wagner, M. Importance of meson-meson and of diquark-antidiquark creation operators for a $\bar{b}\bar{b}ud$ tetraquark. *Phys. Rev. D* **2021**, *103*, 114506. [CrossRef]
176. Junnarkar, P.; Mathur, N.; Padmanath, M. Study of doubly heavy tetraquarks in Lattice QCD. *Phys. Rev. D* **2019**, *99*, 034507. [CrossRef]
177. Richard, J.M.; Valcarce, A.; Vijande, J. Tetraquarks: Relativistic corrections and other issues. *Rev. Mex. Fis. Suppl.* **2022**, *3*, 0308110. [CrossRef]
178. Maiani, L.; Polosa, A.D.; Riquer, V. Hydrogen bond of QCD in doubly heavy baryons and tetraquarks. *Phys. Rev. D* **2019**, *100*, 074002. [CrossRef]
179. Chen, X.; Yang, Y. Doubly-heavy tetraquark states $cc\bar{u}\bar{d}$ and $bb\bar{u}\bar{d}$. *Chin. Phys. C* **2022**, *46*, 054103. [CrossRef]
180. Vijande, J.; Valcarce, A. Tetraquark Spectroscopy: A Symmetry Analysis. *Symmetry* **2009**, *1*, 155–179. [CrossRef]
181. Santowsky, N.; Fischer, C.S. Four-quark states with charm quarks in a two-body Bethe–Salpeter approach. *Eur. Phys. J. C* **2022**, *82*, 313. [CrossRef]
182. Pflaumer, M.; Leskovec, L.; Meinel, S.; Wagner, M. Existence and Non-Existence of Doubly Heavy Tetraquark Bound States. *PoS* **2022**, *396*, 392. [CrossRef]
183. Dai, L.R.; Oset, E.; Feijoo, A.; Molina, R.; Roca, L.; Torres, A.M.; Khemchandani, K.P. Masses and widths of the exotic molecular B(s)(*)B(s)(*) states. *Phys. Rev. D* **2022**, *105*, 074017; Erratum in *Phys. Rev. D* **2022**, *106*, 099904 [CrossRef]
184. Caramés, T.F.; Vijande, J.; Valcarce, A. Exotic $bc\bar{q}\bar{q}$ four-quark states. *Phys. Rev. D* **2019**, *99*, 014006. [CrossRef]
185. Padmanath, M.; Mathur, N. $\bar{b}\bar{c}\,q_1q_2$four-quark states from Lattice QCD. *arXiv* **2021**, arXiv:2111.01147.
186. Hudspith, R.J.; Colquhoun, B.; Francis, A.; Lewis, R.; Maltman, K. A lattice investigation of exotic tetraquark channels. *Phys. Rev. D* **2020**, *102*, 114506. [CrossRef]
187. Wang, Q.N.; Chen, W. Fully open-flavor tetraquark states $bc\bar{q}\bar{s}$ and $sc\bar{q}\bar{b}$ with $J^P = 0^+, 1^+$. *Eur. Phys. J. C* **2020**, *80*, 389. [CrossRef]
188. Dai, L.R.; Molina, R.; Oset, E. Prediction of new T_{cc} states of D*D* and Ds*D* molecular nature. *Phys. Rev. D* **2022**, *105*, 016029. [CrossRef]
189. Karliner, M.; Rosner, J.L. Doubly charmed strange tetraquark. *Phys. Rev. D* **2022**, *105*, 034020. [CrossRef]
190. Gao, X.Y.; Li, Y.; Shen, C.P.; Adachi, I.; Aihara, H.; Asner, D.M.; Atmacan, H.; Aushev, T.; Ayad, R.; Behera, P.; et al. Search for tetraquark states $X_{cc\bar{s}\bar{s}}$ in $D_s^+D_s^+(D_s^{*+}D_s*+)$ final states at Belle. *Phys. Rev. D* **2022**, *105*, 032002. [CrossRef]
191. Wu, Y.; Jin, X.; Liu, R.; Huang, H.; Ping, J. The study of double-charm and double-strange tetraquarks. *arXiv* **2021**, arXiv:2112.05967.
192. Ke, H.W.; Shi, Y.L. Study of possible molecular states of Ds(*)Ds(*) and Bs(*)Bs(*). *Phys. Rev. D* **2022**, *105*, 114019. [CrossRef]
193. Brodsky, S.J.; Schmidt, I.A.; de Teramond, G.F. Nuclear bound quarkonium. *Phys. Rev. Lett.* **1990**, *64*, 1011. [CrossRef]
194. Donnachie, A.; Landshoff, P.V. Elastic Scattering and Diffraction Dissociation. *Nucl. Phys. B* **1984**, *244*, 322. [CrossRef]
195. Wasson, D.A. Comment on 'Nuclear bound quarkonium'. *Phys. Rev. Lett.* **1991**, *67*, 2237. [CrossRef]
196. Dalitz, R.H.; Tuan, S.F. A possible resonant state in pion-hyperon scattering. *Phys. Rev. Lett.* **1959**, *2*, 425–428. [CrossRef]
197. Alston, M.H.; Alvarez, L.W.; Eberhard, P.; Good, M.L.; Graziano, W.; Ticho, H.K.; Wojcicki, S.G. Study of Resonances of the Sigma-pi System. *Phys. Rev. Lett.* **1961**, *6*, 698–702. [CrossRef]
198. Weinstein, J.D.; Isgur, N. The q q $\bar{q}\bar{q}$ System in a Potential Model. *Phys. Rev. D* **1983**, *27*, 588. [CrossRef]
199. Voloshin, M.B.; Okun, L.B. Hadron Molecules and Charmonium Atom. *JETP Lett.* **1976**, *23*, 333–336.
200. De Rujula, A.; Georgi, H.; Glashow, S.L. Molecular Charmonium: A New Spectroscopy? *Phys. Rev. Lett.* **1977**, *38*, 317. [CrossRef]
201. Tornqvist, N.A. On deusons or deuteron-like meson meson bound states. *Nuovo Cim. A* **1994**, *107*, 2471–2476. [CrossRef]

202. Tornqvist, N.A. From the deuteron to deusons, an analysis of deuteron-like meson meson bound states. *Z. Phys. C* **1994**, *61*, 525–537. [CrossRef]
203. Bai, J.Z. Observation of a near threshold enhancement in th $p\bar{p}$ mass spectrum from radiative $J/\psi \to \gamma\ p\bar{p}$ decays. *Phys. Rev. Lett.* **2003**, *91*, 022001. [CrossRef]
204. Datta, A.; O'Donnell, P.J. A New state of baryonium. *Phys. Lett. B* **2003**, *567*, 273–276. [CrossRef]
205. Gao, C.S.; Zhu, S.L. Understanding the possible proton anti-proton bound state observed by BES collaboration. *Commun. Theor. Phys.* **2004**, *42*, 844. [CrossRef]
206. Liu, X.; Zeng, X.Q.; Ding, Y.B.; Li, X.Q.; Shen, H.; Shen, P.N. Can the observed enhancement in the mass spectrum of $p\bar{p}$ in $J/\psi \to \gamma\ p\bar{p}$ be interpreted by a possible $p\bar{p}$ bound state. *arXiv* **2004**, arXiv:hep-ph/0406118.
207. Swanson, E.S. Short range structure in the X(3872). *Phys. Lett. B* **2004**, *588*, 189–195. [CrossRef]
208. Besson, D.; Anderson, S.; Frolov, V.V.; Gong, D.T.; Kubota, Y.; Li, S.Z.; Poling, R.; Smith, A.; Stepaniak, C.J.; Urheim, J.; et al. Observation of a narrow resonance of mass 2.46 GeV/c^2 decaying to $D_s^{*+}\pi^0$ and confirmation of the $D_{sJ}(2317)$ state. *Phys. Rev. D* **2003**, *68*, 032002; Erratum in *Phys. Rev. D* **2007**, *75*, 119908. [CrossRef]
209. Barnes, T.; Close, F.E.; Lipkin, H.J. Implications of a DK molecule at 2.32-GeV. *Phys. Rev. D* **2003**, *68*, 054006. [CrossRef]
210. Szczepaniak, A.P. Description of the $D_s^*(2320)$ resonance as the $D\pi$ atom. *Phys. Lett. B* **2003**, *567*, 23–26. [CrossRef]
211. van Beveren, E.; Rupp, G. Observed $D_s(2317)$ and tentative $D(2100–2300)$ as the charmed cousins of the light scalar nonet. *Phys. Rev. Lett.* **2003**, *91*, 012003. [CrossRef]
212. Hofmann, J.; Lutz, M.F.M. Open charm meson resonances with negative strangeness. *Nucl. Phys. A* **2004**, *733*, 142–152. [CrossRef]
213. Kolomeitsev, E.E.; Lutz, M.F.M. On Heavy light meson resonances and chiral symmetry. *Phys. Lett. B* **2004**, *582*, 39–48. [CrossRef]
214. Guo, F.K.; Shen, P.N.; Chiang, H.C.; Ping, R.G.; Zou, B.S. Dynamically generated 0^+ heavy mesons in a heavy chiral unitary approach. *Phys. Lett. B* **2006**, *641*, 278–285. [CrossRef]
215. Faessler, A.; Gutsche, T.; Lyubovitskij, V.E.; Ma, Y.L. Strong and radiative decays of the $D_{s0}(2317)$ meson in the DK-molecule picture. *Phys. Rev. D* **2007**, *76*, 014005. [CrossRef]
216. Flynn, J.M.; Nieves, J. Elastic s-wave Bπ, Dπ, DK and Kπ scattering from lattice calculations of scalar form-factors in semileptonic decays. *Phys. Rev. D* **2007**, *75*, 074024. [CrossRef]
217. Gamermann, D.; Oset, E.; Strottman, D.; Vicente Vacas, M.J. Dynamically generated open and hidden charm meson systems. *Phys. Rev. D* **2007**, *76*, 074016. [CrossRef]
218. Guo, F.K.; Shen, P.N.; Chiang, H.C. Dynamically generated 1^+ heavy mesons. *Phys. Lett. B* **2007**, *647*, 133–139. [CrossRef]
219. Cleven, M.; Guo, F.K.; Hanhart, C.; Meissner, U.G. Light meson mass dependence of the positive parity heavy-strange mesons. *Eur. Phys. J. A* **2011**, *47*, 19. [CrossRef]
220. Wu, X.G.; Zhao, Q. The mixing of $D_{s1}(2460)$ and $D_{s1}(2536)$. *Phys. Rev. D* **2012**, *85*, 034040. [CrossRef]
221. Cleven, M.; Grießhammer, H.W.; Guo, F.K.; Hanhart, C.; Meißner, U.G. Strong and radiative decays of the $D_{s0}^*(2317)$ and $D_{s1}(2460)$. *Eur. Phys. J. A* **2014**, *50*, 149. [CrossRef]
222. Albaladejo, M.; Jido, D.; Nieves, J.; Oset, E. $D_{s0}^*(2317)$ and DK scattering in B decays from BaBar and LHCb data. *Eur. Phys. J. C* **2016**, *76*, 300. [CrossRef]
223. Aaij, R. Observation of the doubly charmed baryon decay $\Xi_{cc}^{++} \to \Xi_c'^{+}\pi^+$. *J. High Energy Phys.* **2022**, *5*, 38. [CrossRef]
224. Wu, J.J.; Molina, R.; Oset, E.; Zou, B.S. Prediction of narrow N^* and Λ^* resonances with hidden charm above 4 GeV. *Phys. Rev. Lett.* **2010**, *105*, 232001. [CrossRef]
225. Wu, J.J.; Molina, R.; Oset, E.; Zou, B.S. Dynamically generated N^* and Λ^* resonances in the hidden charm sector around 4.3 GeV. *Phys. Rev. C* **2011**, *84*, 015202. [CrossRef]
226. Wang, W.L.; Huang, F.; Zhang, Z.Y.; Zou, B.S. $\Sigma_c\bar{D}$ and $\Lambda_c\bar{D}$ states in a chiral quark model. *Phys. Rev. C* **2011**, *84*, 015203. [CrossRef]
227. Yang, Z.C.; Sun, Z.F.; He, J.; Liu, X.; Zhu, S.L. The possible hidden-charm molecular baryons composed of anti-charmed meson and charmed baryon. *Chin. Phys. C* **2012**, *36*, 6–13. [CrossRef]
228. Yuan, S.G.; Wei, K.W.; He, J.; Xu, H.S.; Zou, B.S. Study of $qqqc\bar{c}$ five quark system with three kinds of quark-quark hyperfine interaction. *Eur. Phys. J. A* **2012**, *48*, 61. [CrossRef]
229. Wu, J.J.; Lee, T.S.H.; Zou, B.S. Nucleon Resonances with Hidden Charm in Coupled-Channel Models. *Phys. Rev. C* **2012**, *85*, 044002. [CrossRef]
230. Garcia-Recio, C.; Nieves, J.; Romanets, O.; Salcedo, L.L.; Tolos, L. Hidden charm N and Delta resonances with heavy-quark symmetry. *Phys. Rev. D* **2013**, *87*, 074034. [CrossRef]
231. Xiao, C.W.; Nieves, J.; Oset, E. Combining heavy quark spin and local hidden gauge symmetries in the dynamical generation of hidden charm baryons. *Phys. Rev. D* **2013**, *88*, 056012. [CrossRef]
232. Chen, R.; Liu, X.; Li, X.Q.; Zhu, S.L. Identifying exotic hidden-charm pentaquarks. *Phys. Rev. Lett.* **2015**, *115*, 132002. [CrossRef] [PubMed]
233. Chen, H.X.; Chen, W.; Liu, X.; Steele, T.G.; Zhu, S.L. Towards exotic hidden-charm pentaquarks in QCD. *Phys. Rev. Lett.* **2015**, *115*, 172001. [CrossRef] [PubMed]
234. Roca, L.; Nieves, J.; Oset, E. LHCb pentaquark as a $\bar{D}^*\Sigma_c - \bar{D}^*\Sigma_c^*$ molecular state. *Phys. Rev. D* **2015**, *92*, 094003. [CrossRef]
235. He, J. $\bar{D}\Sigma_c^*$ and $\bar{D}^*\Sigma_c$ interactions and the LHCb hidden-charmed pentaquarks. *Phys. Lett. B* **2016**, *753*, 547–551. [CrossRef]
236. Yang, G.; Ping, J. The structure of pentaquarks P_c^+ in the chiral quark model. *Phys. Rev. D* **2017**, *95*, 014010. [CrossRef]

237. Meißner, U.G.; Oller, J.A. Testing the χ_{c1} p composite nature of the $P_c(4450)$. *Phys. Lett. B* **2015**, *751*, 59–62. [CrossRef]
238. Xiao, C.W.; Meißner, U.G. $J/\psi(\eta_c)$N and $\Upsilon(\eta_b)$N cross sections. *Phys. Rev. D* **2015**, *92*, 114002. [CrossRef]
239. Chen, R.; Liu, X.; Zhu, S.L. Hidden-charm molecular pentaquarks and their charm-strange partners. *Nucl. Phys. A* **2016**, *954*, 406–421. [CrossRef]
240. Chen, H.X.; Cui, E.L.; Chen, W.; Liu, X.; Steele, T.G.; Zhu, S.L. QCD sum rule study of hidden-charm pentaquarks. *Eur. Phys. J. C* **2016**, *76*, 572. [CrossRef]
241. Azizi, K.; Sarac, Y.; Sundu, H. Analysis of $P_c^+(4380)$ and $P_c^+(4450)$ as pentaquark states in the molecular picture with QCD sum rules. *Phys. Rev. D* **2017**, *95*, 094016. [CrossRef]
242. Lebed, R.F. The Pentaquark Candidates in the Dynamical Diquark Picture. *Phys. Lett. B* **2015**, *749*, 454–457. [CrossRef]
243. Zhu, R.; Qiao, C.F. Pentaquark states in a diquark–triquark model. *Phys. Lett. B* **2016**, *756*, 259–264. [CrossRef]
244. Maiani, L.; Polosa, A.D.; Riquer, V. The New Pentaquarks in the Diquark Model. *Phys. Lett. B* **2015**, *749*, 289–291. [CrossRef]
245. Anisovich, V.V.; Matveev, M.A.; Nyiri, J.; Sarantsev, A.V.; Semenova, A.N. Pentaquarks and resonances in the pJ/ψ spectrum *arXiv* **2015**, arXiv:1507.07652.
246. Ghosh, R.; Bhattacharya, A.; Chakrabarti, B. A study on P_c^* (4380) and P_c^* in the quasi particle diquark model. *Phys. Part. Nucl. Lett.* **2017**, *14*, 550–552. [CrossRef]
247. Wang, Z.G. Analysis of $P_c(4380)$ and $P_c(4450)$ as pentaquark states in the diquark model with QCD sum rules. *Eur. Phys. J. C* **2016**, *76*, 70. [CrossRef]
248. Mironov, A.; Morozov, A. Is the pentaquark doublet a hadronic molecule? *JETP Lett.* **2015**, *102*, 271–273. [CrossRef]
249. Scoccola, N.N.; Riska, D.O.; Rho, M. Pentaquark candidates $P_c^+(4380)$ and $P_c^+(4450)$ within the soliton picture of baryons. *Phys. Rev. D* **2015**, *92*, 051501. [CrossRef]
250. Guo, F.K.; Meißner, U.G.; Wang, W.; Yang, Z. How to reveal the exotic nature of the $P_c(4450)$. *Phys. Rev. D* **2015**, *92*, 071502. [CrossRef]
251. Liu, X.H.; Wang, Q.; Zhao, Q. Understanding the newly observed heavy pentaquark candidates. *Phys. Lett. B* **2016**, *757*, 231–236. [CrossRef]
252. Mikhasenko, M. A triangle singularity and the LHCb pentaquarks. *arXiv* **2015**, arXiv:1507.06552.
253. Skerbis, U.; Prelovsek, S. Nucleon-J/ψ and nucleon-η_c scattering in P_c pentaquark channels from LQCD. *Phys. Rev. D* **2019**, *99*, 094505. [CrossRef]
254. Wang, Z.G. Analysis of the $P_c(4312)$, $P_c(4440)$, $P_c(4457)$ and related hidden-charm pentaquark states with QCD sum rules. *Int. J. Mod. Phys. A* **2020**, *35*, 2050003. [CrossRef]
255. Guo, Z.H.; Oller, J.A. Anatomy of the newly observed hidden-charm pentaquark states: $P_c(4312)$, $P_c(4440)$ and $P_c(4457)$. *Phys. Lett. B* **2019**, *793*, 144–149. [CrossRef]
256. Mutuk, H. Neural Network Study of Hidden-Charm Pentaquark Resonances. *Chin. Phys. C* **2019**, *43*, 093103. [CrossRef]
257. Zhu, R.; Liu, X.; Huang, H.; Qiao, C.F. Analyzing doubly heavy tetra- and penta-quark states by variational method. *Phys. Lett. B* **2019**, *797*, 134869. [CrossRef]
258. Eides, M.I.; Petrov, V.Y.; Polyakov, M.V. New LHCb pentaquarks as hadrocharmonium states. *Mod. Phys. Lett. A* **2020**, *35*, 2050151. [CrossRef]
259. Weng, X.Z.; Chen, X.L.; Deng, W.Z.; Zhu, S.L. Hidden-charm pentaquarks and P_c states. *Phys. Rev. D* **2019**, *100*, 016014. [CrossRef]
260. Wang, F.L.; Chen, R.; Liu, Z.W.; Liu, X. Probing new types of P_c states inspired by the interaction between S-wave charmed baryon and anti-charmed meson in a $\bar{T}$ doublet. *Phys. Rev. C* **2020**, *101*, 025201. [CrossRef]
261. Liu, M.Z.; Pan, Y.W.; Peng, F.Z.; Sánchez Sánchez, M.; Geng, L.S.; Hosaka, A.; Pavon Valderrama, M. Emergence of a complete heavy-quark spin symmetry multiplet: Seven molecular pentaquarks in light of the latest LHCb analysis. *Phys. Rev. Lett.* **2019**, *122*, 242001. [CrossRef]
262. He, J. Study of $P_c(4457)$, $P_c(4440)$, and $P_c(4312)$ in a quasipotential Bethe-Salpeter equation approach. *Eur. Phys. J. C* **2019**, *79*, 393. [CrossRef]
263. Meng, L.; Wang, B.; Wang, G.J.; Zhu, S.L. The hidden charm pentaquark states and $\Sigma_c\bar{D}^{(*)}$ interaction in chiral perturbation theory. *Phys. Rev. D* **2019**, *100*, 014031. [CrossRef]
264. Xiao, C.W.; Nieves, J.; Oset, E. Heavy quark spin symmetric molecular states from $\bar{D}^{(*)}\Sigma_c^{(*)}$ and other coupled channels in the light of the recent LHCb pentaquarks. *Phys. Rev. D* **2019**, *100*, 014021. [CrossRef]
265. Shimizu, Y.; Yamaguchi, Y.; Harada, M. Heavy quark spin multiplet structure of $P_c(4312)$, $P_c(4440)$, and $P_c(4457)$. *arXiv* **2019**, arXiv:1904.00587.
266. He, J.; Chen, D.Y. Molecular states from $\Sigma_c^{(*)}\bar{D}^{(*)} - \Lambda_c\bar{D}^{(*)}$ interaction. *Eur. Phys. J. C* **2019**, *79*, 887. [CrossRef]
267. Chen, R.; Sun, Z.F.; Liu, X.; Zhu, S.L. Strong LHCb evidence supporting the existence of the hidden-charm molecular pentaquarks. *Phys. Rev. D* **2019**, *100*, 011502. [CrossRef]
268. Wang, B.; Meng, L.; Zhu, S.L. Hidden-charm and hidden-bottom molecular pentaquarks in chiral effective field theory. *J. High Energy Phys.* **2019**, *11*, 108. [CrossRef]
269. Lin, Y.H.; Zou, B.S. Strong decays of the latest LHCb pentaquark candidates in hadronic molecule pictures. *Phys. Rev. D* **2019**, *100*, 056005. [CrossRef]
270. Liu, M.Z.; Wu, T.W.; Sánchez Sánchez, M.; Valderrama, M.P.; Geng, L.S.; Xie, J.J. Spin-parities of the $P_c(4440)$ and $P_c(4457)$ in the one-boson-exchange model. *Phys. Rev. D* **2021**, *103*, 054004. [CrossRef]

271. Du, M.L.; Baru, V.; Guo, F.K.; Hanhart, C.; Meißner, U.G.; Oller, J.A.; Wang, Q. Revisiting the nature of the P_c pentaquarks. *J. High Energy Phys.* **2021**, *8*, 157. [CrossRef]
272. Yalikun, N.; Lin, Y.H.; Guo, F.K.; Kamiya, Y.; Zou, B.S. Coupled-channel effects of the $\Sigma_c^{(*)}\bar{D}^{(*)}$-$\Lambda_c(2595)\bar{D}$ system and molecular nature of the Pc pentaquark states from one-boson exchange model. *Phys. Rev. D* **2021**, *104*, 094039. [CrossRef]
273. Pavon Valderrama, M. One pion exchange and the quantum numbers of the $P_c(4440)$ and $P_c(4457)$ pentaquarks. *Phys. Rev. D* **2019**, *100*, 094028. [CrossRef]
274. Yamaguchi, Y.; García-Tecocoatzi, H.; Giachino, A.; Hosaka, A.; Santopinto, E.; Takeuchi, S.; Takizawa, M. P_c pentaquarks with chiral tensor and quark dynamics. *Phys. Rev. D* **2020**, *101*, 091502. [CrossRef]
275. Sakai, S.; Jing, H.J.; Guo, F.K. Decays of P_c into $J/\psi N$ and $\eta_c N$ with heavy quark spin symmetry. *Phys. Rev. D* **2019**, *100*, 074007. [CrossRef]
276. Xiao, C.J.; Huang, Y.; Dong, Y.B.; Geng, L.S.; Chen, D.Y. Exploring the molecular scenario of Pc(4312) , Pc(4440) , and Pc(4457). *Phys. Rev. D* **2019**, *100*, 014022. [CrossRef]
277. Voloshin, M.B. Some decay properties of hidden-charm pentaquarks as baryon-meson molecules. *Phys. Rev. D* **2019**, *100*, 034020. [CrossRef]
278. Guo, F.K.; Jing, H.J.; Meißner, U.G.; Sakai, S. Isospin breaking decays as a diagnosis of the hadronic molecular structure of the $P_c(4457)$. *Phys. Rev. D* **2019**, *99*, 091501. [CrossRef]
279. Xu, Y.J.; Cui, C.Y.; Liu, Y.L.; Huang, M.Q. Partial decay widths of $P_c(4312)$ as a $\bar{D}\Sigma_c$ molecular state. *Phys. Rev. D* **2020**, *102*, 034028. [CrossRef]
280. Cao, X.; Dai, J.P. Confronting pentaquark photoproduction with new LHCb observations. *Phys. Rev. D* **2019**, *100*, 054033. [CrossRef]
281. Wang, G.J.; Xiao, L.Y.; Chen, R.; Liu, X.H.; Liu, X.; Zhu, S.L. Probing hidden-charm decay properties of P_c states in a molecular scenario. *Phys. Rev. D* **2020**, *102*, 036012. [CrossRef]
282. Ling, X.Z.; Lu, J.X.; Liu, M.Z.; Geng, L.S. $P_c(4457) \to P_c$ (4312) π/γ in the molecular picture. *Phys. Rev. D* **2021**, *104*, 074022. [CrossRef]
283. Dong, Y.; Shen, P.; Huang, F.; Zhang, Z. Selected strong decays of pentaquark State $P_c(4312)$ in a chiral constituent quark model. *Eur. Phys. J. C* **2020**, *80*, 341. [CrossRef]
284. Ling, P.; Dai, X.H.; Du, M.L.; Wang, Q. Prompt production of the hidden charm pentaquarks in the LHC. *Eur. Phys. J. C* **2021**, *81*, 819. [CrossRef]
285. Park, I.W.; Cho, S.; Kim, Y.; Lee, S.H. Production of Pc(4312) state in electron-proton collisions. *Phys. Rev. D* **2022**, *105*, 114023. [CrossRef]
286. Winney, D.; Fanelli, C.; Pilloni, A.; Hiller Blin, A.N.; Fernández-Ramírez, C.; Albaladejo, M.; Mathieu, V.; Mokeev, V.I.; Szczepaniak, A.P. Double polarization observables in pentaquark photoproduction. *Phys. Rev. D* **2019**, *100*, 034019. [CrossRef]
287. Chen, H.X. Hidden-charm pentaquark states through current algebra: From their production to decay *. *Chin. Phys. C* **2022**, *46*, 093105. [CrossRef]
288. Yang, Z.; Cao, X.; Liang, Y.T.; Wu, J.J. Identifying hidden charm pentaquark signal from non-resonant background in electron–proton scattering. *Chin. Phys. C* **2020**, *44*, 084102. [CrossRef]
289. Ali, A. First Measurement of Near-Threshold J/ψ Exclusive Photoproduction off the Proton. *Phys. Rev. Lett.* **2019**, *123*, 072001. [CrossRef]
290. Du, M.L.; Baru, V.; Guo, F.K.; Hanhart, C.; Meißner, U.G.; Nefediev, A.; Strakovsky, I. Deciphering the mechanism of near-threshold J/ψ photoproduction. *Eur. Phys. J. C* **2020**, *80*, 1053. [CrossRef]
291. Kubarovsky, V.; Voloshin, M.B. Formation of hidden-charm pentaquarks in photon-nucleon collisions. *Phys. Rev. D* **2015**, *92*, 031502. [CrossRef]
292. Karliner, M.; Rosner, J.L. Photoproduction of Exotic Baryon Resonances. *Phys. Lett. B* **2016**, *752*, 329–332. [CrossRef]
293. Wu, J.J.; Lee, T.S.H.; Zou, B.S. Nucleon resonances with hidden charm in γp reactions. *Phys. Rev. C* **2019**, *100*, 035206. [CrossRef]
294. Yang, G.; Ping, J.; Segovia, J. Tetra- and penta-quark structures in the constituent quark model. *Symmetry* **2020**, *12*, 1869. [CrossRef]
295. Chen, H.X.; Chen, W.; Zhu, S.L. Possible interpretations of the $P_c(4312)$, $P_c(4440)$, and $P_c(4457)$. *Phys. Rev. D* **2019**, *100*, 051501. [CrossRef]
296. Isgur, N.; Wise, M.B. Weak Decays of Heavy Mesons in the Static Quark Approximation. *Phys. Lett. B* **1989**, *232*, 113–117. [CrossRef]
297. Neubert, M. Heavy quark symmetry. *Phys. Rept.* **1994**, *245*, 259–396. [CrossRef]
298. Guo, F.K.; Hanhart, C.; Meissner, U.G. Implications of heavy quark spin symmetry on heavy meson hadronic molecules. *Phys. Rev. Lett.* **2009**, *102*, 242004. [CrossRef]
299. Yamaguchi, Y.; Ohkoda, S.; Hosaka, A.; Hyodo, T.; Yasui, S. Heavy quark symmetry in multihadron systems. *Phys. Rev. D* **2015**, *91*, 034034. [CrossRef]
300. Yan, M.J.; Peng, F.Z.; Sánchez Sánchez, M.; Pavon Valderrama, M. Interpretations of the new LHCb $P_c(4337)^+$ pentaquark state. *Eur. Phys. J. C* **2022**, *82*, 574. [CrossRef]
301. Liu, Y.; Nowak, M.A.; Zahed, I. Holographic charm and bottom pentaquarks. II. Open and hidden decay widths. *Phys. Rev. D* **2021**, *104*, 114022. [CrossRef]

302. Liu, Y.; Mamo, K.A.; Nowak, M.A.; Zahed, I. Holographic charm and bottom pentaquarks. III. Excitations through photoproduction of heavy mesons. *Phys. Rev. D* **2021**, *104*, 114023. [CrossRef]
303. Nakamura, S.X.; Hosaka, A.; Yamaguchi, Y. $P_c(4312)^+$ and $P_c(4337)^+$ as interfering $\Sigma_c\bar{D}$ and $\Lambda_c\bar{D}^*$ threshold cusps. *Phys. Rev. D* **2021**, *104*, L091503. [CrossRef]
304. Giron, J.F.; Lebed, R.F. Fine structure of pentaquark multiplets in the dynamical diquark model. *Phys. Rev. D* **2021**, *104*, 114028. [CrossRef]
305. Wang, J.Z.; Liu, X.; Matsuki, T. Evidence supporting the existence of $P_c(4380)\pm$ from the recent measurements of $B_s \to J/\psi p\bar{p}$. *Phys. Rev. D* **2021**, *104*, 114020. [CrossRef]
306. Chen, R.; He, J.; Liu, X. Possible strange hidden-charm pentaquarks from $\Sigma_c^{(*)}\bar{D}_s^*$ and $\Xi_c^{(\prime,*)}\bar{D}^*$ interactions. *Chin. Phys. C* **2017**, *41*, 103105. [CrossRef]
307. Shen, C.W.; Wu, J.J.; Zou, B.S. Decay behaviors of possible $\Lambda_{c\bar{c}}$ states in hadronic molecule pictures. *Phys. Rev. D* **2019**, *100*, 056006. [CrossRef]
308. Xiao, C.W.; Nieves, J.; Oset, E. Prediction of hidden charm strange molecular baryon states with heavy quark spin symmetry. *Phys. Lett. B* **2019**, *799*, 135051. [CrossRef]
309. Wang, B.; Meng, L.; Zhu, S.L. Spectrum of the strange hidden charm molecular pentaquarks in chiral effective field theory. *Phys. Rev. D* **2020**, *101*, 034018. [CrossRef]
310. Aaij, R. Evidence of a $J/\psi\Lambda$ structure and observation of excited Ξ^- states in the $\Xi_b^- \to J/\psi\Lambda K^-$ decay. *Sci. Bull.* **2021**, *66*, 1278–1287. [CrossRef]
311. Chen, H.X.; Chen, W.; Liu, X.; Liu, X.H. Establishing the first hidden-charm pentaquark with strangeness. *Eur. Phys. J. C* **2021**, *81*, 409. [CrossRef]
312. Wang, Z.G.; Xin, Q. Analysis of hidden-charm pentaquark molecular states with and without strangeness via the QCD sum rules *. *Chin. Phys. C* **2021**, *45*, 123105. [CrossRef]
313. Zhu, J.T.; Song, L.Q.; He, J. $P_{cs}(4459)$ and other possible molecular states from $\Xi_c^{(*)}\bar{D}^{(*)}$ and $\Xi_c'\bar{D}^{(*)}$ interactions. *Phys. Rev. D* **2021**, *103*, 074007. [CrossRef]
314. Liu, M.Z.; Pan, Y.W.; Geng, L.S. Can discovery of hidden charm strange pentaquark states help determine the spins of $P_c(4440)$ and $P_c(4457)$? *Phys. Rev. D* **2021**, *103*, 034003. [CrossRef]
315. Peng, F.Z.; Yan, M.J.; Sánchez Sánchez, M.; Valderrama, M.P. The $P_{cs}(4459)$ pentaquark from a combined effective field theory and phenomenological perspective. *Eur. Phys. J. C* **2021**, *81*, 666. [CrossRef]
316. Chen, R. Can the newly reported $P_{cs}(4459)$ be a strange hidden-charm $\Xi_c\bar{D}^*$ molecular pentaquark? *Phys. Rev. D* **2021**, *103*, 054007. [CrossRef]
317. Chen, R.; Liu, X. Mass behavior of hidden-charm open-strange pentaquarks inspired by the established P_c molecular states. *Phys. Rev. D* **2022**, *105*, 014029. [CrossRef]
318. Chen, R. Strong decays of the newly $P_{cs}(4459)$ as a strange hidden-charm $\Xi_c\bar{D}^*$ molecule. *Eur. Phys. J. C* **2021**, *81*, 122. [CrossRef]
319. Hu, X.; Ping, J. Investigation of hidden-charm pentaquarks with strangeness $S = -1$. *Eur. Phys. J. C* **2022**, *82*, 118. [CrossRef]
320. Giron, J.F.; Lebed, R.F.; Martinez, S.R. Spectrum of hidden-charm, open-strange exotics in the dynamical diquark model. *Phys. Rev. D* **2021**, *104*, 054001. [CrossRef]
321. Wang, Z.G. Analysis of the $P_{cs}(4459)$ as the hidden-charm pentaquark state with QCD sum rules. *Int. J. Mod. Phys. A* **2021**, *36*, 2150071. [CrossRef]
322. Wang, Z.G. Analysis of the $\frac{1}{2}^{\pm}$ pentaquark states in the diquark–diquark–antiquark model with QCD sum rules. *Eur. Phys. J. C* **2016**, *76*, 142. [CrossRef]
323. Anisovich, V.V.; Matveev, M.A.; Nyiri, J.; Sarantsev, A.V.; Semenova, A.N. Nonstrange and strange pentaquarks with hidden charm. *Int. J. Mod. Phys. A* **2015**, *30*, 1550190. [CrossRef]
324. Yang, F.; Huang, Y.; Zhu, H.Q. Strong decays of the $P_{cs}(4459)$ as a $\Xi_c\bar{D}^*$ molecule. *Sci. China Phys. Mech. Astron.* **2021**, *64*, 121011. [CrossRef]
325. Liu, W.Y.; Hao, W.; Wang, G.Y.; Wang, Y.Y.; Wang, E.; Li, D.M. Resonances $X(4140)$, $X(4160)$, and $P_{cs}(4459)$ in the decay of $\Lambda_b \to J/\psi\Lambda\phi$. *Phys. Rev. D* **2021**, *103*, 034019. [CrossRef]
326. Cheng, C.; Yang, F.; Huang, Y. Searching for strange hidden-charm pentaquark state $P_{cs}(4459)$ in $\gamma p \to K + P_{cs}(4459)$ reaction. *Phys. Rev. D* **2021**, *104*, 116007. [CrossRef]
327. Lu, J.X.; Liu, M.Z.; Shi, R.X.; Geng, L.S. Understanding $P_{cs}(4459)$ as a hadronic molecule in the $\Xi_b^- \to J/\psi\Lambda K^-$ decay. *Phys. Rev. D* **2021**, *104*, 034022. [CrossRef]
328. Wu, Q.; Chen, D.Y.; Ji, R. Production of $P_{cs}(4459)$ from Ξ_b Decay. *Chin. Phys. Lett.* **2021**, *38*, 071301. [CrossRef]
329. Azizi, K.; Sarac, Y.; Sundu, H. Investigation of $P_{cs}(4459)^0$ pentaquark via its strong decay to $\Lambda J/\Psi$. *Phys. Rev. D* **2021**, *103*, 094033. [CrossRef]
330. Cheng, H.Y.; Chua, C.K. Bottom Baryon Decays to Pseudoscalar Meson and Pentaquark. *Phys. Rev. D* **2015**, *92*, 096009. [CrossRef]
331. Feijoo, A.; Magas, V.K.; Ramos, A.; Oset, E. A hidden-charm $S = -1$ pentaquark from the decay of Λ_b into $J/\psi, \eta\Lambda$ states. *Eur. Phys. J. C* **2016**, *76*, 446. [CrossRef]
332. Lu, J.X.; Wang, E.; Xie, J.J.; Geng, L.S.; Oset, E. The $\Lambda_b \to J/\psi K^0\Lambda$ reaction and a hidden-charm pentaquark state with strangeness. *Phys. Rev. D* **2016**, *93*, 094009. [CrossRef]

333. Chen, H.X.; Geng, L.S.; Liang, W.H.; Oset, E.; Wang, E.; Xie, J.J. Looking for a hidden-charm pentaquark state with strangeness S = −1 from Ξ_b^- decay into $J/\psi K^-\Lambda$. *Phys. Rev. C* **2016**, *93*, 065203. [CrossRef]
334. Shen, C.W.; Jing, H.J.; Guo, F.K.; Wu, J.J. Exploring Possible Triangle Singularities in the $\Xi_b^- \to K^- J/\psi\Lambda$ Decay. *Symmetry* **2020**, *12*, 1611. [CrossRef]
335. Yang, G.; Ping, J.; Segovia, J. Hidden-bottom pentaquarks. *Phys. Rev. D* **2019**, *99*, 014035. [CrossRef]
336. Shen, C.W.; Rönchen, D.; Meißner, U.G.; Zou, B.S. Exploratory study of possible resonances in heavy meson–heavy baryon coupled-channel interactions. *Chin. Phys. C* **2018**, *42*, 023106. [CrossRef]
337. Wu, J.J.; Zhao, L.; Zou, B.S. Prediction of super-heavy N^* and Λ^* resonances with hidden beauty. *Phys. Lett. B* **2012**, *709*, 70–76. [CrossRef]
338. Xiao, C.W.; Oset, E. Hidden beauty baryon states in the local hidden gauge approach with heavy quark spin symmetry. *Eur. Phys. J. A* **2013**, *49*, 139. [CrossRef]
339. Aitala, E.M. Search for the pentaquark via the $P_{\bar{c}s}^0$ decay. *Phys. Rev. Lett.* **1998**, *81*, 44–48. [CrossRef]
340. Aitala, E.M. Search for the pentaquark via the $P_{\bar{c}s}^0 -> K^{*0}K$-$p$ decay. *Phys. Lett. B* **1999**, *448*, 303–310. [CrossRef]
341. Aktas, A. Evidence for a narrow anti-charmed baryon state. *Phys. Lett. B* **2004**, *588*, 17. [CrossRef]
342. Chekanov, S. Search for a narrow charmed baryonic state decaying to $D^{*\pm}p^{\mp}$ in ep collisions at HERA. *Eur. Phys. J. C* **2004**, *38*, 29–41. [CrossRef]
343. Link, J.M. Search for a strongly decaying neutral charmed pentaquark. *Phys. Lett. B* **2005**, *622*, 229–238. [CrossRef]
344. Aubert, B. [BaBar Collaboration]. Search for the charmed pentaquark candidate $\Theta(c)(3100)^0$ in e^+e^- annihilations at $s^{1/2}$ = 10.58 GeV. *Phys. Rev. D* **2006**, *73*, 091101. [CrossRef]
345. Aubert, B. Measurements of the Decays $B^0 \to \bar{D}^0 p\bar{p}$, $B^0 \to \bar{D}^*0\, p\bar{p}$, $B^0 \to D^- p\bar{p}\pi^+$, and $B^0 \to D^{*-} p\bar{p}\pi^+$. *Phys. Rev. D* **2006**, *74*, 051101. [CrossRef]
346. Aaij, R. Search for weakly decaying b-flavored pentaquarks. *Phys. Rev. D* **2018**, *97*, 032010. [CrossRef]
347. Aaij, R. Observation of the suppressed $\Lambda_b^0 \to DpK^-$ decay with $D \to K^+\pi^-$ and measurement of its CP asymmetry. *Phys. Rev. D* **2021**, *104*, 112008. [CrossRef]
348. Lipkin, H.J. New Possibilities for Exotic Hadrons: Anticharmed Strange Baryons. *Phys. Lett. B* **1987**, *195*, 484–488. [CrossRef]
349. Yamaguchi, Y.; Ohkoda, S.; Yasui, S.; Hosaka, A. Exotic baryons from a heavy meson and a nucleon – Negative parity states –. *Phys. Rev. D* **2011**, *84*, 014032. [CrossRef]
350. An, H.T.; Chen, K.; Liu, X. Manifestly exotic pentaquarks with a single heavy quark. *Phys. Rev. D* **2022**, *105*, 034018. [CrossRef]
351. Richard, J.M.; Valcarce, A.; Vijande, J. Pentaquarks with anticharm or beauty revisited. *Phys. Lett. B* **2019**, *790*, 248–250. [CrossRef]
352. Sarac, Y.; Kim, H.; Lee, S.H. QCD sum rules for the anti-charmed pentaquark. *Phys. Rev. D* **2006**, *73*, 014009. [CrossRef]
353. Stewart, I.W.; Wessling, M.E.; Wise, M.B. Stable heavy pentaquark states. *Phys. Lett. B* **2004**, *590*, 185–189. [CrossRef]
354. Xing, Y.; Liu, W.L.; Xiao, Y.H. The production of singly charmed pentaquark $\bar{c}qqqq$ from bottom baryon. *Eur. Phys. J. C* **2022**, *82*, 1105. [CrossRef]
355. Chen, R.; Hosaka, A.; Liu, X. Heavy molecules and one-σ/ω-exchange model. *Phys. Rev. D* **2017**, *96*, 116012. [CrossRef]
356. Chen, R.; Li, N.; Sun, Z.F.; Liu, X.; Zhu, S.L. Doubly charmed molecular pentaquarks. *Phys. Lett. B* **2021**, *822*, 136693. [CrossRef]
357. Rathaud, D.P.; Tiwari, R.; Rai, A.K. Interaction and identification of meson–baryon molecule. *Indian J. Phys.* **2021**, *95*, 2807–2828. [CrossRef]
358. Zhou, Q.S.; Chen, K.; Liu, X.; Liu, Y.R.; Zhu, S.L. Surveying exotic pentaquarks with the typical $QQqq\bar{q}$ configuration. *Phys. Rev. C* **2018**, *98*, 045204. [CrossRef]
359. Park, W.; Cho, S.; Lee, S.H. Where is the stable pentaquark? *Phys. Rev. D* **2019**, *99*, 094023. [CrossRef]
360. Yang, G.; Ping, J.; Segovia, J. Doubly Charmed Pentaquarks. *Phys. Rev. D* **2020**, *101*, 074030. [CrossRef]
361. Shimizu, Y.; Harada, M. Hidden Charm Pentaquark $P_c(4380)$ and Doubly Charmed Baryon $\Xi_{cc}^*(4380)$ as Hadronic Molecule States. *Phys. Rev. D* **2017**, *96*, 094012. [CrossRef]
362. Giannuzzi, F. Heavy pentaquark spectroscopy in the diquark model. *Phys. Rev. D* **2019**, *99*, 094006. [CrossRef]
363. Yan, M.J.; Liu, X.H.; Gonzàlez-Solís, S.; Guo, F.K.; Hanhart, C.; Meißner, U.G.; Zou, B.S. New spectrum of negative-parity doubly charmed baryons: Possibility of two quasistable states. *Phys. Rev. D* **2018**, *98*, 091502. [CrossRef]
364. Guo, Z.H. Prediction of exotic doubly charmed baryons within chiral effective field theory. *Phys. Rev. D* **2017**, *96*, 074004. [CrossRef]
365. Chen, K.; Wang, B.; Zhu, S.L. Exploration of the doubly charmed molecular pentaquarks. *Phys. Rev. D* **2021**, *103*, 116017. [CrossRef]
366. Wang, Z.G. Analysis of the doubly heavy baryon states and pentaquark states with QCD sum rules. *Eur. Phys. J. C* **2018**, *78*, 826. [CrossRef]
367. Shen, C.W.; Meißner, U.G. Prediction of five-flavored pentaquarks. *Phys. Lett. B* **2022**, *831*, 137197. [CrossRef]
368. Dias, J.M.; Debastiani, V.R.; Xie, J.J.; Oset, E. Doubly charmed Ξ_{cc} molecular states from meson-baryon interaction. *Phys. Rev. D* **2018**, *98*, 094017. [CrossRef]
369. Hofmann, J.; Lutz, M.F.M. D-wave baryon resonances with charm from coupled-channel dynamics. *Nucl. Phys. A* **2006**, *776*, 17–51. [CrossRef]
370. Romanets, O.; Tolos, L.; Garcia-Recio, C.; Nieves, J.; Salcedo, L.L.; Timmermans, R.G.E. Charmed and strange baryon resonances with heavy-quark spin symmetry. *Phys. Rev. D* **2012**, *85*, 114032. [CrossRef]

371. Azizi, K.; Sarac, Y.; Sundu, H. Possible Molecular Pentaquark States with Different Spin and Quark Configurations. *Phys. Rev. D* **2018**, *98*, 054002. [CrossRef]
372. Chen, R.; Hosaka, A.; Liu, X. Prediction of triple-charm molecular pentaquarks. *Phys. Rev. D* **2017**, *96*, 114030. [CrossRef]
373. Wang, F.L.; Chen, R.; Liu, Z.W.; Liu, X. Possible triple-charm molecular pentaquarks from $\Xi_{cc}D_1/\Xi_{cc}D_2^*$ interactions. *Phys. Rev. D* **2019**, *99*, 054021. [CrossRef]
374. Li, S.Y.; Liu, Y.R.; Liu, Y.N.; Si, Z.G.; Wu, J. Pentaquark states with the $QQQq\bar{q}$ configuration in a simple model. *Eur. Phys. J. C* **2019**, *79*, 87. [CrossRef]
375. Wang, Z.G. Analysis of the triply-charmed pentaquark states with QCD sum rules. *Eur. Phys. J. C* **2018**, *78*, 300. [CrossRef]
376. An, H.T.; Chen, K.; Liu, Z.W.; Liu, X. Fully heavy pentaquarks. *Phys. Rev. D* **2021**, *103*, 074006. [CrossRef]
377. Zhang, J.R. Fully-heavy pentaquark states. *Phys. Rev. D* **2021**, *103*, 074016. [CrossRef]
378. Wang, Z.G. Analysis of the fully-heavy pentaquark states via the QCD sum rules. *Nucl. Phys. B* **2021**, *973*, 115579. [CrossRef]
379. Yan, Y.; Wu, Y.; Hu, X.; Huang, H.; Ping, J. Fully heavy pentaquarks in quark models. *Phys. Rev. D* **2022**, *105*, 014027. [CrossRef]
380. Yelton, J. Observation of an Excited Ω^- Baryon. *Phys. Rev. Lett.* **2018**, *121*, 052003. [CrossRef]
381. Barnes, V.E. Observation of a Hyperon with Strangeness Minus Three. *Phys. Rev. Lett.* **1964**, *12*, 204–206. [CrossRef]
382. Patrignani, C. Review of Particle Physics. *Chin. Phys. C* **2016**, *40*, 100001. [CrossRef]
383. Hyodo, T.; Niiyama, M. QCD and the strange baryon spectrum. *Prog. Part. Nucl. Phys.* **2021**, *120*, 103868. [CrossRef]
384. Kolomeitsev, E.E.; Lutz, M.F.M. On baryon resonances and chiral symmetry. *Phys. Lett. B* **2004**, *585*, 243–252. [CrossRef]
385. Sarkar, S.; Oset, E.; Vicente Vacas, M.J. Baryonic resonances from baryon decuplet-meson octet interaction. *Nucl. Phys. A* **2005**, *750*, 294–323; Erratum in *Nucl. Phys. A* **2006**, *780*, 90. [CrossRef]
386. Yuan, S.G.; An, C.S.; Wei, K.W.; Zou, B.S.; Xu, H.S. Spectrum of low-lying $s^3Q\bar{Q}$ configurations with negative parity. *Phys. Rev. C* **2013**, *87*, 025205. [CrossRef]
387. Xu, S.Q.; Xie, J.J.; Chen, X.R.; Jia, D.J. The $\Xi^*\bar{K}$ and $\Omega\eta$ interaction within a chiral unitary approach. *Commun. Theor. Phys.* **2016**, *65*, 53–56. [CrossRef]
388. Capstick, S.; Isgur, N. Baryons in a relativized quark model with chromodynamics. *Phys. Rev. D* **1986**, *34*, 2809–2835. [CrossRef]
389. Loring, U.; Metsch, B.C.; Petry, H.R. The Light baryon spectrum in a relativistic quark model with instanton induced quark forces: The Strange baryon spectrum. *Eur. Phys. J. A* **2001**, *10*, 447–486. [CrossRef]
390. Pervin, M.; Roberts, W. Strangeness -2 and -3 baryons in a constituent quark model. *Phys. Rev. C* **2008**, *77*, 025202. [CrossRef]
391. Faustov, R.N.; Galkin, V.O. Strange baryon spectroscopy in the relativistic quark model. *Phys. Rev. D* **2015**, *92*, 054005. [CrossRef]
392. Xiao, L.Y.; Zhong, X.H. Possible interpretation of the newly observed $\Omega(2012)$ state. *Phys. Rev. D* **2018**, *98*, 034004. [CrossRef]
393. Wang, Z.Y.; Gui, L.C.; Lü, Q.F.; Xiao, L.Y.; Zhong, X.H. Newly observed $\Omega(2012)$ state and strong decays of the low-lying Ω excitations. *Phys. Rev. D* **2018**, *98*, 114023. [CrossRef]
394. Aliev, T.M.; Azizi, K.; Sarac, Y.; Sundu, H. Nature of the $\Omega(2012)$ through its strong decays. *Eur. Phys. J. C* **2018**, *78*, 894. [CrossRef]
395. Aliev, T.M.; Azizi, K.; Sarac, Y.; Sundu, H. Interpretation of the newly discovered $\Omega(2012)$. *Phys. Rev. D* **2018**, *98*, 014031. [CrossRef]
396. Liu, M.S.; Wang, K.L.; Lü, Q.F.; Zhong, X.H. Ω baryon spectrum and their decays in a constituent quark model. *Phys. Rev. D* **2020**, *101*, 016002. [CrossRef]
397. Arifi, A.J.; Suenaga, D.; Hosaka, A.; Oh, Y. Strong decays of multistrangeness baryon resonances in the quark model. *Phys. Rev. D* **2022**, *105*, 094006. [CrossRef]
398. Wang, K.L.; Lü, Q.F.; Xie, J.J.; Zhong, X.H. Toward discovering the excited Ω baryons through nonleptonic weak decays of Ω_c. *Phys. Rev. D* **2023**, *107*, 034015. [CrossRef]
399. Polyakov, M.V.; Son, H.D.; Sun, B.D.; Tandogan, A. $\Omega(2012)$ through the looking glass of flavour SU (3). *Phys. Lett. B* **2019**, *792*, 315–319. [CrossRef]
400. Huang, Y.; Liu, M.Z.; Lu, J.X.; Xie, J.J.; Geng, L.S. Strong decay modes $\bar{K}\Xi$ and $\bar{K}\Xi\pi$ of the $\Omega(2012)$ in the $\bar{K}\Xi(1530)$ and $\eta\Omega$ molecular scenario. *Phys. Rev. D* **2018**, *98*, 076012. [CrossRef]
401. Valderrama, M.P. $\Omega(2012)$ as a hadronic molecule. *Phys. Rev. D* **2018**, *98*, 054009. [CrossRef]
402. Lin, Y.H.; Zou, B.S. Hadronic molecular assignment for the newly observed Ω^* state. *Phys. Rev. D* **2018**, *98*, 056013. [CrossRef]
403. Zeng, C.H.; Lu, J.X.; Wang, E.; Xie, J.J.; Geng, L.S. Theoretical study of the $\Omega(2012)$ state in the $\Omega_c^0 \to \pi^+\Omega(2012)^- \to \pi^+(\bar{K}\Xi)^-$ and $\pi^+(\bar{K}\Xi\pi)^-$ decays. *Phys. Rev. D* **2020**, *102*, 076009. [CrossRef]
404. Lin, Y.H.; Wang, F.; Zou, B.S. Reanalysis of the newly observed Ω^* state in a hadronic molecule model. *Phys. Rev. D* **2020**, *102*, 074025. [CrossRef]
405. Gutsche, T.; Lyubovitskij, V.E. Strong decays of the hadronic molecule $\Omega^*(2012)$. *J. Phys. G* **2020**, *48*, 025001. [CrossRef]
406. Ikeno, N.; Toledo, G.; Oset, E. Molecular picture for the $\Omega(2012)$ revisited. *Phys. Rev. D* **2020**, *101*, 094016. [CrossRef]
407. Lu, J.X.; Zeng, C.H.; Wang, E.; Xie, J.J.; Geng, L.S. Revisiting the $\Omega(2012)$ as a hadronic molecule and its strong decays. *Eur. Phys. J. C* **2020**, *80*, 361. [CrossRef]
408. Pavao, R.; Oset, E. Coupled channels dynamics in the generation of the $\Omega(2012)$ resonance. *Eur. Phys. J. C* **2018**, *78*, 857. [CrossRef]
409. Liu, X.; Huang, H.; Ping, J.; Chen, D. Investigating $\Omega(2012)$ as a molecular state. *Phys. Rev. C* **2021**, *103*, 025202. [CrossRef]
410. Jia, S. Search for $\Omega(2012) \to K\Xi(1530) \to K\pi\Xi$ at Belle. *Phys. Rev. D* **2019**, *100*, 032006. [CrossRef]

411. Oset, E. Weak decays of heavy hadrons into dynamically generated resonances. *Int. J. Mod. Phys. E* **2016**, *25*, 1630001. [CrossRef]
412. Sumihama, M. Observation of $\Xi(1620)^0$ and evidence for $\Xi(1690)^0$ in $\Xi_c^+ \to \Xi^- \pi^+ \pi^+$ decays. *Phys. Rev. Lett.* **2019**, *122*, 072501. [CrossRef]
413. Li, Y. Evidence for the decay $\Omega_c^0 \to \pi^+ \Omega(2012)^- \to \pi^+ (\bar{K}\Xi)^-$. *Phys. Rev. D* **2021**, *104*, 052005. [CrossRef]
414. The Belle Collaboration Observation of $\Omega(2012)^- \to \Xi(1530)\bar{K}$ and measurement of the effective couplings of $\Omega(2012)^-$ to $\Xi(1530)\bar{K}$ and $\Xi\bar{K}$. *arXiv* **2022**, arXiv:2207.03090. [CrossRef]
415. Ikeno, N.; Liang, W.H.; Toledo, G.; Oset, E. Interpretation of the $\Omega c \to \pi + \Omega(2012) \to \pi + (K^-\Xi)$ relative to $\Omega c \to \pi + K^-\Xi$ from the $\Omega(2012)$ molecular perspective. *Phys. Rev. D* **2022**, *106*, 034022. [CrossRef]
416. Hu, X.; Ping, J. Analysis of $\Omega(2012)$ as a molecule in the chiral quark model. *Phys. Rev. D* **2022**, *106*, 054028. [CrossRef]
417. Abazov, V.M. Inclusive production of the P_c resonances in $p\overline{p}$ collisions. *arXiv* **2019**, arXiv:1910.11767.
418. Hiller Blin, A.N.; Fernández-Ramírez, C.; Jackura, A.; Mathieu, V.; Mokeev, V.I.; Pilloni, A.; Szczepaniak, A.P. Studying the $P_c(4450)$ resonance in J/ψ photoproduction off protons. *Phys. Rev. D* **2016**, *94*, 034002. [CrossRef]
419. Kubarovsky, V.; Voloshin, M.B. Search for Hidden-Charm Pentaquark with CLAS12. *arXiv* **2016**, arXiv:1609.00050.
420. Meziani, Z.E. A Search for the LHCb Charmed 'Pentaquark' using Photo-Production of J/ψ at Threshold in Hall C at Jefferson Lab. *arXiv* **2016**, arXiv:1609.00676.
421. Joosten, S.; Meziani, Z.E. Heavy Quarkonium Production at Threshold: From JLab to EIC. *PoS* **2018**, *308*, 17. [CrossRef]
422. Lutz, M.F.M. [PANDA Collaboration]. Physics Performance Report for PANDA: Strong Interaction Studies with Antiprotons *arXiv* **2009**, arXiv:0903.3905.
423. Martinou, A.; Bonatsos, D.; Mertzimekis, T.J.; Karakatsanis, K.E.; Assimakis, I.E.; Peroulis, S.K.; Sarantopoulou, S.; Minkov, N. The islands of shape coexistence within the Elliott and the proxy-SU(3) Models. *Eur. Phys. J. A* **2021**, *57*, 84. [CrossRef]
424. Barucca, G. [PANDA Collaboration]. Feasibility studies for the measurement of time-like proton electromagnetic form factors from $\bar{p}p \to \mu^+\mu^-$ at $\overline{\text{P}}$ANDA at FAIR. *Eur. Phys. J. A* **2021**, *57*, 30. [CrossRef]
425. Xu, Q. Isospin asymmetry of the pseudospin symmetry in nuclear resonant states. *Eur. Phys. J. A* **2019**, *55*, 54. [CrossRef]
426. Barucca, G. [PANDA Collaboration], The potential of Λ and Ξ^- studies with PANDA at FAIR. *Eur. Phys. J. A* **2021**, *57*, 154. [CrossRef]
427. Barucca, G. PANDA Phase One. *Eur. Phys. J. A* **2021**, *57*, 184. [CrossRef]
428. Barucca, G. [PANDA Collaboration]. Study of excited Ξ baryons with the PANDA detector. *Eur. Phys. J. A* **2021**, *57*, 149. [CrossRef]
429. Weinberg, S. *The Quantum Theory of Fields. Vol. 1: Foundations*; Cambridge University Press: Cambridge, UK, 2005. [CrossRef]
430. Richard, J.M. About the J/ψ J/ψ peak of LHCb: Fully-charmed tetraquark? *Sci. Bull.* **2020**, *65*, 1954–1955. [CrossRef]
431. Becchi, C.; Ferretti, J.; Giachino, A.; Maiani, L.; Santopinto, E. A study of $cc\bar{c}\bar{c}$ tetraquark decays in 4 muons and in $D^{(*)}\bar{D}^{(*)}$ at LHC. *Phys. Lett. B* **2020**, *811*, 135952. [CrossRef]
432. Chen, H.X.; Chen, W.; Liu, X.; Zhu, S.L. Strong decays of fully-charm tetraquarks into di-charmonia. *Sci. Bull.* **2020**, *65*, 1994–2000. [CrossRef]
433. Sonnenschein, J.; Weissman, D. Deciphering the recently discovered tetraquark candidates around 6.9 GeV. *Eur. Phys. J. C* **2021**, *81*, 25. [CrossRef]
434. Giron, J.F.; Lebed, R.F. Simple spectrum of $c\bar{c}c\bar{c}$ states in the dynamical diquark model. *Phys. Rev. D* **2020**, *102*, 074003. [CrossRef]
435. Maiani, L. J/ψ-pair resonance by LHCb: A new revolution? *Sci. Bull.* **2020**, *65*, 1949–1951. [CrossRef]
436. Wang, J.Z.; Chen, D.Y.; Liu, X.; Matsuki, T. Producing fully charm structures in the J/ψ -pair invariant mass spectrum. *Phys. Rev. D* **2021**, *103*, 071503. [CrossRef]
437. Chao, K.T.; Zhu, S.L. The possible tetraquark states $cc\bar{c}\bar{c}$ observed by the LHCb experiment. *Sci. Bull.* **2020**, *65*, 1952–1953. [CrossRef] [PubMed]
438. Maciuła, R.; Schäfer, W.; Szczurek, A. On the mechanism of $T_{4c}(6900)$ tetraquark production. *Phys. Lett. B* **2021**, *812*, 136010. [CrossRef]
439. Gordillo, M.C.; De Soto, F.; Segovia, J. Diffusion Monte Carlo calculations of fully-heavy multiquark bound states. *Phys. Rev. D* **2020**, *102*, 114007. [CrossRef]
440. Wu, J.; Liu, Y.R.; Chen, K.; Liu, X.; Zhu, S.L. Heavy-flavored tetraquark states with the $QQ\bar{Q}\bar{Q}$ configuration. *Phys. Rev. D* **2018**, *97*, 094015. [CrossRef]
441. Kuang, Z.; Serafin, K.; Zhao, X.; Vary, J.P. All-charm tetraquark in front form dynamics. *Phys. Rev. D* **2022**, *105*, 094028. [CrossRef]
442. Wang, G.J.; Meng, L.; Oka, M.; Zhu, S.L. Higher fully charmed tetraquarks: Radial excitations and P-wave states. *Phys. Rev. D* **2021**, *104*, 036016. [CrossRef]
443. liu, M.S.; Liu, F.X.; Zhong, X.H.; Zhao, Q. Full-heavy tetraquark states and their evidences in the LHCb di-J/ψ spectrum. *arXiv* **2020**, arXiv:2006.11952.
444. Liu, F.X.; Liu, M.S.; Zhong, X.H.; Zhao, Q. Higher mass spectra of the fully-charmed and fully-bottom tetraquarks. *Phys. Rev. D* **2021**, *104*, 116029. [CrossRef]
445. Faustov, R.N.; Galkin, V.O.; Savchenko, E.M. Masses of the $QQ\bar{Q}\bar{Q}$ tetraquarks in the relativistic diquark–antidiquark picture. *Phys. Rev. D* **2020**, *102*, 114030. [CrossRef]
446. Lü, Q.F.; Chen, D.Y.; Dong, Y.B. Masses of fully heavy tetraquarks $QQ\bar{Q}\bar{Q}$ in an extended relativized quark model. *Eur. Phys. J. C* **2020**, *80*, 871. [CrossRef]

447. Zhao, Z.; Xu, K.; Kaewsnod, A.; Liu, X.; Limphirat, A.; Yan, Y. Study of charmoniumlike and fully-charm tetraquark spectroscopy. *Phys. Rev. D* **2021**, *103*, 116027. [CrossRef]
448. Asadi, Z.; Boroun, G.R. Masses of fully heavy tetraquark states from a four-quark static potential model. *Phys. Rev. D* **2022**, *105*, 014006. [CrossRef]
449. Karliner, M.; Rosner, J.L. Interpretation of structure in the di- J/ψ spectrum. *Phys. Rev. D* **2020**, *102*, 114039. [CrossRef]
450. Li, Q.; Chang, C.H.; Wang, G.L.; Wang, T. Mass spectra and wave functions of $T_{QQ\bar{Q}\bar{Q}}$ tetraquarks. *Phys. Rev. D* **2021**, *104*, 014018. [CrossRef]
451. Ke, H.W.; Han, X.; Liu, X.H.; Shi, Y.L. Tetraquark state $X(6900)$ and the interaction between diquark and antidiquark. *Eur. Phys. J. C* **2021**, *81*, 427. [CrossRef]
452. Zhu, R. Fully-heavy tetraquark spectra and production at hadron colliders. *Nucl. Phys. B* **2021**, *966*, 115393. [CrossRef]
453. Zhang, J.R. 0^+ fully-charmed tetraquark states. *Phys. Rev. D* **2021**, *103*, 014018. [CrossRef]
454. Wu, R.H.; Zuo, Y.S.; Wang, C.Y.; Meng, C.; Ma, Y.Q.; Chao, K.T. NLO results with operator mixing for fully heavy tetraquarks in QCD sum rules. *J. High Energy Phys.* **2022**, *11*, 23. [CrossRef]
455. Dong, X.K.; Baru, V.; Guo, F.K.; Hanhart, C.; Nefediev, A.; Zou, B.S. Is the existence of a J/ψJ/ψ bound state plausible? *Sci. Bull.* **2021**, *66*, 2462–2470. [CrossRef] [PubMed]
456. Nefediev, A.V. X(6200) as a compact tetraquark in the QCD string model. *Eur. Phys. J. C* **2021**, *81*, 692. [CrossRef]
457. Gong, C.; Du, M.C.; Zhao, Q.; Zhong, X.H.; Zhou, B. Nature of X(6900) and its production mechanism at LHCb. *Phys. Lett. B* **2022**, *824*, 136794. [CrossRef]
458. Wang, J.Z.; Liu, X.; Matsuki, T. Fully-heavy structures in the invariant mass spectrum of $J/\psi\psi(3686)$, $J/\psi\psi(3770)$, $\psi(3686)\psi(3686)$, and $J/\psi\Upsilon(1S)$ at hadron colliders. *Phys. Lett. B* **2021**, *816*, 136209. [CrossRef]
459. Zhuang, Z.; Zhang, Y.; Ma, Y.; Wang, Q. Lineshape of the compact fully heavy tetraquark. *Phys. Rev. D* **2022**, *105*, 054026. [CrossRef]
460. Guo, Z.H.; Oller, J.A. Insights into the inner structures of the fully charmed tetraquark state $X(6900)$. *Phys. Rev. D* **2021**, *103*, 034024. [CrossRef]
461. Albuquerque, R.M.; Narison, S.; Rabetiarivony, D.; Randriamanatrika, G. Doubly hidden 0++ molecules and tetraquarks states from QCD at NLO. *Nucl. Part. Phys. Proc.* **2021**, *312–317*, 120–124. [CrossRef]
462. Wang, Q.N.; Yang, Z.Y.; Chen, W. Exotic fully-heavy $Q\bar{Q}Q\bar{Q}$ tetraquark states in $\mathbf{8}_{[Q\bar{Q}]} \otimes \mathbf{8}_{[Q\bar{Q}]}$ color configuration. *Phys. Rev. D* **2021**, *104*, 114037. [CrossRef]
463. Yang, B.C.; Tang, L.; Qiao, C.F. Scalar fully-heavy tetraquark states $QQ'\bar{Q}\bar{Q}'$ in QCD sum rules. *Eur. Phys. J. C* **2021**, *81*, 324. [CrossRef]
464. Zhu, J.W.; Guo, X.D.; Zhang, R.Y.; Ma, W.G.; Li, X.Q. A possible interpretation for $X(6900)$ observed in four-muon final state by LHCb—A light Higgs-like boson? *arXiv* **2020**, arXiv:2011.07799.
465. Wan, B.D.; Qiao, C.F. Gluonic tetracharm configuration of $X(6900)$. *Phys. Lett. B* **2021**, *817*, 136339. [CrossRef]
466. Berezhnoy, A.V.; Likhoded, A.K.; Luchinsky, A.V.; Novoselov, A.A. Double J/psi-meson Production at LHC and 4c-tetraquark state. *Phys. Rev. D* **2011**, *84*, 094023. [CrossRef]
467. Karliner, M.; Nussinov, S.; Rosner, J.L. $QQ\bar{Q}\bar{Q}$ states: Masses, production, and decays. *Phys. Rev. D* **2017**, *95*, 034011. [CrossRef]
468. Wang, Z.G. Analysis of the X(6600), X(6900), X(7300) and related tetraquark states with the QCD sum rules. *Nucl. Phys. B* **2022**, *985*, 115983. [CrossRef]
469. Wang, Z.G. Revisit the tetraquark candidates in the $J/\psi J/\psi$ mass spectrum. *Int. J. Mod. Phys. A* **2021**, *36*, 2150014. [CrossRef]
470. Khachatryan, V. Observation of Y(1S) pair production in proton-proton collisions at $\sqrt{s} = 8$ TeV. *J. High Energy Phys.* **2017**, *5*, 13. [CrossRef]
471. Aaij, R. Search for beautiful tetraquarks in the $\Upsilon(1S)\mu^+\mu^-$ invariant-mass spectrum. *J. High Energy Phys.* **2018**, *10*, 86. [CrossRef]
472. Mutuk, H. Nonrelativistic treatment of fully-heavy tetraquarks as diquark-antidiquark states. *Eur. Phys. J. C* **2021**, *81*, 367. [CrossRef]
473. Tiwari, R.; Rathaud, D.P.; Rai, A.K. Mass-spectroscopy of $[bb][\bar{b}\bar{b}]$ and $[bq][\bar{b}\bar{q}]$ tetraquark states in a diquark–antidiquark formalism. *Eur. Phys. J. A* **2021**, *57*, 289. [CrossRef]
474. Chen, W.; Chen, H.X.; Liu, X.; Steele, T.G.; Zhu, S.L. Hunting for exotic doubly hidden-charm/bottom tetraquark states. *Phys. Lett. B* **2017**, *773*, 247–251. [CrossRef]
475. Aaij, R. Observation of New Resonances Decaying to $J/\psi K^+$+ and $J/\psi\phi$. *Phys. Rev. Lett.* **2021**, *127*, 082001. [CrossRef] [PubMed]
476. Aaltonen, T. Evidence for a Narrow Near-Threshold Structure in the $J/\psi\phi$ Mass Spectrum in $B^+ \to J/\psi\phi K^+$ Decays. *Phys. Rev. Lett.* **2009**, *102*, 242002. [CrossRef] [PubMed]
477. Aaij, R. Search for the $X(4140)$ state in $B^+ \to J/\psi\phi K^+$ decays. *Phys. Rev. D* **2012**, *85*, 091103. [CrossRef]
478. Chatrchyan, S. Observation of a Peaking Structure in the $J/\psi\phi$ Mass Spectrum from $B^\pm \to J/\psi\phi K^\pm$ Decays. *Phys. Lett. B* **2014**, *734*, 261–281. [CrossRef]
479. Abazov, V.M. Search for the $X(4140)$ state in $B^+ \to \mathrm{J}_{\psi,\phi}K^+$ decays with the D0 Detector. *Phys. Rev. D* **2014**, *89*, 012004. [CrossRef]
480. Lees, J.P. Study of $B^{\pm,0} \to J/\psi K^+K^-K^{\pm,0}$ and search for $B^0 \to J/\psi\phi$ at BABAR. *Phys. Rev. D* **2015**, *91*, 012003. [CrossRef]
481. Aaltonen, T. Observation of the $Y(4140)$ Structure in the $J/\psi\phi$ Mass Spectrum in $B^\pm \to J/\psi\phi K^\pm$ Decays. *Mod. Phys. Lett. A* **2017**, *32*, 1750139. [CrossRef]

482. Aaij, R. Observation of $J/\psi\phi$ structures consistent with exotic states from amplitude analysis of $B^+ \to J/\psi\phi K^+$ decays. *Phys. Rev. Lett.* **2017**, *118*, 022003. [CrossRef]
483. Aaij, R. Amplitude analysis of $B^+ \to J/\psi\phi K^+$ decays. *Phys. Rev. D* **2017**, *95*, 012002. [CrossRef]
484. Liu, X.; Luo, Z.G.; Liu, Y.R.; Zhu, S.L. X(3872) and Other Possible Heavy Molecular States. *Eur. Phys. J. C* **2009**, *61*, 411–428. [CrossRef]
485. Wang, Z.G. Analysis of the Y(4140) with QCD sum rules. *Eur. Phys. J. C* **2009**, *63*, 115–122. [CrossRef]
486. Albuquerque, R.M.; Bracco, M.E.; Nielsen, M. A QCD sum rule calculation for the Y(4140) narrow structure. *Phys. Lett. B* **2009**, *678*, 186–190. [CrossRef]
487. Wang, Z.G.; Liu, Z.C.; Zhang, X.H. Analysis of the Y(4140) and related molecular states with QCD sum rules. *Eur. Phys. J. C* **2009**, *64*, 373–386. [CrossRef]
488. Wang, Z.G. Analysis of the Y(4274) with QCD sum rules. *Int. J. Mod. Phys. A* **2011**, *26*, 4929–4943. [CrossRef]
489. Liu, X.; Luo, Z.G.; Zhu, S.L. Novel charmonium-like structures in the $J/\psi\phi$ and $J/\psi\omega$ invariant mass spectra. *Phys. Lett. B* **2011**, *699*, 341–344; Erratum in *Phys. Lett. B* **2012**, *707*, 577. [CrossRef]
490. He, J.; Liu, X. The open-charm radiative and pionic decays of molecular charmonium Y(4274). *Eur. Phys. J. C* **2012**, *72*, 1986. [CrossRef]
491. Finazzo, S.I.; Nielsen, M.; Liu, X. QCD sum rule calculation for the charmonium-like structures in the $J/\psi\phi$ and $J/\psi\omega$ invariant mass spectra. *Phys. Lett. B* **2011**, *701*, 101–106. [CrossRef]
492. Hidalgo-Duque, C.; Nieves, J.; Valderrama, M.P. Light flavor and heavy quark spin symmetry in heavy meson molecules. *Phys. Rev. D* **2013**, *87*, 076006. [CrossRef]
493. Stancu, F. Can Y(4140) be a $c\bar{c}s\bar{s}$ tetraquark? *J. Phys. G* **2010**, *37*, 075017; Erratum in *J. Phys. G* **2019**, *46*, 019501. [CrossRef]
494. Patel, S.; Shah, M.; Vinodkumar, P.C. Mass spectra of four-quark states in the hidden charm sector. *Eur. Phys. J. A* **2014**, *50*, 131. [CrossRef]
495. Molina, R.; Oset, E. The Y(3940), Z(3930) and the X(4160) as dynamically generated resonances from the vector-vector interaction. *Phys. Rev. D* **2009**, *80*, 114013. [CrossRef]
496. Branz, T.; Molina, R.; Oset, E. Radiative decays of the Y(3940), Z(3930) and the X(4160) as dynamically generated resonances. *Phys. Rev. D* **2011**, *83*, 114015. [CrossRef]
497. Danilkin, I.V.; Simonov, Y.A. Channel coupling in heavy quarkonia: Energy levels, mixing, widths and new states. *Phys. Rev. D* **2010**, *81*, 074027. [CrossRef]
498. Chen, W.; Zhu, S.L. The Vector and Axial-Vector Charmonium-like States. *Phys. Rev. D* **2011**, *83*, 034010. [CrossRef]
499. Chen, H.X.; Cui, E.L.; Chen, W.; Liu, X.; Zhu, S.L. Understanding the internal structures of the $X(4140)$, $X(4274)$, $X(4500)$ and $X(4700)$. *Eur. Phys. J. C* **2017**, *77*, 160. [CrossRef]
500. Wang, Z.G. Reanalysis of $X(4140)$ as axial-vector tetraquark state with QCD sum rules. *Eur. Phys. J. C* **2016**, *76*, 657. [CrossRef]
501. Wang, Z.G. Analysis of the mass and width of the $Y(4274)$ as axialvector molecule-like state. *Eur. Phys. J. C* **2017**, *77*, 174. [CrossRef]
502. Wang, Z.G. Scalar tetraquark state candidates: $X(3915)$, $X(4500)$ and $X(4700)$. *Eur. Phys. J. C* **2017**, *77*, 78. [CrossRef]
503. Agaev, S.S.; Azizi, K.; Sundu, H. Exploring the resonances $X(4140)$ and $X(4274)$ through their decay channels. *Phys. Rev. D* **2017**, *95*, 114003. [CrossRef]
504. Liu, X.; Huang, H.; Ping, J.; Chen, D.; Zhu, X. The explanation of some exotic states in the $cs\bar{c}\bar{s}$ tetraquark system. *Eur. Phys. J. C* **2021**, *81*, 950. [CrossRef]
505. Wang, Z.G.; Di, Z.Y. Analysis of the mass and width of the $X(4140)$ as axialvector tetraquark state. *Eur. Phys. J. C* **2019**, *79*, 72. [CrossRef]
506. Wang, Z.G. Revisit the $X(4274)$ as the Axialvector Tetraquark State. *Acta Phys. Polon. B* **2020**, *51*, 435. [CrossRef]
507. Zhu, R. Hidden charm octet tetraquarks from a diquark-antidiquark model. *Phys. Rev. D* **2016**, *94*, 054009. [CrossRef]
508. Ghalenovi, Z.; Sorkhi, M.M. Spectroscopy of hidden-charm tetraquarks in diquark model. *Eur. Phys. J. Plus* **2020**, *135*, 399. [CrossRef]
509. Maiani, L.; Polosa, A.D.; Riquer, V. Interpretation of Axial Resonances in $J/psi/phi$ at LHCb. *Phys. Rev. D* **2016**, *94*, 054026. [CrossRef]
510. Shi, P.P.; Huang, F.; Wang, W.L. Hidden charm tetraquark states in a diquark model. *Phys. Rev. D* **2021**, *103*, 094038. [CrossRef]
511. Wu, J.; Liu, Y.R.; Chen, K.; Liu, X.; Zhu, S.L. $X(4140)$, $X(4270)$, $X(4500)$ and $X(4700)$ and their $cs\bar{c}\bar{s}$ tetraquark partners. *Phys. Rev. D* **2016**, *94*, 094031. [CrossRef]
512. Deng, C.; Chen, H.; Ping, J. Can the state $Y(4626)$ be a P-wave tetraquark state $[cs][\bar{c}\bar{s}]$? *Phys. Rev. D* **2020**, *101*, 054039. [CrossRef]
513. Lü, Q.F.; Dong, Y.B. X(4140) , X(4274) , X(4500) , and X(4700) in the relativized quark model. *Phys. Rev. D* **2016**, *94*, 074007. [CrossRef]
514. Anwar, M.N.; Ferretti, J.; Santopinto, E. Spectroscopy of the hidden-charm $[qc][\bar{q}\bar{c}]$ and $[sc][\bar{s}\bar{c}]$ tetraquarks in the relativized diquark model. *Phys. Rev. D* **2018**, *98*, 094015. [CrossRef]
515. Olsen, S.L.; Skwarnicki, T.; Zieminska, D. Nonstandard heavy mesons and baryons: Experimental evidence. *Rev. Mod. Phys.* **2018**, *90*, 015003. [CrossRef]
516. Li, H.B. Physics in the τ-charm Region at BESIII. *arXiv* **2022**, arXiv:2204.08943.
517. Aaij, R. Study of the lineshape of the $\chi_{c1}(3872)$ state. *Phys. Rev. D* **2020**, *102*, 092005. [CrossRef]

518. Aaij, R. Study of the $\psi_2(3823)$ and $\chi_{c1}(3872)$ states in $B^+ \to (J\psi\pi^+\pi^-)K^+$ decays. *J. High Energy Phys.* **2020**, *8*, 123. [CrossRef]
519. Choi, S.K. Bounds on the width, mass difference and other properties of $X(3872) \to \pi^+\pi^- J/\psi$ decays. *Phys. Rev. D* **2011**, *84*, 052004. [CrossRef]
520. Dubynskiy, S.; Voloshin, M.B. Pionic transitions from $X(3872)$ to chi(cJ). *Phys. Rev. D* **2008**, *77*, 014013. [CrossRef]
521. Ablikim, M. Search for$X(3872) \to \pi^0\chi_{c0}$ and $X(3872) \to \pi\pi\chi_{c0}$ at BESIII. *Phys. Rev. D* **2022**, *105*, 072009. [CrossRef]
522. Barnes, T. Higher charmonium. *J. Phys. Conf. Ser.* **2005**, *9*, 127–131. [CrossRef]
523. Eichten, E.J.; Lane, K.; Quigg, C. New states above charm threshold. *Phys. Rev. D* **2006**, *73*, 014014; Erratum in *Phys. Rev. D* **2006**, *73*, 079903. [CrossRef]
524. Ablikim, M. Observation of the decay $X(3872) \to \pi^0\chi_{c1}(1P)$. *Phys. Rev. Lett.* **2019**, *122*, 202001. [CrossRef]
525. Zhou, Z.Y.; Yu, M.T.; Xiao, Z. Decays of $X(3872)$ to $\chi_{cJ}\pi^0$ and $J/\psi\pi^+\pi^-$. *Phys. Rev. D* **2019**, *100*, 094025. [CrossRef]
526. Guo, F.K.; Hanhart, C.; Li, G.; Meissner, U.G.; Zhao, Q. Effect of charmed meson loops on charmonium transitions. *Phys. Rev. D* **2011**, *83*, 034013. [CrossRef]
527. Fleming, S.; Mehen, T. Hadronic Decays of the X(3872) to χ_{cJ} in Effective Field Theory. *Phys. Rev. D* **2008**, *78*, 094019. [CrossRef]
528. Badalian, A.M.; Orlovsky, V.D.; Simonov, Y.A.; Bakker, B.L.G. The ratio of decay widths of X(3872) to $\psi'\gamma$ and $J/\psi\gamma$ as a test of the X(3872) dynamical structure. *Phys. Rev. D* **2012**, *85*, 114002. [CrossRef]
529. Dong, Y.; Faessler, A.; Gutsche, T.; Lyubovitskij, V.E. $J\psi\gamma$ and $\psi(2S)\gamma$ decay modes of the X(3872). *J. Phys. G* **2011**, *38*, 015001. [CrossRef]
530. Cincioglu, E.; Nieves, J.; Ozpineci, A.; Yilmazer, A.U. Quarkonium Contribution to Meson Molecules. *Eur. Phys. J. C* **2016**, *76*, 576. [CrossRef]
531. Besson, D. Observation of a narrow resonance of mass 2.46 GeV/c^2 in the $D_s^{*+}\pi^0$ final state, and confirmation of the $D_{sJ}^*(2317)$. *AIP Conf. Proc.* **2004**, *698*, 497–502. [CrossRef]
532. Mikami, Y. Measurements of the D_{sJ} resonance properties. *Phys. Rev. Lett.* **2004**, *92*, 012002. [CrossRef] [PubMed]
533. Ablikim, M. Measurement of the absolute branching fraction of $D_{s0}^{*\pm}(2317) \to \pi^0 D_s^{\pm}$. *Phys. Rev. D* **2018**, *97*, 051103. [CrossRef]
534. Browder, T.E.; Pakvasa, S.; Petrov, A.A. Comment on the new $D_s^{*+}\pi^0$ resonances. *Phys. Lett. B* **2004**, *578*, 365–368. [CrossRef]
535. Hwang, D.S.; Kim, D.W. Mass of $D_{sJ}^*(2317)$ and coupled channel effect. *Phys. Lett. B* **2004**, *601*, 137–143. [CrossRef]
536. Zhou, Z.Y.; Xiao, Z. Hadron loops effect on mass shifts of the charmed and charmed-strange spectra. *Phys. Rev. D* **2011**, *84*, 034023. [CrossRef]
537. Ortega, P.G.; Segovia, J.; Entem, D.R.; Fernandez, F. Molecular components in P-wave charmed-strange mesons. *Phys. Rev. D* **2016**, *94*, 074037. [CrossRef]
538. Martinez Torres, A.; Dai, L.R.; Koren, C.; Jido, D.; Oset, E. Unitary chiral dynamics of two hadrons in a finite volume: The KD, ηD_s system and the $D_{s0}^*(2317)$ resonance. *J. Phys. Conf. Ser.* **2012**, *374*, 012008. [CrossRef]
539. Tan, Y.; Ping, J. $D_{s0}^*(2317)$ and $D_{s1}(2460)$ in an unquenched quark model *arXiv* **2021**, arXiv:2111.04677.
540. Dougall, A.; Kenway, R.D.; Maynard, C.M.; McNeile, C. The Spectrum of D_s mesons from lattice QCD. *Phys. Lett. B* **2003**, *569*, 41–44. [CrossRef]
541. Moir, G.; Peardon, M.; Ryan, S.M.; Thomas, C.E.; Liu, L. Excited spectroscopy of charmed mesons from lattice QCD. *J. High Energy Phys.* **2013**, *5*, 21. [CrossRef]
542. Lang, C.B.; Leskovec, L.; Mohler, D.; Prelovsek, S.; Woloshyn, R.M. Ds mesons with DK and D*K scattering near threshold. *Phys. Rev. D* **2014**, *90*, 034510. [CrossRef]
543. Simonov, Y.A.; Tjon, J.A. The Coupled-channel analysis of the D and D_s mesons. *Phys. Rev. D* **2004**, *70*, 114013. [CrossRef]
544. Feshbach, H. Unified theory of nuclear reactions. *Ann. Phys.* **1958**, *5*, 357–390. [CrossRef]
545. Badalian, A.M.; Simonov, Y.A.; Trusov, M.A. The Chiral transitions in heavy-light mesons. *Phys. Rev. D* **2008**, *77*, 074017. [CrossRef]
546. Burkert, V.D.; Roberts, C.D. Colloquium : Roper resonance: Toward a solution to the fifty year puzzle. *Rev. Mod. Phys.* **2019**, *91*, 011003. [CrossRef]
547. Richard, J.M. The Nonrelativistic three-body problem for baryons. *Phys. Rept.* **1992**, *212*, 1–76. [CrossRef]
548. Hogaasen, H.; Richard, J.M. Nucleon Resonances and the Quark Model. *Phys. Lett. B* **1983**, *124*, 520–522. [CrossRef]
549. Glozman, L.Y.; Plessas, W.; Varga, K.; Wagenbrunn, R.F. Unified description of light and strange baryon spectra. *Phys. Rev. D* **1998**, *58*, 094030. [CrossRef]
550. Isgur, N. Critique of a pion exchange model for interquark forces. *Phys. Rev. D* **2000**, *62*, 054026. [CrossRef]
551. Yang, G.; Ping, J.; Segovia, J. The S- and P-Wave Low-Lying Baryons in the Chiral Quark Model. *Few Body Syst.* **2018**, *59*, 113. [CrossRef]
552. Qing, D.; Chen, X.S.; Wang, F. Spin content of the nucleon in a valence and sea quark mixing model. *Phys. Rev. C* **1998**, *57*, R31–R34. [CrossRef]
553. Liu, B.C.; Zou, B.S. Mass and K Lambda coupling of N*(1535). *Phys. Rev. Lett.* **2006**, *96*, 042002. [CrossRef] [PubMed]
554. Li, Q.B.; Riska, D.O. The Role of $q\bar{q}$ components in the N(1440) resonance. *Phys. Rev. C* **2006**, *74*, 015202. [CrossRef]
555. Yuan, S.G.; An, C.S.; He, J. Contributions of $qqqq\bar{q}$ components to axial charges of proton and N(1440). *Commun. Theor. Phys.* **2010**, *54*, 697–700. [CrossRef]
556. Morel, D.; Capstick, S. Baryon meson loop effects on the spectrum of nonstrange baryons. *arXiv* **2002**, arXiv:nucl-th/0204014.

557. Adlarson, P. ABC Effect in Basic Double-Pionic Fusion—Observation of a new resonance? *Phys. Rev. Lett.* **2011**, *106*, 242302. [CrossRef] [PubMed]
558. Adam, J. The Proton-Ω correlation function in Au+Au collisions at $\sqrt{s_{NN}}$=200 GeV. *Phys. Lett. B* **2019**, *790*, 490–497. [CrossRef]
559. Godfrey, S. Testing the nature of the D(sJ)*(2317)+ and D(sJ)(2463)+ states using radiative transitions. *Phys. Lett. B* **2003**, *568*, 254–260. [CrossRef]
560. Zou, B.S. On the nature of the lowest $1/2^-$ baryon nonet and decuplet. *Eur. Phys. J. A* **2008**, *35*, 325–328. [CrossRef]